To the Graduate Council:
I am submitting herewith a thesis written by Shems-Eddine Belhout entitled "Image Based Processing for Weld Defect Detection." I have examined the final electronic copy of this thesis for form and content and recommend that it be accepted in partial fulfillment of the requirements for the degree of Master of Science, with a major in Mechanical Engineering.

Dr. Bradley Howell Jared, Major Professor

We have read this thesis
and recommend its acceptance:

Dr. Jindong Tan

Dr. Sudarsanam Suresh Babu

Accepted for the Council:

Dr. Dixie Thompson

Vice Provost and Dean of the Graduate School

(Original signatures are on file with official student records.)

Image Based Processing for Weld Defect Detection

A Thesis Presented for

The Master of Science

Degree

The University of Tennessee, Knoxville

Shems-Eddine Belhout

December 2022

© by Shems-Eddine Belhout, 2022
All Rights Reserved.

dedication...

To the people in my life who supported and believed in me during the hardest of times.

Acknowledgements

I would like to thank...

Dr. Bradley Jared for always being there for me as an advisor, and supporting my growth through incredibly harsh times. Ethan Vals for connecting me to the lab and supporting me as a friend through grad school. Sam Robertson for hiring me, and initially training me before his departure. Dr. William Bill Hamel for advice and assistance the transition of the project to us. Devon Goodspeed, Dylan Lewis, John Codevilla for continuing to support me during my research efforts to make this robot operational. David Hansen for the expertise and repairs on the Liburdi Welding Systems. Josh Penney and Logan McNeill for their help with coding and support. The many people who assisted me in the making of this custom welding robot. Ken Porterfield for his assistance with the Faulhaber motors and controllers. Daryl Dennison for his help with Kollmorgen communication. Jay West with his knowledge on the P300, weld sequence, and modbus interface. Mark Da Costa with his Liburdi field maintenance knowledge. Alan Bumgardner with his engineering skills for Liburdi repairs. Beckhoff Application Engineer Alec Abkemeier with his software development on the TF3710. Keyence technical expert Nathan White for his assistance with filtering the arc light. Cavitar sales manager James Primo and technical support Erkki Lassila & Aku Savolainen for fixing our cameras. My family for for the constant encouragement and for always believing in me. Brendon Michelle Blair for assistance and companionship in writing of this thesis.

Quotation...

"If we knew what it was we were doing, it would not be called research, would it?"

— Albert Einstein

"I haven't failed. I've just found 10,000 ways that won't work"

- Thomas Edison

"I am credited with being one of the hardest workers and perhaps I am, if thought is the equivalent of labour, for I have devoted to it almost all of my waking hours. But if work is interpreted to be a definite performance in a specified time according to a rigid rule, then I may be the worst of idlers."

- Nikola Tesla

Abstract

There is a growing need for automation in the welding industry due to a growing shortage in skilled welders. TIG (tungsten inert gas) welding, a method of welding that uses an electrode shielded by gas and a wire fed externally into the weld pool, is incredibly advantageous for its precise heat control. TIG welding is considered the standard for nuclear application which requires highly precise welds to be performed. Robotic welding can address this issue, and one major problem that occurs during welding is welding defects.

Typical weld defect detection requires a highly knowledgeable welder or destructive and nondestructive evaluation. Destructive evaluation such as sanding or cutting destroys part of the weld to investigate if a defect has occurred. Nondestructive evaluation such as x-rays ad ultrasonic imaging work well and do not require any damage to be done on the weld. However, these traditional measures must be done after a weld finishes due to the amount of heat that is dissipated from the system.

The challenges associated with defect detection are that they are time consuming and often expensive to repair. If a defect is detected, then a repair must be done to ensure the structural integrity of the weld. The only way to repair a weld is by removing material until the defect is reached and the weld is redone. The sooner a defect is detected then the easier the rework will be. Therefore, robotic real time detection would be weld defects.

Image processing is a solution for real time weld defect detection. This is especially useful so that an operator does not have to constantly monitor the weld camera to

check for a defect and how much a defect is occurring. There are three types of defects that are commonly associated with TIG welding will be investigated. Surface porosity is described by its hole patterns in the surface of the solidification of the weld. A weld characteristic known as tie-in is the interface or connection of overlapping weld beads in a multi-pass weld. Tie-in is described by its nonlinear weld characteristics and jagged edges. Void formation physically looks like a cavern underneath the weld. Currently an automated adaptive welding robot is in development by the University of Tennessee Knoxville in partnership with the Electric Power Research Institute. The goal of this research will be to incorporate the weld defect detection algorithm into the operational robot. Therefore, image processing algorithms will be developed in LabVIEW to detect surface porosity, tie-in, and if possible void formation.

Table of Contents

1 Introduction **1**

2 Background **4**

2.1 TIG Weld Pool & Solidification 4

2.2 Weld Defects 5

2.3 Robotic Welding 5

2.3.1 Liburdi F Head 5

2.3.2 Mark I Modified Head 6

2.3.3 Mark II Adaptive Welding Head 7

2.3.4 EPRI Liburdi G Head 7

2.4 Sensors 8

2.4.1 Cameras 8

2.4.2 Laser Profilometer 8

2.4.3 Power Supply 9

2.5 Software 9

2.5.1 LabVIEW 9

2.5.2 NI Vision Assistant 10

2.6 Past Methods for Weld Image Processing 10

2.6.1 Weld Pool Width Tracking Image Algorithm 10

2.6.2 Wire Feed Tracking Image Algorithm 11

2.6.3 Tungsten Location Tracking Image Algorithm 11

3 Experimental Method **12**

3.1 EPRI Liburdi G Head Setup . . . 12

3.2 Data Collection Software . . . 13

3.2.1 Liburdi P300 Power Supply . . . 13

3.2.2 LJ-V7080 Keyence Laser Profilometer . . . 14

3.2.3 C300 Cavitar Welding Cameras . . . 15

3.2.4 Weld State Activation . . . 15

3.3 Experimental Plan . . . 17

3.3.1 Robot & Groove System . . . 17

3.3.2 Data Collection Software . . . 17

3.3.3 Weld & Sensor Settings . . . 18

3.3.4 Surface Porosity Test Cases . . . 18

3.3.5 Tie-In Test Cases . . . 18

4 Experimental Results **19**

4.1 Surface Porosity . . . 19

4.1.1 Gas Flow Coverage Discontinued . . . 19

4.1.2 Oil Contaminants . . . 20

4.1.3 Paint Contaminants . . . 20

4.1.4 Accelerated Rust . . . 21

4.1.5 Varying Groove Geometry . . . 21

4.1.6 Compressed Air in Varying Groove Geometry . . . 22

4.1.7 Possible Explanations for Difficulty to Induce Porosity . . . 22

4.2 Void Formation . . . 23

4.3 Keyence Solidification Edge Tracking . . . 23

4.4 P300 Power Supply Monitoring . . . 24

5 Tie-In Image Processing Algorithm **26**

5.1 LabVIEW Tie-In Algorithm . . . 26

5.1.1 Image Warping . . . 26

5.1.2 Image Configuration . . . 28
5.1.3 Cropping . . . 29
5.1.4 Line Profile . . . 30
5.1.5 Peak Detection . . . 31
5.1.6 Region of Interest Filtering . . . 32
5.2 Tie-In Algorithm Test Cases . . . 33
5.2.1 Good Centered Weld Bead in an Empty Groove . . . 33
5.2.2 Good Inner & Outer Weld Bead in a Filled Groove . . . 33
5.2.3 Adaptive Cropping Conditions . . . 34
5.2.4 Poor Camera Angle & Focal Length . . . 35
5.2.5 Awful Weld Conditions . . . 35
5.3 Algorithm Limitations . . . 36
5.3.1 Detecting Stray Defects . . . 37
5.3.2 Wall Reflections & Divergences . . . 38
5.4 Tie-In Defect Quantification . . . 39

6 MK II Custom Weld Head **40**
6.1 Current State of the Robot . . . 40
6.2 Software . . . 41
6.2.1 P300 Power Supply . . . 41
6.2.2 Keyence Laser Profilometer . . . 41
6.2.3 Motor Encoder Position & Velocity . . . 41
6.2.4 Cavitar Trail & Lead Cameras . . . 42
6.2.5 System Operation's Panel . . . 43
6.2.6 Data Collection . . . 44
6.2.7 Live Tie-In Detection Algorithm . . . 44
6.3 Live Tie-in Algorithm Test . . . 45

7 Conclusions & Future Steps **46**
7.1 Conclusion . . . 46

7.2 Future Work 47

A Appendix **50**

A.1 Introduction 50

A.2 Background 51

A.3 Experimental Method 60

A.4 Experimental Results 67

A.5 Tie-In Image Algorithm 83

A.6 Tie-In Algorithm Results 92

A.7 MK II Custom Weld Head 101

A.8 LabVIEW Code 104

Vita **106**

List of Tables

A.1 P300 Power Supply Registers Monitored 61
A.2 Weld States on the Liburdi P300 Registers 63
A.3 Liburdi G Head Power Settings 64
A.4 Data Collection Settings 65
A.5 Surface Porosity Test Matrix 65
A.6 Tie-In Test Matrix 66
A.7 Surface Porosity Results 67

List of Figures

A.1 Tungsten Inert Gas (TIG) Welding Operation [Shirsat (2021)] 50
A.2 TIG Leading Camera of Weld Pool (Top) Trailing Camera of Solidification (Bottom) 51
A.3 Weld Defects: Surface Porosity (Top) Aquasol (2021) Poor Tie-in (Middle) Void Formation (Bottom) 52
A.4 Welding Robots Used [Top to Bottom]: (1) EPRI Donated Liburdi F Head at UTK (2) MK I Modified F Head (3) MK II Custom CAD Model Prototype Design (4) Liburdi G Head 53
A.5 Liburdi and Cavitar Camera Image Quality Comparison 54
A.6 LJ-V7080 Keyence Laser Profilometer (Top) Liburdi Dimetrics P300 Power Supply (Bottom) 55
A.7 NI Vision Assistant Software Interface (Top) LabVIEW Front Panel (Middle) LabVIEW Back Panel (Bottom) 56
A.8 Weld Pool Width Tracking Image Process on Lead Camera 57
A.9 Weld Pool Width Tracking Image Process on Lead Camera 58
A.10 Tungsten Tip Edge Detection Tracking 59
A.11 Liburdi G Head Initial Setup 60
A.12 EPRI Liburdi G Head Mod 1 Cavitar Lead (Left) & Trail (Right) View 60
A.13 EPRI Liburdi G Head Final Setup 61
A.14 Keyence Laser Profilometer Scan Plot 62
A.15 Groove Geometry 63

A.16 EPRI G Head Data Collection Interface - LabVIEW Front Panel . . . 64
A.17 Cut Gas Coverage Test Case for Surface Porosity 67
A.18 Cut Gas Coverage Resulting Weld Bead 68
A.19 Oil Contaminants for Surface Porosity 69
A.20 Oil Contaminants Resulting Weld Bead 70
A.21 Paint Contaminants for Surface Porosity 71
A.22 Paint Contaminants Resulting Weld Bead 72
A.23 Induced Rusted Surface Contaminants 73
A.24 Rusted Surface Contaminants Resulting Weld Bead 74
A.25 Different Groove Geometry Test Case 75
A.26 Slotted Plate Resulting Weld Bead 76
A.27 Slotted Plate Compressed Air Damage 77
A.28 Slotted Plate Compressed Air Inner Wall Resulting Weld Bead 78
A.29 Void Instance in Surface Porosity Test with Tapmatic 79
A.30 Keyence Failed Detection 80
A.31 Heavily Filtered Keyence 3D Weld Groove Scan 80
A.32 P300 Power Supply Raw Current & Voltage Telemetry 81
A.33 Cut Gas Coverage Raw Volts Spike Locations 82
A.34 Tie-In Edge Detection System Diagram 83
A.35 Image Warping in NI Vision Assistant 83
A.36 Image Warping Before & After 84
A.37 LabVIEW Tie-In Configuration 85
A.38 LabVIEW Static Crop 86
A.39 Edge Detection Cropping 86
A.40 Y Axis Oscillation Motor Encoder Position Cropping on MK II Head 87
A.41 Image to Matrix to Line Profile Plot 87
A.42 NI Vision Assistant Line Profile 88
A.43 Average Smoothing Line Profile Peak Detection & Edge Tracking . . 89
A.44 Tungsten Tracking Line Profile Peak Detection 90

A.45 ROI Data Filter Process Diagram 91
A.46 Clean Weld Center Bead Tie-In Algorithm Test 92
A.47 Clean Weld Outer Wall Tie-In Algorithm Test 93
A.48 Clean Weld Inner Wall Tie-In Algorithm Test 94
A.49 Adaptive Cropping Moving Y-Axis Oscillation Tie-In Algorithm Test 95
A.50 Poor Camera Angle from First Test Run Comparison 95
A.51 Poor Camera Angle & Focal Length for Tie-In Algorithm Test 96
A.52 Tie-In Cut Argon Gas Coverage 97
A.53 Result of Bad Algorithm Start Data (Bottom) Example of Bad Start Data (Top): Welding Near Edge of Groove (Top Left) Welding Started with Arc Formation 98
A.54 Algorithm Detects Oxide Close to Right Edge 99
A.55 Instance of Algorithm Diverging from Poor Start Data 100
A.56 Current MK II Weld Head Actively Welding: Front View (Top) Side View (Bottom) 101
A.57 Evolution of Robot & Comparison 102
A.58 Current State of MK II Weld Head LabVIEW Interface 103
A.59 Live Tie-in Robot Control 103
A.60 Results of the Live Tie-In Algorithm on the MK II System 104
A.61 LabVIEW Front Panel - Standalone Tie-in Algorithm 104
A.62 LabVIEW Back Panel - Standalone Tie-in Algorithm 105

Nomenclature

AVC	automated voltage control
csv	comma separated values
EPRI	Electric Power Research Institute
FFT	Fast Fourier Transform
HDR	high dynamic range
HMI	human machine interface
IR	infrared
NI	National Instruments
ROI	region of interest
TCP	transmission control protocol
TDMS	LabVIEW binary technical data management system
TIG	tungsten inert gas welding
UT	University of Tennessee Knoxville
VI	LabVIEW visual instrument

Chapter 1

Introduction

There is a growing need for automation in the welding industry due to the increasing shortage of skilled welders. TIG (tungsten inert gas) welding, a method of welding that uses an electrode shielded by gas and is fed externally by a wire, is incredibly advantageous for its precise heat control and cleanliness as seen in Figure A.1. TIG welding is considered the standard for nuclear application which requires highly precise welds. As the population of expert welders decreases, there is a growing demand to fill in the market. Robotic welding can fill that market. Liburdi, a Canadian welding robot company, has shown the capability of welding orbitally around the circumference of a pipe using robots. Liburdi partners with the nuclear power industry to perform repairs on existing power plant pipes. Liburdi's system provides a great tool for automated welding, but their system is lacking. Their systems have to be manually operated within proximity of the welding robot. A skilled welder would still need to be required to ensure the robot welds optimally. There also exists no feedback with any of the motors or sensors. Many existing orbital TIG welding robots lack any real-time control feedback for movement and weld conditions. Hence, the University of Tennessee Knoxville (UTK), partnered with the Electric Power Research Institute (EPRI), was developing a TIG welding robot intended for adaptive welding and defect detection.

In addition to the lack of control, there's also a lack of real-time image processing. A group from the University of Wollongon in Australia developed deep learning algorithms for defect detection [Xia (2020)]. They researched and discovered high dynamic range (HDR) cameras that can filter the arc light somewhat similar to the Cavitar cameras that were used for this thesis. Their group developed convolutions neural network which combines deep learning with an image processing technique that applies a filter to highlight certain color spectrum's through kernels. Convolutions were what the image software like Photoshop uses to apply photo altering changes. Using a convolution neural network, the Australian group was able to categorize defects such as good weld, misalignment, burn through, under cut, and under penetration. There was one severe limitation to their algorithm. It cannot operate in real-time. The group relies on post-processing to categorize when a defect occurs. This was not viable for real-time defect detection. AIMEN Technology Centre, a Spanish-based technology firm developed an artificial intelligence model to categorize different components of the weld pool as seen in Figure A.2. AIMEN showed that it was possible to identify the components of the weld, but they require intensive post-processing artificial intelligence [Landín (2022)]. Multiple companies and research groups have shown that it was possible to identify defects using image processing, however, they use very complex and computer-intensive algorithms. Very recently new revolutionary welding cameras have been introduced to the market. They filter the arc light using laser illumination and allow for accurate real-time image processing which was not possible. The extent of the camera's capabilities was discussed in the background section of the thesis. These cameras clearly show the weld pool features without any noise that HDR or heavily filtered cameras present. There's no need for artificial intelligence or neural networks to perform image processing for weld defects.

With the introduction of robotic control and sensing, other information can be documented such as power supply telemetry or robot positioning. If a defect occurs at some time, perhaps other data at that time could indicate if a defect has formed. Common defects that plague TIG were poor tie-in. Traditionally, if a defect has

occurred, the weld would be aborted, the solidified weld would then be ground down, and the weld would be repeated. Because of this, the faster a defect was detected, the quicker it can be prevented. By observing the solidification trailing cameras, we can monitor and track the edges of the solidification over time. Using a real-time image processing algorithm can identify defects by measuring the location of the tungsten tip, the solidified melt pool edges, and the groove geometry. The real-time monitoring of these features can inform the operator if a particular defect was present.

Chapter 2

Background

2.1 TIG Weld Pool & Solidification

In Figure A.2, the leading camera view of the weld pool was visible. Parts of the welding robot were also visible such as the shielding glass cup. This cup, attached to the flow regulator in the torch' directs 100% pure Argon gas for shielding the arc. The Tungsten tip electrode acts as the conductor of electricity from the power supply to the work plate. After the formation of the arc, the surface gets to temperatures of at least 2,600°F to form the molten weld pool. The system fed 316 stainless steel wire and instantly melted upon entry into the weld pool. The robot welded in the motion towards the camera from the leading perspective as labeled in Figure A.2.

The wire was visible behind the Tungsten electrode in the trail camera view. The transition between the molten weld pool and solidified weld bead was visible. This boundary was identifiable when the chevrons, curved edges in the solidified weld, end right before the weld pool. The developed image processing algorithm focused on the rear or trailing camera that shows the solidification of the groove clearly for defect detection.

2.2 Weld Defects

Surface porosity is a common weld defect that occurs when gases are in the molten weld pool. The gases attempt to rise, but some never reach the surface. This results in a weld bead that appears porous. There are two notable ways that surface porosity can form: contaminants on the weld plate, and reduced gas coverage over the Tungsten electrode. Once surface porosity starts forming it will not go away unless welding stops and the causing issue was addressed.

A prevalent weld defect was the occurrence of poor tie-in as seen in Figure A.3. This defect was categorized by the edges of the groove. An ideal weld bead has straight edges and good fusion to the surface. Welding over abnormal surfaces can cause this defect to occur. Poor control of the robot can also cause poor tie-in. The wire being fed differently into the pool can also cause this flaw. This was the most common defect that plagues the welding industry and robotic control can eliminate the risk.

This defect is the equivalent of a cavern that forms underneath the weld bead. Unfortunately, this is a challenging defect to observe. The defect is often internal and would require destructive evaluation to determine its impact as seen in the cross-section in Figure A.3. It would not be obvious to the human eye. The key to detecting void formation was knowing exactly when the void forms. The sensors are needed to monitor the transition from a normal weld solidification to a void formation.

2.3 Robotic Welding

2.3.1 Liburdi F Head

Liburdi is an Ontario, Canada based technology company. They produce a wide range of products such as power supplies, gas turbine engines, and welding services. Liburdi (2010) Liburdi Dimetrics are known for their orbital welding heads. With a donation from EPRI, The University of Tennessee Knoxville (UTK) acquired a Liburdi F head

for research purposes. A picture of the donated Liburdi F Head. Robotic control eliminated almost all human error from movement. Before, a welder would need to control the distance between the torch and the plate, travel at a constant speed, and constantly feed wire in the correct direction. Making a good weld was challenging and used to require decades of experience. Now, robotic control can eliminate most defects caused by motion.

Despite these benefits, there were design flaws of the Liburdi F head. The weld head required to be manual control by an operator. Only three out of the six axes were motorized. This included the track (x-axis), perpendicular to the track (y-axis), and vertically to the track [Z axis or Arc Voltage Control (AVC)]. None of the motor's positioning were capable of monitoring or control via encoder feedback. There are no sensors for monitoring the weld. This system cannot be operated remotely nor was it capable of automation. These problems need to be addressed before it could get to the state of adaptive control.

2.3.2 Mark I Modified Head

In response to all the limitations of the F head, a prior UT student modified the exiting F head that could be capable of automation. The front assembly on the F Head was completely redesigned. New axes were motorized with encoder feedback. A laser profilometer and two Liburdi cameras were integrated. The new modified F head has capabilities of control and remote monitoring.

However, there were many issues associated with this head's operation. The original Liburdi F head was not designed to support the added weight to the front half of its assembly. In the original F head, the AVC motor only needed to support the torch and wire feed. Instead the AVC supported sensors, motors, and machined assemblies. The Liburdi motors were prone to failing and dying from the amount of torque required to support the newly added weight. Another challenge was having the system be repeatable over multiple runs. The modifications made the F head not

as robust as its original counterpart. A majority of the parts were 3D printed adding to the instability. All of these issues led to the decision for a completely brand new redesign.

2.3.3 Mark II Adaptive Welding Head

In this new weld head redesign, all parts were completely machined and fabricated either in-house or outsourced. The design took inspiration from the F head. Many aspects and designs were reworked into this design such as the roller track. The only parts that were reused from the Liburdi F Head were the motherboard controller, the torch, water/gas lines, and the Liburdi P300 power supply. This system used original motors decoupled from Liburdi's welding system and offered real-time control with encoder feedback. There were many challenges associated with such an ambitious project. Many components that were reused from the F head were simply not designed for such a larger welding system. Originally, the goal was to integrate image-based processing into the Mark II, but due to the many challenges associated with this project this head was not used for the initial scope of this thesis. However, the new head would eventually become operational and one of the algorithms was tested live. This was discussed in Chapter 6.

2.3.4 EPRI Liburdi G Head

The Liburdi G Welding Head was the next generation series that Liburdi manufactured after the F Head. It was significantly more stable than the F head. This system introduced a motorized wire height adjustment, a brand new power supply, and options to add encoder feedback for the travel and oscillation axes. Due to delays in the MK II weld head, EPRI agreed to experimentation on their G head for the development of defect detection algorithms. This welding system was later modified to incorporate sensors originally seen in the MK II Custom Weld Head. The details

of the setup was addressed in Chapter 3. Images of all past weld heads used by the University and EPRI collaboration can be seen in Figure A.4.

2.4 Sensors

2.4.1 Cameras

Liburdi Welding Cameras were preinstalled on the MK I Modified Head as well as all newly built Liburdi Heads. They provide a view of the weld pool and solidification without any damage from the heat of the arc. However, the arc light introduced extreme amounts of exposure that made it incredibly challenging to develop image algorithms. The resolution is low and the arc washes out the images extensively. In contrast, Cavitar C300 welding cameras provide a significant increase in image quality. Unlike the Liburdi cameras that use intense filtering, Cavitar uses class 3R laser illumination to produce a greyscale image. Cavitar (2021) Figure A.5 compares the image quality between the Liburdi and Cavitar cameras. The Cavitar image shows great detail of the weld pool. In some cases, the brightness of the arc was eliminated. Some identifying features in this image include the weld pool, Tungsten tip, wire feed, and weld solidification.

2.4.2 Laser Profilometer

This was a new sensor that's not traditionally used with a welding environment. Keyence is a large technology company that produces microscopes and metrology instrumentation. Both the MK I modified head and the MK II custom head integrated a Keyence LJ-V7080 laser profilometer. This particular model of Keyence uses a visible blue laser with a wavelength of 405 nanometers. Keyence (2022) A laser profilometer uses laser displacement sensor that emits a band of light onto the target and the reflected light was received using a 2D CMOS to calculate the height across the laser line. Keyence (2022) to detect the reflections of the laser from the surface.

This resulted in a 2D vector of the topology of the surface. Using multiple scans can generate a 3D representation of the surface without ever making contact with the material as seen in Figure A.6. Ideally, for our welding application, the sensor can be integrated to track the edges of the groove. Other welding applications can include detecting weld geometry, topology, and surface characteristics.

2.4.3 Power Supply

The Liburdi F Head and MK II custom head uses a P300 Liburdi Dimetrics Power Supply as seen in A.6. The P300 controls the coolant, gas, voltage, current, power, and motors for an orbital welding head. When used as a stand-alone power supply it can fully control and program a Liburdi Welding Head in all of the welding phases. This power supply has a Modbus interface that can remotely read and/or write the power supply's many registers including telemetry and weld settings.

2.5 Software

2.5.1 LabVIEW

LabVIEW is a visual-based programming language developed by National Instruments. The program has two main interfaces. The front panel is where code is converted into a graphical user interface for the operator to see and interact with data, sensors, etc. The back panel contains all of the hard code of the front panel and is where all of the background processes occur. The code flows like a circuit where data travels through the wires and goes through operations inside Visual Instruments. (VI) are smaller, modular functions of LabVIEW code. The software can interface between many different types of sensors and data acquisition. It was advantageous for developing control and monitoring of systems with its built-in graphical user interface and custom applications.

2.5.2 NI Vision Assistant

Vision Assistant is a plug-in developed for LabVIEW by National Instruments. The program is a prototyping interface for image processing. It's much more user-friendly compared to LabVIEW and can export the project into LabVIEW code that can later be modified. The program has many built-in functions that perform image processing such as masking, threshold, binary, tracking, and more. It's a great tool for quickly performing image analysis. An example of LabVIEW code as well as the interface for NI Vision Assistant can be seen in Figure A.7.

2.6 Past Methods for Weld Image Processing

2.6.1 Weld Pool Width Tracking Image Algorithm

This was an image algorithm developed by a prior student whose goal was to monitor the weld pool width over time. The algorithm used a local adaptive threshold that created a binary image that outlines outlines high contrast areas. This image process can be seen in Figure A.8. After thresholding, an aggressive particle grouping filter was applied to reduce the noise level in the image. A finer particle filter was used to remove objects that remain outside the estimated weld pool area. The weld groove geometry was known to be 0.75 inches. This known length can be scaled down to monitor the estimated weld width in inches and the location of the left and right pool edges with respect to the torch tip. The information was overlaid on the original image, and concatenated frame by frame to form a plot over time of the values. This width tracking resulted in a plot that monitors the weld pool pulsing over time. This algorithm operated well for one image set. However, it would fail on any other test case. That was the main flaw with using a binary method. There would need to be some sort of adaptive setting changed in response to different kinds of welds, or the algorithm needed to learn and have patterns to recognize what kind of model needs to be used.

2.6.2 Wire Feed Tracking Image Algorithm

This was an algorithm developed to mimic the image processing method developed by the prior Ph.D. student who worked on the project. The steps to this method was shown in Figure A.9. It used a similar threshold, cluster, and filter method to attempt to track the wire's entry location into the weld pool. This algorithm was prone to failing continuously. It had difficulty tracking the wire entry into the weld pool and often lose track. This was the main downside to the binary threshold methods. They were dependent on the variation in the bright and dark parts of the image. As soon as any amount of exposure or movement changed the threshold criteria were no longer valid.

2.6.3 Tungsten Location Tracking Image Algorithm

This algorithm uses an edge detection method for tracking the edges of the Tungsten tip as seen in Figure A.10. Edge detection observes the pixels of a given region of interest (ROI) and separates them. Like the prior two algorithms, this algorithm would fail consistently. The algorithm fails whenever the brightness of the image changes i.e. whenever the welding arc pulses. Later in the thesis, it would be discovered that it's redundant to track the Tungsten electrode for this case. The cameras were kinematically fixed to the robot head, and anytime the robot moves the Tungsten will always be in the same location. Hence there was no need to track the Tungsten.

Chapter 3

Experimental Method

3.1 EPRI Liburdi G Head Setup

Due to the major delays in the development of the MK II head at UT, the image processing algorithms were developed by modifying an existing Liburdi G Head at EPRI's lab in Charlotte, NC. The goal was to replicate the MK II's setup as closely as possible with the G head. The first version of the setup was developed and can be seen in Figure A.11. The goal was to modify the G head without destructively changing any existing components such that the G head could be reassembled to its original state. In this version, the Keyence laser was seven inches away from the torch tip. The leading camera was at a 45 degree angle with respect to the plate.

The trailing camera was not located at an optimal position relative to the tungsten tip. The C300 Cavitar camera's working distance was 200 mm. In this setup, the trail camera lens was 250 mm away from the tungsten tip. This resulted in an out of focus view as seen in Figure A.12. The trailing camera should also have been oriented at a similar angle to the leading cameras. The trail camera was at a 45 degree angle with respect to the plate. A steeper camera angle provides a smaller region of interest that image processing can be performed.

The Keyence was also positioned too far away from the torch. The laser profilometer would not collect any data until the torch reaches halfway into the plate. A potential workaround to this delay would be to scan the groove after solidification. However, this was not a good solution as the key to this study was to pinpoint from start to finish where a defect occurred in the cameras live. This would make the timing of all of the defects with all of the other sensors incredibly challenging as well. Especially since at the time, there were no encoders for travel. The eventual goal for the MK II will be for a real-time weld defect detection capability so all of the sensors would ideally collect the data as soon as defect forms to stop welding or flag any spots.

The new redesign was in response to all of the issues from the first iteration. The Keyence support was redesigned to mount directly to the side of the torch on the G head. There were extra threaded holes to adjust the height of the Keyence Support. The Cavitar camera support brackets were also redesigned to have larger adjustments. The trail camera was at a better angle for viewing the feed. The wire support window was redesigned with a larger opening to hold the wire in place.

3.2 Data Collection Software

3.2.1 Liburdi P300 Power Supply

Currently, the P300 power supply values were documented using Modbus communication. Modbus is a communication protocol that enables two devices to send information and communicate. In Modbus there is a master, for the current welding system, it was the computer running the software, that will act as the device to send instructions for what it wants and receives it. There was also the slave device, the P300, which receives instructions from the master device and responds accordingly.

The LabVIEW code opens the command prompt and pings the Liburdi P300 Power Supply to confirm that the main computer can communicate with the P300

over Ethernet. For most Ethernet devices this was normally not required, but the P300 power supply needs to be notified that it expects communication between itself and the PC. Once there was a successful ping, the VI prepares a Transmission Control Protocol packet (TCP). TCP was a standard transport protocol for Ethernet networks. In Modbus TCP, a Modbus message was placed inside a TCP packet so it can be transmitted over an Ethernet network. You can imagine TCP as the truck that has a map that will transport information between the computer and the device. Modbus was the cargo that the truck or TCP transports between the two devices.

After creating a TCP packet, a register was chosen on the P300 that we want to read off of. A register was a quickly accessible location on a processor that stores small sets of data such as a binary or double value. Depending on what register was chosen, we can read anything on the P300 such as current, voltage, wire feed, etc. See Table A.1 for the full list of registers that were monitored. There were two types of registers, input, and output, where each determines the purpose of that specific register the P300 uses it for. Once a register number, type, and TCP packet were created. It was sent via Ethernet to the P300's Modbus server. The P300 then receives the order and responds immediately with the value of the register at that time.

The P300's reply was then saved into a Binary Technical data management system (TDMS) file. This was a data collection file developed by National Instruments that organizes data into channels. The power supply was sampled at 16 Hz, although it would later be discovered that the power supply needed to be sampled at least 100 Hz to capture the full voltage square wave from the arc pulsing.

3.2.2 LJ-V7080 Keyence Laser Profilometer

There were standalone VI's provided by the Keyence Company to allow for easy integration into LabVIEW. The controller used for the LJ-V7080 was the Keyence Controller LJ-V7001. In the controller, there were two modes. The high-speed mode

optimizes the controller for high data acquisition and removes some information about the profile. Advanced mode was slower, but provides a much more in-depth analysis of the geometry. The data collection software uses the high-speed option. Any settings that were modified for the Keyence were automatically stored inside the controller.

LabVIEW connects to the Keyence over a specific IP address that LabVIEW attempts to locate and find. Once connected LabVIEW reads the data from the Keyence controller. The data exported results in three bits of data. Y0 was the starting position of the laser. Xd represents the indices of each point from the Keyence. 800 Z height values were produced from the Keyence scan. This data gets sent to a TDMS file to be saved on the computer during every scan. Once again this sensor was sampled at 16 Hz despite being capable of going up to 150 Hz.

3.2.3 C300 Cavitar Welding Cameras

The Cavitar cameras behave like normal cameras that plug into a PC. This makes the cameras natively LabVIEW compatible. Due to this feature, the cameras connect to LabVIEW easily as there were built-in drivers that LabVIEW can detect and view data off of the sensor. The Cavitar cameras communicate over Ethernet, much like the other sensors do. The data was being saved off of the cameras as an image sequence. Pictures were more advantageous than video. If there was a frame rate drop it will result in a non-constant frame rate. Video also produces motion blur which a photograph would reduce. Image analysis works more efficiently on image sequences than videos as well. Similar image acquisition methods performed in this data collection section were later adapted to the image processing section of this thesis.

3.2.4 Weld State Activation

As stated prior, the key to defect detection was ensuring that the timing of all sensors was accurate. All data were recorded at the same sample rate albeit it was later

determined that some sensors needed to be recorded at a much higher rate. All sensors started and stopped recording data at the same time. As suggested by EPRI researchers, they recommended an automatic start and stop recording capability. Before the recording would need to be manually triggered. Now the data collection would be triggered by the arc forming on the G head and stopping when the arc was no longer present. There exists a specific register on the P300 that can read out when the arc formed on the head. As seen in Table A.2, this indicates the possible weld states the welding robot can be in. Recording would begin at the start of the segment state, which was the longest state during welding. Recording stopped at the arc stops. There was an initial challenge in reading the welding state while recording data. During arc initiation, the P300 Power Supply temporarily halts all communication. If the Modbus Server was temporarily unable to service a request, the communication protocol requires that it issues a Modbus Exception, indicating that the server was busy. In the case of arc initiation, the power supply was moving the tungsten electrode toward the work piece. The control system must stop the torch movement the moment that the tip of the tungsten makes contact as it was sampling well over 500 Hz. To guarantee immediate recognition of the touch, the processor suspends servicing any requests from the Modbus Master. This prevents the Master from flooding the Server with requests that take time to service. If this were to happen it's possible that the controller would not immediately recognize a touch when it occurs because it was too busy generating Modbus responses. Internally there was a circuit with a small voltage that normally was not in the welding circuit. This circuit activates whenever the native Power Supply jogs the AVC motor. When jogging the axes, it flips a relay and a 2-3 voltage will appear on the parallel circuit. That voltage signal drops whenever the tungsten on the weld head makes contact with the work piece and closes the loop. By doing that, the P300 stops movement, pushes current into the system, pushes the tungsten up, and forms the arc. There were still a few registers that were readable during the arc initiation sequence. Weld

state was one of them. The code merely pauses reading the power supply data until the weld state changes to the segmented stage.

3.3 Experimental Plan

3.3.1 Robot & Groove System

The EPRI Liburdi G Head was used for all experimental runs for this thesis. It was modified as explained earlier in the thesis. The sensors were placed at their respective optimal focal length for the best results. The Keyence was placed at a height of 80 mm from the work piece. The Cavitar cameras were oriented 200 mm away from the object of interest which was the tungsten. All trials were done in a modified V groove composed of 316 stainless steel. The dimensions of the groove can be seen in Figure A.15.

3.3.2 Data Collection Software

Figure A.16 shows the software used to record sensor data from the power supply, cameras, and laser profilometer. This program has the option to choose which sensor the operator wants to record in case one of the sensors was no longer accessible. There was a manual record option that starts and stops recording whenever the operator chooses. There was also an automatic start and stop recording that was triggered via the Liburdi Weld State Register as discussed earlier in the thesis. Finally, there was an option to save all of the data to four different data format types. Microsoft Excel, Binary TDMS, Binary TDM, and CSV were the options. All data started and stopped at the same time, as well as the time stamp for when it was sampled relative to the start time in seconds.

3.3.3 Weld & Sensor Settings

The weld settings seen in Table A.3 were chosen by an EPRI expert welder. These operating settings were typically much higher than what the manufacturer recommendations are. These settings often produce better welds. Whenever the weld operated at high voltage and current, the temperatures get incredibly hot which burns any material in the weld path that may cause defects. Welds that operate at higher temperatures were more forgiving and hence recommended.

All of the sensors were recorded at 16 Hz. This sample rate was chosen for the Cavitar Cameras. At the time of software development, 16 Hz was the max possible sample rate that could be achieved in LabVIEW for the Cavitar Cameras. EPRI was keen on the timing and proximity of the data hence all data was sampled the same. 16 Hz was plenty sufficient for the cameras. However, it would later be discovered that the power supply and Keyence needed to be sampled at least 100 Hz. The camera frame rate could also be increased by improving Ethernet traffic as they transfer 4K images (1920x1080) resolution at 200 FPS over Ethernet natively.

3.3.4 Surface Porosity Test Cases

Unfortunately, this defect was shown to be incredibly difficult or near impossible to create. As stated prior, there were two main methods for inducing porosity on the surface of the weld. Introduce contaminants or cut the gas flow. The entire experimental matrix for surface porosity can be seen in Table A.5.

3.3.5 Tie-In Test Cases

The poor tie-in was the easiest defect to create. The bead geometry can be manipulated in three main ways. Moving the robot position in the Y axis oscillation or other motion axes. Manipulating the wire entry into the weld pool. Welding over contaminants or varying weld geometries. The poor tie-in was tested for all of these three cases in addition to welding on different parts of the groove.

Chapter 4

Experimental Results

4.1 Surface Porosity

After rigorous testing on the modified Liburdi G head, there were no signs of surface porosity. The conditions were rendered to the point that the testing damaged the gas flow cup on the g head robot. This was replaced before the next series of trials. Even the worst welds showed no signs of porosity. The complete test matrix and the weld's results can be seen in Table A.7. There was not a single documented case of surface porosity under any weld condition for this system.

4.1.1 Gas Flow Coverage Discontinued

Removing the gas coverage for a weld has been known to cause porosity. However, surface porosity was identified during the trials on the modified Liburdi G Head. For this particular test case, the Argon tank's flow regulator was periodically cut from the system. Decreasing the flow rate greatly reduces the gas coverage. This was done for one second, and the regulator immediately increased the flow again. The weld pool gets extremely unstable when the Argon gas coverage was no longer present. This results in molten metal spattering the entire area. In Figure A.18, the spots in the weld bead where it appears to be puddling were moments when the Argon gas was

cut. Anytime the gas was cut, smoke spews from the weld pool as seen in the leaf image in Figure A.17. The weld pool becomes extremely unstable resulting in poor tie-in. The few black spots on the weld bead were categorized as oxides. Oxides are compounds oxidizing during the weld and some residue was left over. It was obvious that cutting the gas flow results in a bad weld, but there were no instances of surface porosity present. There were no characteristics of pores forming on the surface of the bead.

4.1.2 Oil Contaminants

It has been known that welding over contaminants will oxidize or change the molecular composition of the weld. Singh (2014) This was due to all the concentrated heat put into the weld causing a chemical reaction in the oils. Knowing this, various oil-based contaminants were applied onto the surface of the groove. Marvel air tool oil, Texaco way lubricant 68 oil, mobile vactra oil no.2, and hydraulic mobile dte 24 were welded over during these trials. Four 1/8 inch holes were drilled into the plate each filled with their respective oil as seen in Figure A.19. The few discolored spots seen in Figure A.20 were oxides formed on the weld bead. There were also instances of poor tie-in near the left edges of the bead. This was due to the weld pool entering parts of the 1/8 inch hole of oil. These spots reflect light the most in the bead image. There were no signs of porosity within the weld bead. Overall this was a good weld bead with minor oxides and poor tie-in in some parts.

4.1.3 Paint Contaminants

There were no signs of surface porosity from introducing paint into the groove, so paint was also tested. After the weld trials paint had no defects other than some poor tie-in. This test case used two types of paints. A strip of UNI paint and a strip of Sharpie paint. In addition to the strips of paint as seen in Figure A.21, a separate case study for paint contaminants was done where a 1/8 inch hole was

drilled into the weld plate and filled with paint. There were small circular divots in the weld plate. This was welded over and the resulting weld bead appears somewhat deformed. There were no defects present in this weld. There was a brief moment of poor tie-in occurring higher in the bead. In the current position of the robot welding in the groove, the robot welded over multiple holes of paint. There was one particular paint hole that was too close to the edge of the weld pool. Hence the pool could not fill up in time. All other drilled holes fell in the middle of the robot's path and were filled up. The strips of paint showed no signs of impacting the weld in any way.

4.1.4 Accelerated Rust

Rust was accelerated on the stainless steel groove. This was done by adding vinegar and hydrogen peroxide to the surface to further accelerate the surface. This resulted in a dirty oxide-filled groove as seen in Figure A.23. After welding over the rusted surface, the resulting weld bead had no defects. The poor tie-in was very minimal, and there were no oxides present. Overall rust appears to not impact the quality of the weld in any noticeable ways.

4.1.5 Varying Groove Geometry

After speaking with Professor Suresh Babu, he recommended changing the weld groove geometry. EPRI typically uses the stainless steel flat V groove for welding testing purposes. Porosity in MIG typically occurs when there's room for air to get underneath the weld. EPRI welds on a flat surface and slowly build up over time. The plate has remained constant for all testing purposes so far, so a series of 0.05-inch slots were machined into the groove. Various horizontal, vertical, and angled slots were machined. The system was able to weld without any issues over the various gaps. Some poor tie-in was present, but overall the weld appears to be fairly good. No oxides or other abnormalities were present. The robot was able to weld right over the groove without any issues. The weld bead merely filled the groove partially or

completely depending on the geometry. Regardless of the penetration, the outside weld bead was near perfect as seen in Figure A.26.

4.1.6 Compressed Air in Varying Groove Geometry

None of the varying groove geometries resulted in porosity. Professor Suresh Babu also mentioned that air needs to be flowing underneath the groove for the porous gases to form. During a weld, compressed air was blown through the slotted gap. This trial resulted in the worst damage done to the weld groove. It burnt the material resulting in a damaged bead. Once the air stopped, the weld bead resumed as normal for the rest of the weld. Despite this burnt weld, there were no signs of porosity.

4.1.7 Possible Explanations for Difficulty to Induce Porosity

After the compressed air in a slotted groove was performed; the committee agreed that it was no longer viable to continue researching surface porosity. If in the future surface porosity does occur, it can be documented and algorithms can be developed to further investigate it. The likely reason why porosity was so difficult to induce was likely due to the operating conditions. The Liburdi G Head pulses at 270/170 Amps with a voltage of 11/0 Volts as seen in Table A.3. The max current their power supply can output was 300 Amps hence the name of the P300 Power Supply. These were higher than normal operating welding conditions. Higher operating conditions result in a better bead due to the higher temperatures. There's no logical reason to go lower as that would reduce the quality of the weld. When welding over contaminants, the system would burn through contaminants instantly and burn them before they could make an impact on the weld solidification. TIG as a welding process has been known as an incredibly stable weld process compared to MIG. There's very effective temperature control throughout the system. In addition to that, robotic welding reduces all of the variability that can happen from an operator manually welding

using TIG. It's a highly controlled environment and there's a chance that porosity was no longer a concern for this system.

4.2 Void Formation

Similar to porosity, voids were near impossible to reliably cause and control. Voids typically form when welding over a surface with contaminants or unusual geometries. Due to the current weld settings, the robot welded over any potential locations where a void could form. Even during instances where a hole was drilled into the plate, the system filled the hole. There was only one recorded instance of a void occurring. In the surface porosity test case for propylene glycol & tapmatic; a void can be seen 80 seconds into the image sequence which was identified in Figure A.29. Unfortunately, this was not enough data to build an image algorithm off of. Like porosity, ideally in the future if voids continue to occur an image algorithm can be developed to accurately identify when that occurs.

4.3 Keyence Solidification Edge Tracking

The Keyence's purpose was to track the edges of the weld bead for tie-in detection. By orienting the Keyence close to the solidification boundary, we would have a real-time measurement of the bead width. Unfortunately, testing showed that the Keyence, in its current state, was not consistent or reliable. The brightness of the arc was not taken into account during weld recording. The welding arc introduces noise into the Keyence sensor that the bead geometry was no longer visible. The Keyence laser also had difficulty detecting reflective surfaces due to the stray laser reflections. For the duration of the experimentation, there was no solution to fix this issue. However, very recently it was discovered that Liburdi recently incorporated the same Keyence model into their orbital welding systems. They discovered a method for using the Keyence during a welding process. They used a 405-nanometer bandpass filter to

filter the arc light. In addition to the filter, they incorporated masking and manual filtering to remove any stray reflections. This would be the next step for this research and would remain outside of the scope of this thesis. The initial goal of this thesis was to use the Keyence for poor tie-in defect detection, but that was no longer viable. Therefore, tie-in detection was further investigated through image processing. The trailing camera was chosen to monitor tie-in as most of the weld solidification can be seen in that view.

4.4 P300 Power Supply Monitoring

This thesis focused on defect detection for surface porosity, tie-in, and void formation. Other potential defects were not investigated such as internal porosity, but in the weld defect trials there were cases where the weld solidification and pool were not good, but there were no signs of the prior mentioned defects except for poor tie-in. It would be challenging to develop an image-based processing algorithm for all types of defects. However, there exists a method for measuring when the weld was going wrong without image-based processing under certain conditions.

Five different outputs were measured from the Power Supply as stated in Table A.1. Out of these five registers, raw volts changed dramatically during the surface porosity test case for cutting Argon gas flow. Traditionally the voltage telemetry was supposed to look like a fairly constant square wave with the upper and lower bounds representative of the welding arc pulsing. This was similar to the first 20 seconds in Figure A.32. The moment the Argon gas was cut, the weld pool sputtered and the solidification was warped as seen in Figure A.17. The raw volts spiked up in correlation with the gas as seen in Figure A.33. Drastic changes were correlated in raw volts with defect occurrences. If the image processing algorithm fails to see a defect then the power supply will notice unusual behavior.

In LabVIEW, a peak detection algorithm was developed to measure the occurrences of raw volts peaks. If the weld was operating under normal conditions, the raw

volt telemetry should show a fairly constant square wave. If the square wave changes dramatically then there must be an anomaly occurring. Given the most recent N samples, if the current value for raw volts was greater than the average + twice the standard deviation then it's considered a spike in the data, and a flag to the user would occur. Another method to trigger this flag would be to monitor the raw volts' upper and lower bounds. The upper and lower thresholds were supposed to be given the power supply settings. If those bounds exceed in any way then the software could flag it.

$$RawVolts_i > mean_N + 2 * standarddeviation$$

The chances of this algorithm ever being useful was very low. The only documented case where the raw volts changed was when the Argon gas was cut. In every other poor case, the raw volts remained fairly constant. The Argon gas flow should not practically decrease unless someone was intentionally doing so, the flow regulator broke, or the tank was running low on gas. There were other major signs of the gas flow decreasing: the sound of the weld changes when compared to welding with continuous gas, and [when] physical sparks begin to fly from the weld. This particular test should also be repeated by sampling the raw volts at a higher sample rate of 100 Hz or more. This will ensure that the entire spectrum of raw volts was captured. The square wave voltage telemetry would also need to be measured to ensure any changes. The lack of gas coverage could be a sign of the voltage between the tungsten and plate changing because the argon gas was no longer effectively shielding the tungsten.

Chapter 5

Tie-In Image Processing Algorithm

5.1 LabVIEW Tie-In Algorithm

Both binary threshold clustering method and an edge detection method were used to track the edges of the bead. An algorithm can be designed to work incredibly well for one case study, but once anything changes, the algorithm no longer operates. The largest challenge with past methods for image processing were their robustness. A new novel method for image processing was developed that had the ability to change based on user input. The algorithm cannot use methods that can fail if the brightness or exposure of an image changes. The algorithm also needed to adaptively change in response to some user input.

5.1.1 Image Warping

To produce an accurate measure of tie-in, an accurate scale of the weld was needed. The current weld groove appears like a trapezoid or train tracks going off into the distance. This was due to the camera's perspective angled 45 degrees to the plate.. If the image analysis was performed in the middle of the image versus the bottom of the image there would need to be some scaling to make the results accurate. Fortunately,

image warping can address this. This transformed the image as if the camera was looking top-down parallel to the surface.

Inside LabVIEW's NI Vision Assistant, two commands assist in warping the image which were Image Calibration and Image Correction. Image Calibration defines the distortion mesh and real-life measurements of the image. There were multiple methods to perform the calibration such as defining a known grid mesh, defining tracker markers, or defining a camera model. This algorithm used the point-to-point calibration where the user defines points of known dimensions. A series of measurements were made on the weld plate. The width of the groove was known to be 0.75 inches as that remains constant for how wide the groove was (y-axis). The vertical distance was less straightforward. There were no obvious physical objects to track vertically in the trail image. The software needed to identify a frame of reference for what the real-life distances were along the groove (x-axis). Eventually, a ruler was incorporated into the photos to get an accurate camera distortion model.

As seen in Figure A.36 , the image gets warped, but now the edges of the groove were completely parallel. The resulting image has a top-down view. This algorithm addition ensures that the weld bead edges were trackable and more accurate than before. The camera's position and rotation can, unfortunately, change during each weld simply due to human error and the weld being modified. This system was built as a prototype with the capability for future modification. The camera supports were designed to be adjustable. If the camera supports were adjusted then the warping model would need to be recalculated. All of the test cases that were performed were not at the same camera orientation. Despite this, with minimal adjustments, this method works for other camera angles and rotations.

A future potential method to fix this issue would be to add tracking dots to the weld geometry. The dots would be equally separated from each other, so the real-life measurement could be easily calculated. With the tracking dots added, there would be an obvious reference to track during every trial. This would be the next step in regards to this portion of the Tie-In Detection Algorithm.

5.1.2 Image Configuration

Now that the image was warped, next, the settings needed to be configurable based on the current model. One of these settings was defining three lines. Two of the lines were used to manually define where the edge of the groove was located in the image as seen in Figure A.37. The cyan line was used to define the left edge of the groove. The dark blue line was used to define the right edge of the groove. It was crucial to identify the edges of the groove as it was necessary for cropping and defining the conversion from pixels to inches. The distance between these two blue lines should be equal to 0.75 inches. This scaling was necessary to determine the real dimensions of the bead width. The third line was horizontal black line that defines where the tie-in algorithm takes place.

Another changeable setting was the edge detection model to track lines inside the image. More specifically, the edges of the weld plate groove were being tracked. This configuration was only relevant if the adaptive edge detection cropping was used. This was addressed in the Cropping section of the Tie-In Algorithm. With the line detection working, an adaptive region of interest (ROI) crop can be applied. What makes this ROI adaptive was its ability to change during welding. The goal with all methods used in image processing so far was to isolate the solidified weld bead. Making this adaptive removes everything in the image except for the groove. This will still work even when the oscillation y-axis motor was moving the camera view. The groove edge tracking coordinates were sent to the ROI and updated the algorithm where in the image the crop should occur. Now it always isolates the groove even if the camera moves before or during a weld. This was done to make the algorithm more robust.

5.1.3 Cropping

Static Cropping

Cropping in general helps to reduce the amount of information present in the image, as it filters out unnecessary data. Static cropping was only viable when the robot only moves in a straight line along the X axis for travel, and the groove was also parallel to the path of travel. Static cropping resulted in the most stable results for the algorithm as adaptively cropping can add noise to the robustness of the algorithm. During the configuration stage of the algorithm, the edges were manually defined. An example of the algorithm's static cropping ability can be seen in Figure A.38.

The most common method for introducing poor tie-in was by manipulating the robot's oscillation y-axis movement. An ideal weld bead should be a straight line parallel to the X axis of travel. If the robot moves in any other direction it would impact the weld bead and also move the image. The adjustment of the Y-axis can easily cause this particular defect. In the camera feed, the weld groove appears to move whenever the Y-axis oscillation moves because the cameras were fixed to the torch. The tungsten was always kinematically in the same spot on the image. A method was needed to stabilize the camera view and hence edge detection or encoder cropping was necessary.

Edge Detection Cropping

In an instance where the robot was not moving in a straight line and/or the groove was not parallel to the travel then adaptive cropping using edge detection can be used. During the configuration stage, an ROI was added for both edges of the groove. In the configuration stage, a preview of the edge detection can be seen where it estimates where a straight line was located within the ROI. If it cannot find a straight line the algorithm fails. In most of the test cases, one side of the edge was more clearly defined than the other edge. The user chooses which edge the algorithm should focus on tracking. Once the algorithm detects an edge, the image gets cropped to the

location of the edge. The effectiveness of this algorithm was dependent on how well defined the edge was inside the image. In Figure A.39, the groove was intentionally rotated at an angle to the camera to test the effectiveness of this cropping. Based on the results, as long as the algorithm can detect an edge, then the crop will go through. Ideally, the groove appears as close to a straight vertical line as possible.

Motor Encoder Cropping

If the robot has a position encoder read out for the y-axis oscillation then it can be incorporated into the image analysis to control the size of cropping. Both the new MK II Adaptive Head and the Liburdi G head have an encoder read out for the y axis. Unfortunately, during all of the experimentation done for this thesis, it was only recently discovered that the Liburdi G head had an encoder readout for this axis. Fortunately, this portion of the algorithm was tested on the new MK II custom head. The groove's edges were manually defined in the configuration stage of the tie-in algorithm. This creates a zero home position relative to the current encoder position. Whenever the position encoder for the y-axis moves, the position in inches was scaled to image pixels appropriately. This scaling would adaptively crop the image keeping the groove in place at all times as seen in Figure A.40. As this adaptive cropping takes place, the tungsten tip appears to be moving in the image when in wheras in the original image the groove should appear to be moving.

5.1.4 Line Profile

All images can be represented as a matrix. Traditional color images will have three elements for each respective pixel. R, G, and B for each of the three color channels. This results in an (nxnx3) matrix. Cavitar cameras use laser illumination and result in a greyscale image. This results in an (nxnx1) matrix where each element was an integer between 0 and 256. Where 0 represents pure black, 256 represents pure

white, and the numbers in between represent some variation of grey. An graphic visualization of this process can be seen in Figure A.41.

The image was then convert into a matrix. The camera's resolution was 1440x1080p hence one image produced a matrix of that size. If a single row from this matrix plotted, an interesting pattern should appear as seen in the NI Vision Assistant line profile function in Figure A.42. In this figure, the green line was drawn in the middle of the bead and plotted. There were three distinct peaks. The peaks represent the brightest part of that line profile in the image. The left and right peaks represent the left and right edges of the weld bead. The middle peak represents the arc reflection on the solidified bead. The welding arc illuminates the solidified bead and reflects light the most at the edges of the bead. Multiple lines can be placed within the image to see how the pixels change throughout the image. For the case of this tie-in algorithm, only two line profiles were documented. One at the top of the image to track the location of the tungsten. Another one was right below the weld pool and arc to capture a real-time weld solidification. The location of the latter line may vary within the image depending on how the camera configuration may change.

5.1.5 Peak Detection

The algorithm now has a 2D plot that shows the change in pixel intensity. The peaks within these plots need to be tracked. Fortunately, there were existing algorithms built into LabVIEW designed to locate peaks. An averaging filter was applied to the line profile to filter extra noise as seen in the two plots in Figure A.43. In the peak detection algorithm, two definitions were defined. The threshold ignores any peaks below some value defined by the threshold criteria. Width which ignores any peaks that aren't at least as wide as the width criteria. The algorithm produces an array of peaks if it finds multiple peaks that meet the threshold and width criteria. For the left edge of the bead, the first element was chosen in the peak location array. For the right bead, the last element of the array was chosen. A cursor marker was applied on

the plot and image to confirm that the correct objects were being tracked within the line profile or image.

The tungsten tracking worked more reliably when compared to the bead edge peak detection tracking. A line profile was applied to the top of the image. As seen in Figure A.44, the brightest part of the plot was in the middle where the tungsten was located. The tungsten was the brightest part of the image and often created a large peak that creates a line profile that maxes out the white intensities. It was the largest and only peak present in the image therefore there was no need to perform any average smoothing.

5.1.6 Region of Interest Filtering

In an ideal weld, the line profile peaks remain fairly obvious and consistent. However, this will more than often not be the case. The peaks can decrease in intensity, or external noise could be introduced into the system and the algorithm detects something else that it's not supposed to. Hence filtering was required to maintain the robustness of the algorithm. A visualization of this ROI filtering can be seen in Figure A.45. After the peak detection was configured to reliably track the designated peak, it stores the location history into an array of size n as defined by the user. There will be some noise in this array as the peak detection may detect stray peaks that fit the threshold criteria. If the majority of data was correct in tracking, the filter should work properly. Once the array size was equal to n, the average of all the locations in that array was taken. An equal upper and lower bounds were assigned to that average for where it thinks the peak was located on the line profile. All other data was removed that was not within that ROI. Within the ROI, the max value inside the data was chosen such that it should ideally be the edge of the groove. By using an adaptive filtering, the peak's location should always be captured even if the edge line profile does not produce a large peak. This method also consistently tracks

the edges even when the peak detection algorithm fails. In reality, the peaks should not move that quickly such that the moving average ROI will keep track of the edge.

This concludes the algorithm process. After the ROI Data filter, LabVIEW plots the peaks onto a plot and the image to ensure that the tracking was accurate. It then saves the data into a data format such as excel or binary TDMS. This program can edit any prior step live during the edge detection algorithm. This was the most robust method that has been developed for this project. Despite this, there were some algorithm limitations and their robustness shall be discussed.

5.2 Tie-In Algorithm Test Cases

5.2.1 Good Centered Weld Bead in an Empty Groove

This was the most basic test for this algorithm. Assuming the best conditions with a static crop, no defects, clean groove - how well does the algorithm track the edges? In Figure A.46, the algorithm works incredibly well. The plot appears to be fairly straight vertically as it was supposed to. Please note that the image was warped to closely resemble the tracking of the algorithm. The image sequence was merged into one large panoramic photo which may not always be accurate in size. A straight edge was a sign of good tie-in. It's noted that the edges were not in a perfectly straight line. There were some signs of horizontal oscillations in the plot. These oscillations were due to the arc pulsing during the tracking. There were moments when the algorithm appears to pick up some noise. This noise can be seen in Figure A.46 whenever there was a jump in the data. However, that will be discussed in the algorithm limitations section.

5.2.2 Good Inner & Outer Weld Bead in a Filled Groove

There were three main paths a weld bead can fall inside the groove. The center bead where the weld does not make any contact with the edges. The inner wall, where the

weld bead makes contact with the groove, and left most wall with respect to the trail camera view. The outer wall, where the weld bead makes contact with the groove and right most wall with respect to the trail camera view. Examples of an outer and inner wall trial can be seen in Figure A.47 for an outer wall trial and Figure A.48 for an inner wall trial. Due to the angle of the camera, configuring the camera to track the edges of the bead closest to the wall was challenging when compared to the center. However, once the configuration was set, the algorithm still functions very well. In both cases for the inner and outer wall, the algorithm functions more accurately in the weld bead edge closest to the center of the groove away from the wall. There was more room for the algorithm's filtering to operate effectively. In the center there were less places for light to reflect and add unwanted noise to the line profile. The algorithm still operates fairly well on the wall edges. Due to the camera angle and the behavior of the pool on an incline, there was little work the algorithm needs to do to track the edges. The main issue with the edges was the potential spots for noise to occur.

5.2.3 Adaptive Cropping Conditions

These test cases used the edge detection method for adaptive cropping. The green line seen in Figure A.49 represents the movement of the Tungsten in the image. In actuality, the tungsten never moves in the image. Whenever the robot moves in the y-axis oscillation, the groove appeared to move with respect to the camera. With adaptive cropping, the algorithm always focuses on just the groove edges. Hence, the tungsten movement was trackable. Anytime there was a change in the green tungsten tracking plot, the robot was moving and hence alters the weld bead geometry. It can be observed that anytime the tungsten moved, the weld bead moved as well. Moving the tungsten changes where the weld pool was located inside the groove therefore impacting the solidification. This was reflected on the graph in Figure A.49. The edge detection adaptive cropping does introduce noise into the measuring system. The

abnormal spikes in data were moments when the tracking fails. If done accurately, the algorithm was minimally impacted. The edge detection can occasionally not pick up the edge and make the program choose a crop location that was not consistent. Cropping via encoder feedback was more accurate and not prone to failure. At the time of data collection, it was not known that the Liburdi G Head had built-in motor encoders. Future tests would document the encoder position data to produce a more accurate adaptive cropping result.

5.2.4 Poor Camera Angle & Focal Length

This was one of the earliest test cases for the robot. Figure A.51 shows the first trial iteration of the modified Liburdi G Head and eventually needed correction. The algorithm successfully tracked the edges incredibly well despite the lack of reflections. The Cavitar camera was not angled or positioned at the optimal 200 mm focal length resulting in a blurry unfocused image. Hence there was less data for the algorithm to detect. Regardless of this, the algorithm was still able to track the edges effectively. The edges appear incredibly straight. The details of the weld solidification were not as good compared to the newer images. It would appear that less information from the cameras can make the algorithm more forgiving. Especially since the output of the Cavitar cameras were 4K images. The cameras consume a large amount of Ethernet bandwidth. If LabVIEW does not need a 4K image to track the edges then it would optimize the program for speed and performance.

5.2.5 Awful Weld Conditions

In Figure A.52, the flow of Argon gas was temporarily cut multiple times during the weld. This resulted in the weld pool splashing throughout the groove. The tie-in algorithm was tested on this data. Overall, the weld shown in Figure A.52 was considerably poor quality. Due to the cutting of gas, the weld pool changes dramatically. The algorithm can handle changes, but it was not optimized for these

rapidly changing weld bead geometries. Despite this, the algorithm managed to track the edges somewhat well. There were points on this figure the gas was cut which impacted the weld pool size. This can be seen in the algorithm. Anytime there was a jump in the data, it indicates that the gas was cut. At Y-travel 0.35 inches the left edge began to stray off outside the edges of the groove. In reality, the weld never goes outside of the groove. The weld bead goes too close to the edges and this was an instance when the algorithm fails. Normally when this occurs, the algorithm will hit a divergence and continue to predict the edge location to stretch out to infinity. This time the algorithm was able to correct itself and not diverge to infinity.

5.3 Algorithm Limitations

There were two main conditions that make tracking difficult. The moment the robot starts welding, and if the weld started at the edge of the groove plate as seen in Figure A.53. The algorithm needs some form of the weld bead to be present while tracking. Right after the arc forms, there was a transition period for the molten pool to form and begin welding. During this sequence, there was not a weld bead that can be monitored. After the Liburdi's start delay, amount of time after the formation of the arc before the robot begins moving, does the algorithm have enough data to begin monitoring the edges. The other condition that causes issues was when the edge of the plate was visible as seen in the top left image in Figure A.53. The laser illumination from the camera reflects light the most on this surface making it incredibly bright. This edge was also an unusual geometry that the algorithm was not normally used to interpreting. In an ideal situation, this surface would not be present, so the algorithm can detect the weld bead effectively without any external noise. All past figures show the edge detection plot starts at an offset from the location where the bead formed. This delay was manually added to the algorithm to ensure that the edges were appropriate for tracking. 10-20 seconds after the arc forms was normally appropriate to begin the algorithm.

If the the starting images have no trackable data then the algorithm can have a bad start. Assuming that the delay has occurred, the algorithm would ideally begin tracking the line profile peaks on the bead. The algorithm then stores a history of where it thinks the peak detection was located and uses it to apply a region of interest to the data. The ROI filter must receive the correct estimation of where the location of the edge was located. If the data has bad data then the region of interest will be somewhere that the peak was not supposed to be located and hence result in an inaccurate bead edge location prediction. This was the main reason why the algorithm cannot start when the conditions in Figure A.53 were present. This also applies if the threshold and width settings for the peak detection do not accurately represent the edge of the weld bead. Bad data will quite simply cause the algorithm to fail as seen in Figure A.53.

5.3.1 Detecting Stray Defects

The algorithm was a function of the pixel greyscale intensities. Once the adaptive data filtering executed, the algorithm searches for the max value within a region of interest. Ideally, the algorithm stays working as long as the max value in that region represents the real location of the weld bead's edge. However, this was not always the case. Light from the arc reflects the brightest on nonlinear geometries such as the edges. There were instances where if a defect occurs either on the weld bead or in the groove the algorithm will detect that defect. An additional filter can be added to the algorithm to take into account of any abnormal changes. An average filter will look at the most recent N locations points and, if the current data strays too far from the average, it will replace the current value with the average. This can work in instances where an oxide was detected in the bead as as seen in Figure A.54. An average filter has been used for additional filtering, but there were limitations to this particular filter. The average filters fails if there was a sudden change in the weld bead, which it will assume was a mistake. If the filter continues to flag a location it will continue

replacing the false location with the average. This can result in a divergence where the algorithm no longer knows where to detect the edge. This can also happen if the threshold % was too small and needs to be used sparingly. Unfortunately, this may just be a limitation of the current algorithm that cannot be addressed. Despite that, the algorithm can give information about other potential defects. If the edge detection indicates that at some point in the weld it was not straight then there could be a sign of a defect.

5.3.2 Wall Reflections & Divergences

Multiple test cases showed that the algorithm struggled close to a wall. Light reflected differently on unusual geometries and especially on the highly reflective wall surfaces. The current camera orientation focuses on the weld bead centroid and was parallel to the robot's x axis for travel. With the current camera angle, it was difficult to observe the the weld pool behavior on the wall effectively. The complete border of the weld pool on the inclined surface was not fully visible and would have required an additional camera oriented parallel to the oscillation y-axis. Due to this limitation, it was challenging to ensure the algorithm's accuracy in detecting the weld bead's border on the wall's edge.

In addition to the prior challenge, the reflections on a clean wall surface, when the groove was machined, makes the surface incredibly smooth and reflective. That reflective surface acts as a mirror for the Cavitar Camera's laser illumination. This further adds to the challenge of tracking the edges. However, with the right configuration, the algorithm can still function effectively under these conditions. This was only possible after a precise algorithm configuration, but it was more challenging to fine tune the algorithm compared to configuring for a centered weld bead.

The largest side effect of tracking an edge on a wall was the chance of a divergence. The algorithm can fail if a line profile peak was detected outside of the image's ROI. The edge tracking algorithm indicated that a bead's edge location extended to infinity

as seen in Figure A.55. Due to the divergence, the line profile was estimated to be outside the bounds of the image itself. The yellow line in that figure represents the left edge location for the weld bead. The algorithm had a poor starting configuration and hence began to stray from the expected location. The right edge closest to the center of the groove continued to track the edges fairly well. In this test case, it was important to configure the algorithm correctly to ensure accurate tracking.

5.4 Tie-In Defect Quantification

There were currently no standards for the quantification of poor tie-in. EPRI has definitions for bad welds, but not a definition for the quantification of how bad the weld was. Current code standards for EPRI contractors state that there can only be a few defects in every inch of weld to be considered good. EPRI ignores that definition and believes that if a defect occurs then the whole weld was bad and needs to be addressed. That being said there were no guidelines for the quantification of defects. It was either no defects or some defects which were bad. A potential tie-in quantification can involve performing a Fast Fourier Transform (FFT) analysis on the edges to monitor any unusual changes. An ideal weld should have a fairly constant edge. Granted, how much variation equates to a bad weld or pie tie-in was up for debate and should be discussed further in future studies.

Chapter 6

MK II Custom Weld Head

6.1 Current State of the Robot

This custom MK II Weld Head has gone through a long period of redesigns and modifications to get the system to a state of welding operation. It was stated that this thesis was not dependant on the completion of the MK II Custom Weld Head. Work has been completed to design, build, integrate and demonstrate a five-axis TIG welding system targeted for nuclear piping. The system is currently operational and capable of welding with real time monitoring and data collection. Figure A.56 shows the custom weld head welding on a groove similar to that of the modified G Head trials. The white light seen in Figure A.56 was the weld arc. Figure A.57 shows the current capabilities of the custom weld head compared to all past weld head iterations that have been used. The newly functioning custom head clearly exceeds all past heads in its new capabilities. The most notable of which was the addition of encoder feedback in all motors.

6.2 Software

6.2.1 P300 Power Supply

Similar to the Liburdi G Head, this system can monitor power supply telemetry during a weld. This includes current, voltage, wire feed, and AVC error telemetry. Unlike the Liburdi G Head, this system operates using a custom arc initiation sequence that was decoupled from the power supply. The Liburdi G Head uses its own native Liburdi motors that was directly controlled through the power supply. The MK II system does not use any Liburdi motors for moving the robot in 3D space. The only Liburdi motor used on the MK II was strictly for the wire feed draw. This system can also write and save weld settings in the settings configuration section of the interface. Before the G head's pendant was required to start, stop, and move the weld head. In this system, everything was entirely remotely controlled in LabVIEW through mod bus communication.

6.2.2 Keyence Laser Profilometer

This system uses the same Keyence series as the Liburdi Modified G Head. This Keyence was mounted to the left of the torch to monitor a real time topology of the weld solidification. The Keyence operates in high speed mode which samples the Keyence monitor in LabVIEW at 200 Hz. Unfortunately, the Keyence at UTK was experiencing similar issues of noise as the EPRI system during active welds.

6.2.3 Motor Encoder Position & Velocity

This system was capable of monitoring and controlling the encoder position and velocity from five motors. There was the X axis, or Travel axis, which moves the robot along the track and along the weld groove. This axis can be jogged, or move at a constant velocity. The Y axis, or the Oscillation axis, was perpendicular to travel. This axis can also be jogged. The X and Y axes use Kollmorgen servo motor

controllers. They were known for their high power and compact size. These motors communicate to LabVIEW over an HMI service port over TCP Ethernet.

The main axis that used real time control was the Automatic Voltage Control (AVC Z Axis) for vertical height travel. The axis can respond to the voltage telemetry and adjust the height to maintain a constant arc gap to the plate. This resulted in a stable high and low voltage during the weld. Wire feed height (WF Z Axis) allows for the adjustment of height for the wire manipulation. Wire feed rotation (WF yaw axis) allows for adjustment of rotation from side to side of the wire entry into the weld pool. The X, WFZ, and WFR axes use Faulhaber motor controllers. These controllers communicate over EtherCAT and were connected to a C6015 Beckhoff EtherCAT Master. This device acts as a mini computer that processes Ethernet traffic through the TwinCAT Software. The Beckhoff has capabilities to communicate directly to LabVIEW using the TF3710 plugin. This plugin provided incredibly fast and real-time control of all axes. Unfortunately, the current Kollmorgen motor controller does not have EtherCAT communication. The current Kollmorgen controller was capable of real time control. However, this can easily be fixed by acquiring a new updated EtherCAT Kollmorgen controller. The Faulhaber motors were capable of real time control because they use an EtherCAT communication protocol.

Future efforts hope to integrate two more axes: a lead/lag (roll axis) and a theta (pitch axis). As well as purchase an EtherCAT Kollmorgen motor controller to connect to the Beckhoff EtherCAT Master for real time control.

6.2.4 Cavitar Trail & Lead Cameras

These were the same Cavitar C300 cameras used on the Liburdi Modified G Head. They eliminate the brightness of the arc using laser illumination. They were both mounted at the optimal focal length of 200 mm away from the weld pool. There was one notable difference from the EPRI system compared to the UTK system. The MK II used the Cavitar trail camera feed for the live tie-in algorithm.

6.2.5 System Operation's Panel

Figure A.58 shows the full LabVIEW interface used to monitor and control the entire MK II custom weld head. The system's operation panel shows a side view image of the robot with some arrow buttons on the side of the panel. This control panel was designed with the intention to be as easy to understand as possible. There were arrow buttons that indicate the modes of movement in the system. There were six LED buttons that adjust the welding process parameters. Such buttons include "weld mode" which makes the P300 power supply be in weld mode if welding starts. "Purge gas", which releases Argon gas into the weld torch. These two buttons were automatically enabled whenever the "Begin Welding" Button is pressed. "Wire On" button enables wire draw into the weld groove during welding. "Travel FWD" enables the robot to move at a constant velocity in the X-axis travel. When "TRAV FWD" is disabled the X-axis does not move, or can be manually jogged. These four buttons were cloned from the Liburdi P300 controller that would have manually required to begin welding. The new buttons unique to this system were "AVC" which enables the automatic adjustment of the Z axis during welds to maintain a constant arc gap. When "AVC" is disabled the AVC can be manually jogged. "Tie-in Detect" button enables the live tie-in algorithm during welding.

The main control system buttons were "Begin Welding" which starts the arc initiation sequence. "Stop Welding" which stops welding and begins the shutoff and post-purge sequence. The yellow "Shutdown System" Button begins the shutdown sequence for all sensors and properly disconnects them from LabVIEW. The orange triangle "Clear All Errors?" button clears errors on the Beckhoff, Kollmorgen, and P300. The "ESTOP" button executes an emergency halt on all of the motors and turns off welding on the P300. Lastly, there were two indicators that tells you if the weld arc is on, and an indicator that writes what weld state the P300 is in. This is the exact same weld state list as seen in Table A.2.

6.2.6 Data Collection

All of the sensors and monitors previously discussed can be documented and saved. Pressing the "record button" as seen in Figure A.58 will trigger the creation of a folder with all of the folders and blank TDMS data files named and organized. This system monitors and timestamps motor encoder position & velocity, Keyence topology scan, Cavitar trail & lead images, P300 power supply settings & telemetry. There is documentation of all errors that the system experiences during welds. There is further documentation of when the robot begins arc initiation, forms the arc, and stops welding. Each sensor was decoupled from each other and hence can operate at different sample rates depending on what was desired. Once welding begins, the program writes to all of the blank files or empty folders. Once the system repeats, data collection can repeat again, and the program generates more files.

6.2.7 Live Tie-In Detection Algorithm

The live tie-in algorithm behaves very similarly to the stand alone algorithm. Once the MK II connects to all of the sensors, the tie-in algorithm can be activated. The algorithm requires the Cavitar trail camera, the Kollmorgen X-axis travel, and the Liburdi P300 to have travel weld mode enabled. If the Y-axis oscillation is active then the encoder adaptive cropping can be used, but it's not required for operation of the algorithm. Assuming the prior conditions have been met, the algorithm proceeds to the configuration setup. The configuration behaves exactly the same as the stand alone program. The user defines the edges of the groove and the bounds for the adaptive edge detection cropping. The program will begin the peak detection once welding starts in the system. Afterwards, the thresholds for the peak detection algorithm can be changed until the appropriate edges were tracking accurately. Once satisfied, the operator presses a button that begins the algorithm and edge tracking.

6.3 Live Tie-in Algorithm Test

Once welding began, the peak detection algorithm was modified until it was accurately tracking the peaks for edge detection. The results of this weld produced one of the best weld beads the MK II systems has welded to date. There was almost no poor tie-in or defects present in Figure A.60. There exists only one defect in the middle of the bead, but that was intentionally caused to test the live tie-in algorithm. Everything else in the weld bead was untouched. The minor defect halfway into the bead was done by moving the oscillation y-axis. There were some minor noise present in the edge tracking, but overall the algorithm worked as intended. Albeit, it was challenging to configure the algorithm just right for operation. This took approximately 30 seconds to configure for the algorithm.

Chapter 7

Conclusions & Future Steps

7.1 Conclusion

The MK II custom weld head is operational and robust. The robot was capable of welding and data collection. In addition to an operational head, the tie-in algorithm was shown to be robust and capable of real-time operation. The algorithm can detect the edges of the center multilayered weld bead even during harsh welding conditions. The outer and inner edges were also possible to track using the same algorithm. Welding over an existing bead does not impact the effectiveness of the algorithm. The adaptive cropping, however, can impact the effectiveness of the algorithm only if the software does not have a good groove edge to track. Surface porosity was originally thought to be a common defect that can occur in robotic TIG welding. After rigorous testing on the Liburdi G Head, it was shown that surface porosity would not cause any issues during welding. The most severe welding conditions were tested which includes cutting the gas coverage, introducing multiple types of contaminants, and changing the weld groove geometry. With the high operating conditions and robotic control, defects were greatly reduced in the system. Ideally in the future, if surface porosity occurs then it will be documented and future image processing algorithms can be developed to detect this defect.

7.2 Future Work

There are currently no standards for the quantification of poor tie-in. EPRI has definitions for bad welds, but not a definition for the quantification of how bad the weld is. Current code standards for EPRI contractors state that there can only be a few defects in every inch of weld to be considered good. EPRI ignores that definition and believes that if a defect occurs then the whole weld is bad and needs to be addressed. That being said there are no guidelines for the quantification of defects. Guidelines should be introduced either by creating a new convention or new code.

There are issues with the live and stand-alone tie-in algorithm that needs to be addressed before it can be reliably used for real time welding robot operation. Automation is needed to ensure the algorithm's effectiveness. No one configuration could be repeated in all prior experimental runs. Every experimental trial had multiple variables change. Whether that is a different start position, a different location in the groove, welding over a different surface, etc. Configuring the algorithm to work for the current weld takes time and requires some complexity. There were too many conditions that needed to be accounted for. The groove was never in the same location of the image. The camera supports were adjustable and that changed how the camera feed appears. The bounds for the edge detection need to be updated. If the robot moved in the y-axis oscillation; the algorithm needed to be configured for adaptive cropping. The location of the line profile for the tie-in algorithm needed to be configured. The peak detection settings needed to be adjusted before the algorithm starts monitoring the edges. This system was incredibly complex and the process needs to be severely simplified. There needs to be automation for this algorithm to function effectively. Creating fixed camera supports that won't change the camera view is crucial to minimize modification to the algorithm. If the camera's position in 3D space relative to the tungsten changes; the algorithm needs to be modified as well. Assuming the camera's exposure/ brightness stays the same; this would greatly minimize having to change the peak detection settings. Adding a homing position

or automatic alignment of the robot onto the groove would also greatly assist the algorithm. The robot identifying where it is located in the groove would automate the configuration stage of the tie-in detection algorithm. This would minimize the need to manually define the edges of the groove and the edge detection ROI for the adaptive edge detection cropping.

As stated earlier in in Chapter **??**, the original goal was to develop the image processing algorithms for the MK II Adaptive Welding Head. It has been demonstrated that the algorithm can operate live. However, this system is not adaptive. The first step was getting the robot operational. A significant amount of work needs to be done to reach a full feedback control system. There has been discussion with collaborators in EPRI about working with European teams such as Fraunhofer and AIMEN about integrating machine learning with the MK II system. Such machine learning capabilities would make the image processing algorithms more precise and robust. Instead of having one algorithm working, there would be an adaptive algorithm that will learn and get better over time. Another future incorporation of this algorithm would be the adaptive capability of the robot. The goal of this thesis was to detect defects and determine the severity of a defect. If a defect was occurring, what should the operator do? For porosity, assuming it occurs, the robot should immediately stop and address the forming porosity. Once that defect starts, it will not go away. The only way to fix defects would be to remove the defect with a grinder and weld over the new spot. However, tie-in can be fixed. The robot's kinematics are known because the new custom head has encoder feedback in all motors. If the cameras show a lack of fusion against the wall then there can be a control loop that moves the robot closer to the wall. If the wire feed into the pool was further away from the ideal location then the wire can be adjusted into the correct position. Assuming no prior defects on the existing weld, it would make poor tie-in highly unlikely to occur. This would create a fully adaptive feedback welding robot.

Bibliography

Aquasol, C. (2021). Aluminum welding procedure: Best practices to prevent defects. xiii, 52

Cavitar (2021). Cavitar welding camera. 8

Keyence (2022). Cavitar welding camera. 8

Landín, S. M. (2022). Artificial intelligence for categorizing the tig weld pool components. 2

Liburdi, D. E. (2010). *Enabling technologies globally for orbital tube and pipe welding applications*. Liburdi Engineering. 5

Shirsat, A. (2021). Mig vs tig: Welding types, materials, and applications - a guide. xiii, 50

Singh, R. (2014). A review of porosity formation and recommendations on the avoidance of porosity in tig welding of steels. *International Journal of Mechanical Engineering And Information Technology*, 2(8):700–712. 20

Xia, C. (2020). Vision based defects detection for keyhole tig welding using deep learning with visual explanation. 2

Appendix A

Appendix

A.1 Introduction

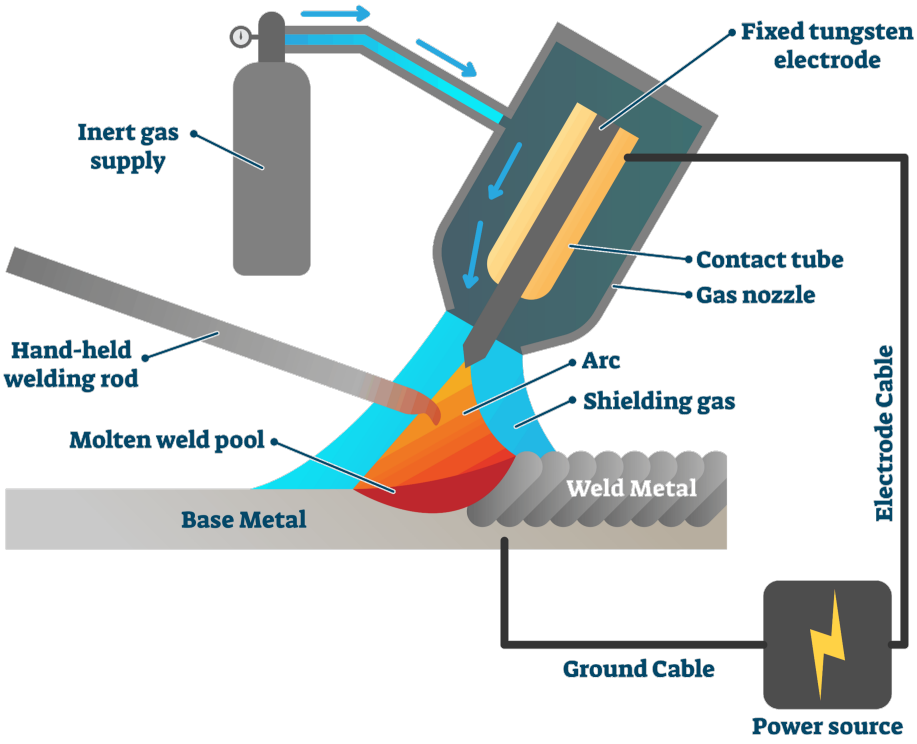


Figure A.1: Tungsten Inert Gas (TIG) Welding Operation [Shirsat (2021)]

A.2 Background

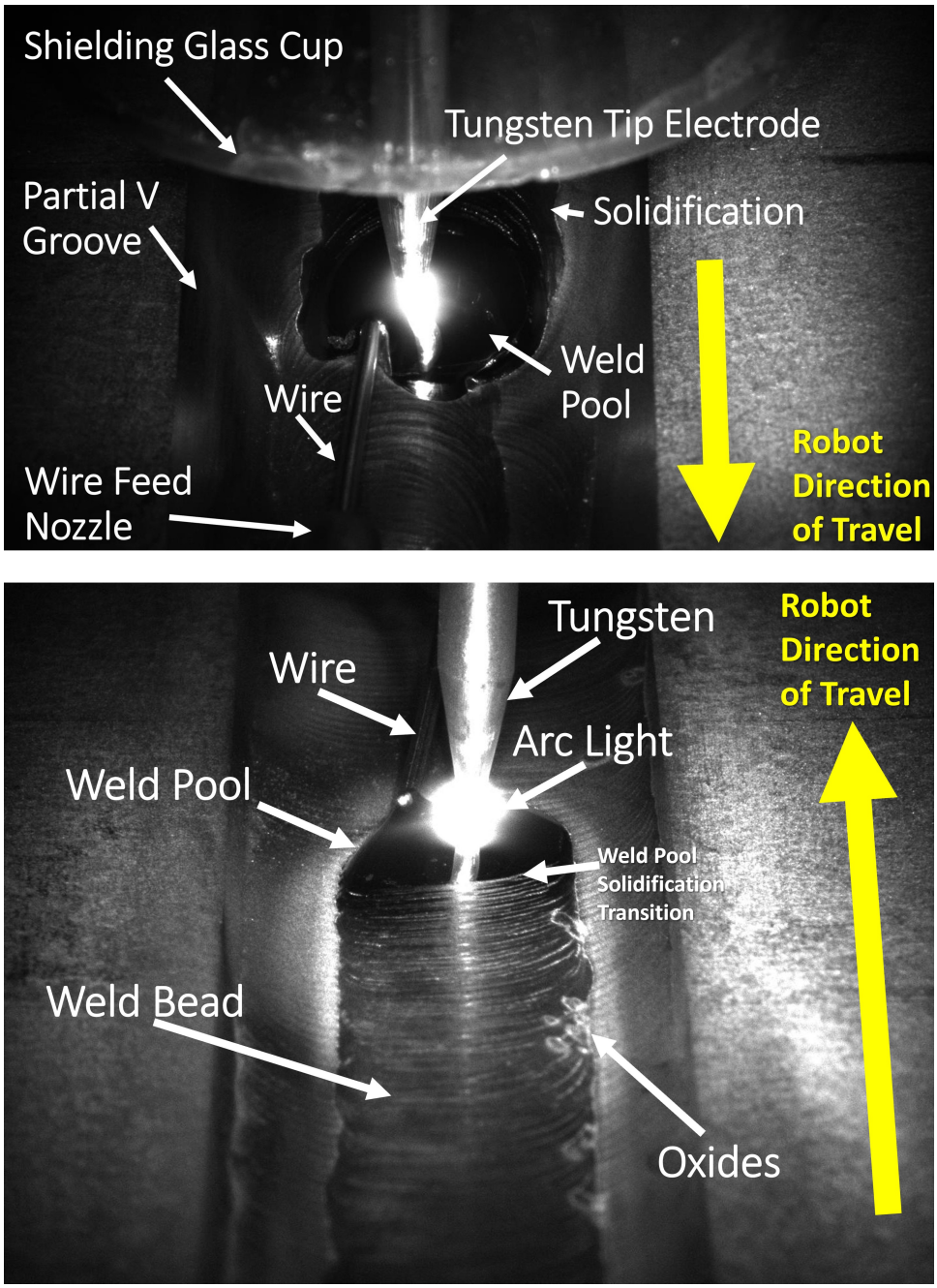


Figure A.2: TIG Leading Camera of Weld Pool (Top)
Trailing Camera of Solidification (Bottom)

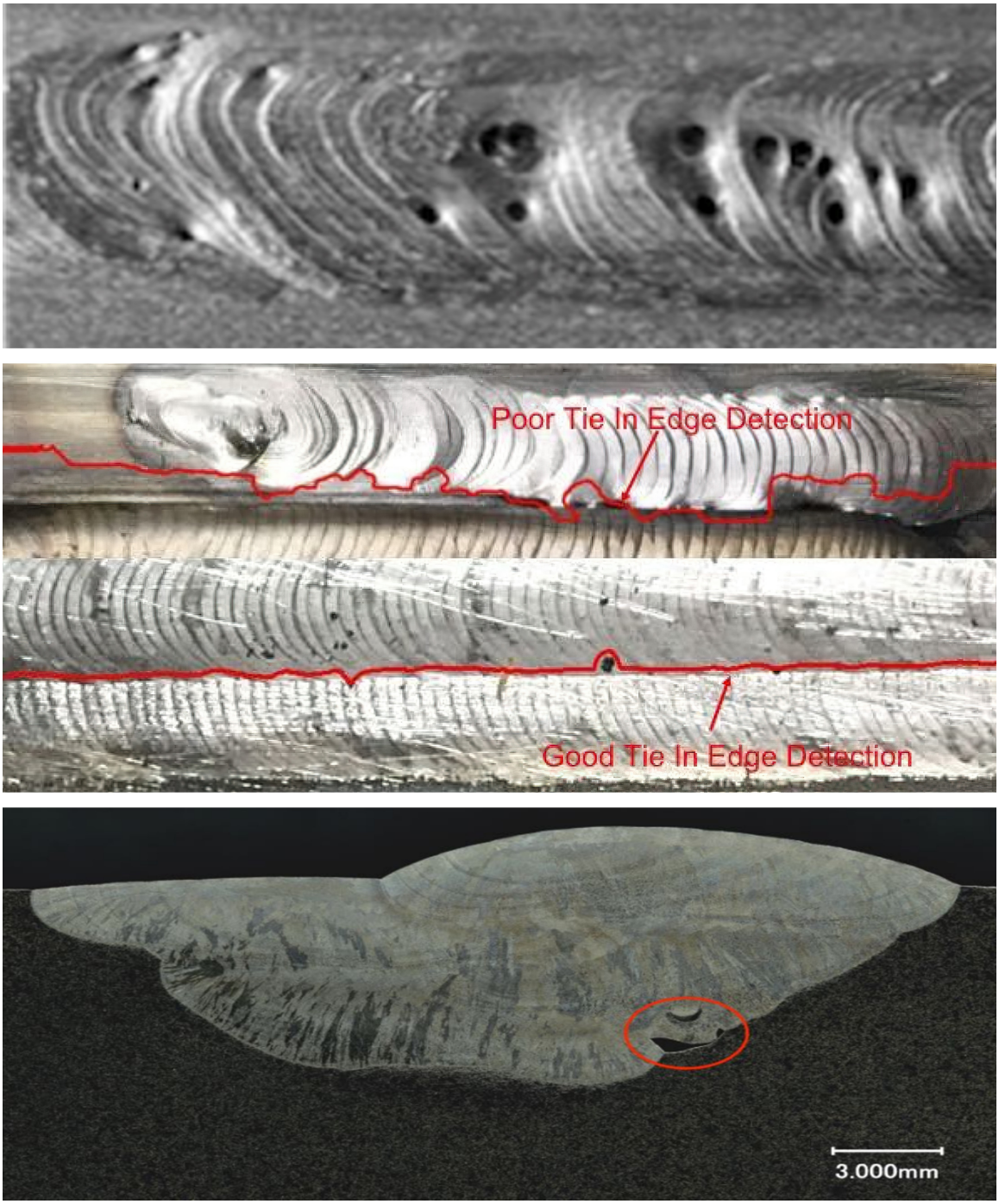


Figure A.3: Weld Defects: Surface Porosity (Top) Aquasol (2021)
Poor Tie-in (Middle)
Void Formation (Bottom)

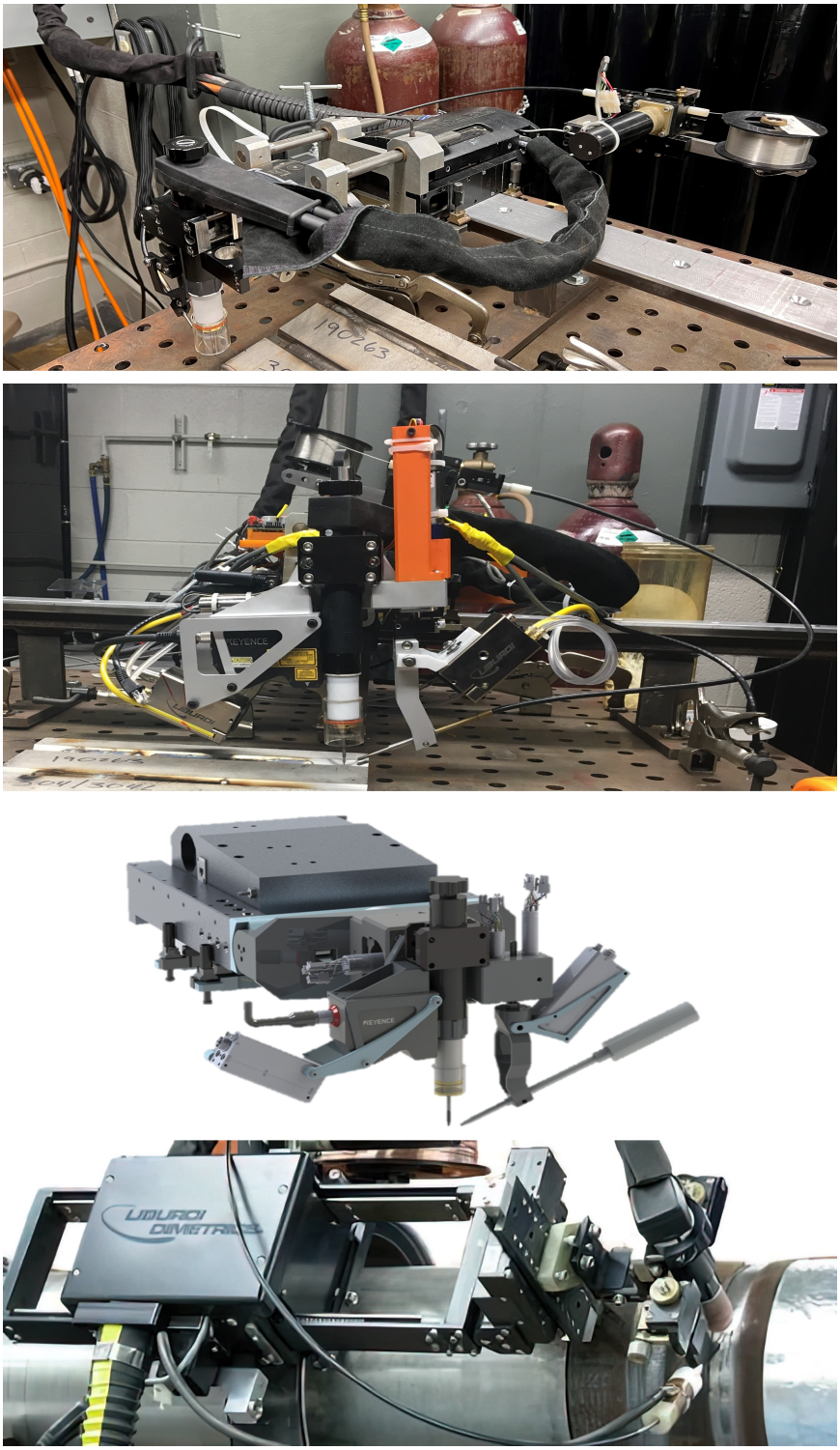


Figure A.4: Welding Robots Used [Top to Bottom]:
(1) EPRI Donated Liburdi F Head at UTK
(2) MK I Modified F Head
(3) MK II Custom CAD Model Prototype Design
(4) Liburdi G Head

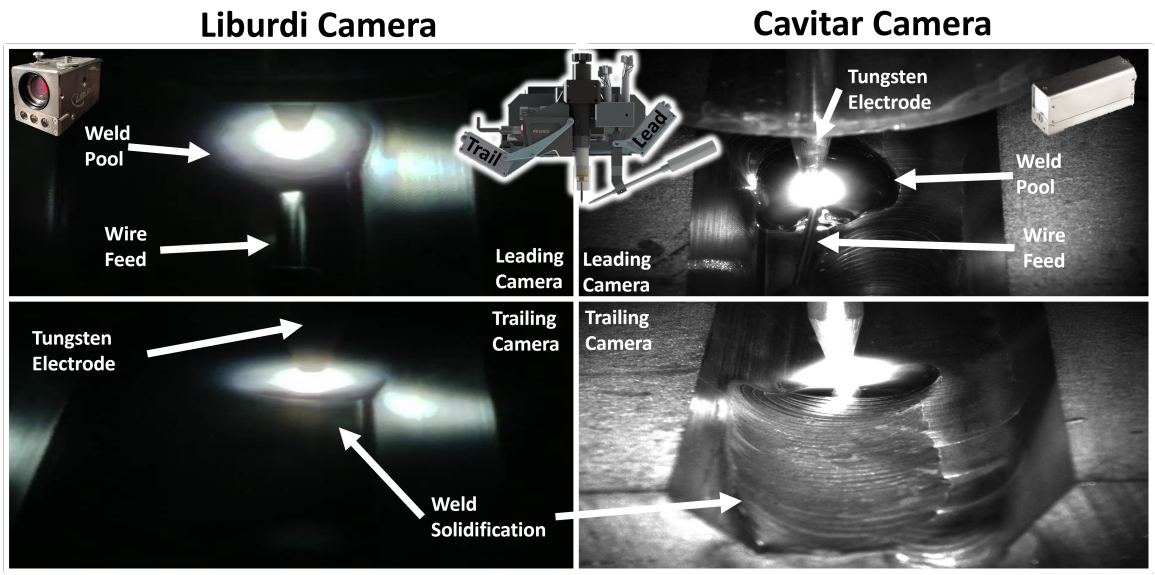


Figure A.5: Liburdi and Cavitar Camera Image Quality Comparison



Figure A.6: LJ-V7080 Keyence Laser Profilometer (Top)
Liburdi Dimetrics P300 Power Supply (Bottom)



Figure A.7: NI Vision Assistant Software Interface (Top)
LabVIEW Front Panel (Middle)
LabVIEW Back Panel (Bottom)

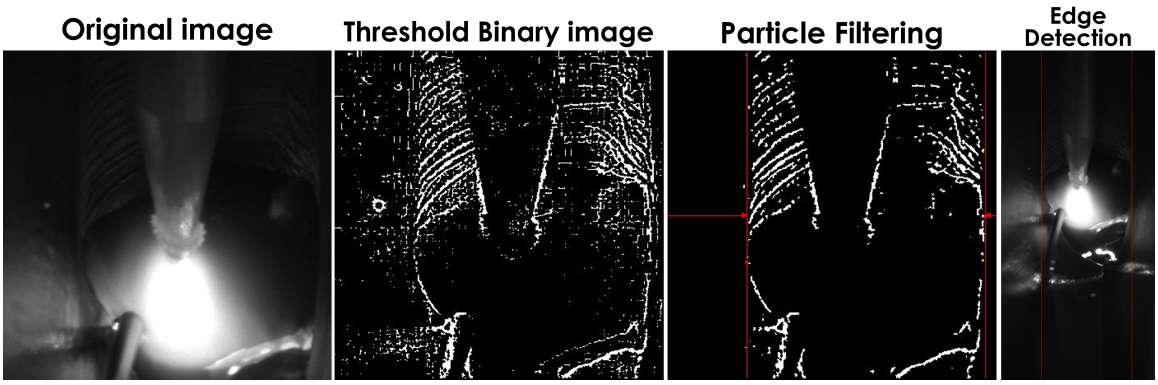


Figure A.8: Weld Pool Width Tracking Image Process on Lead Camera

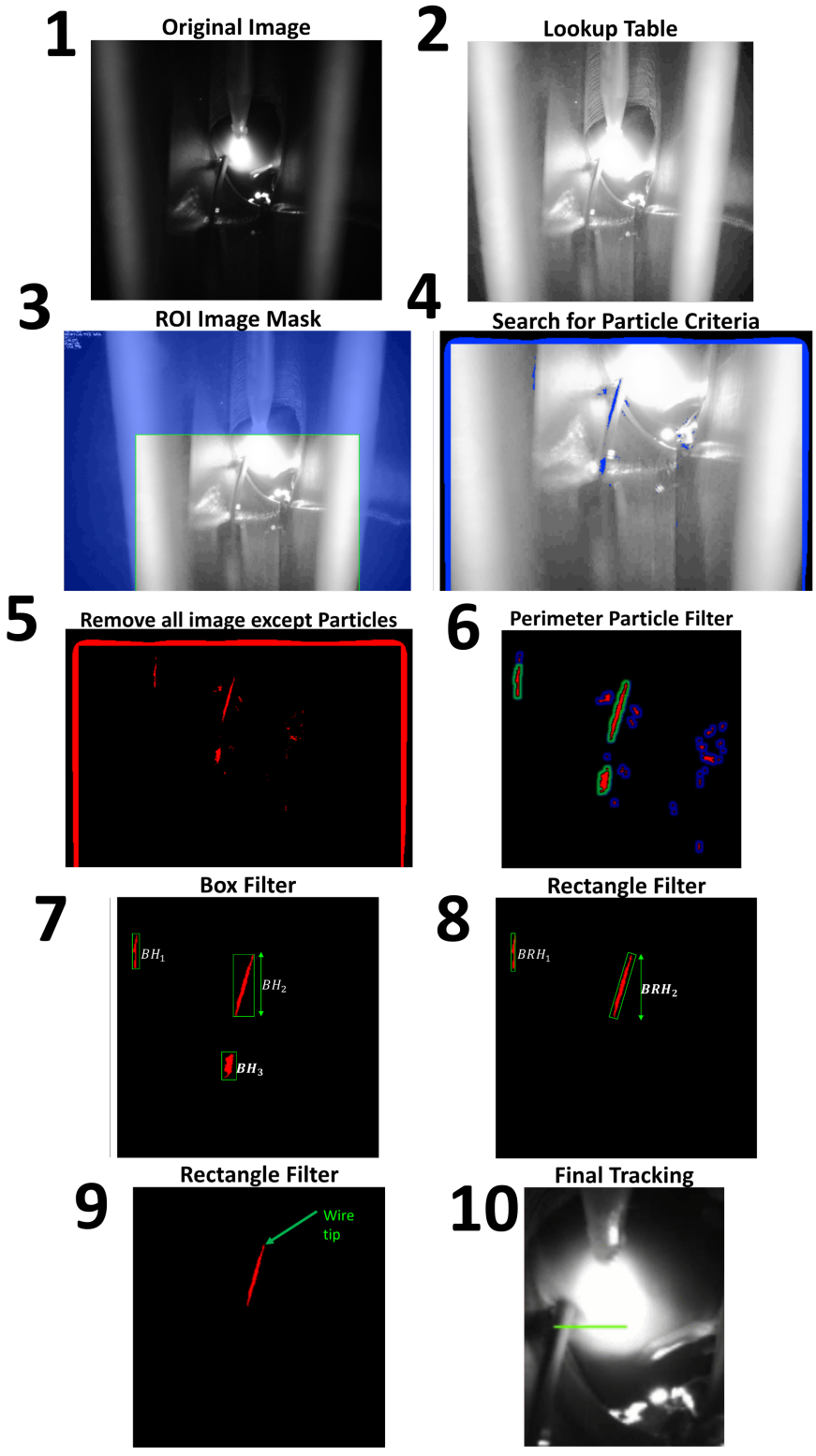


Figure A.9: Weld Pool Width Tracking Image Process on Lead Camera

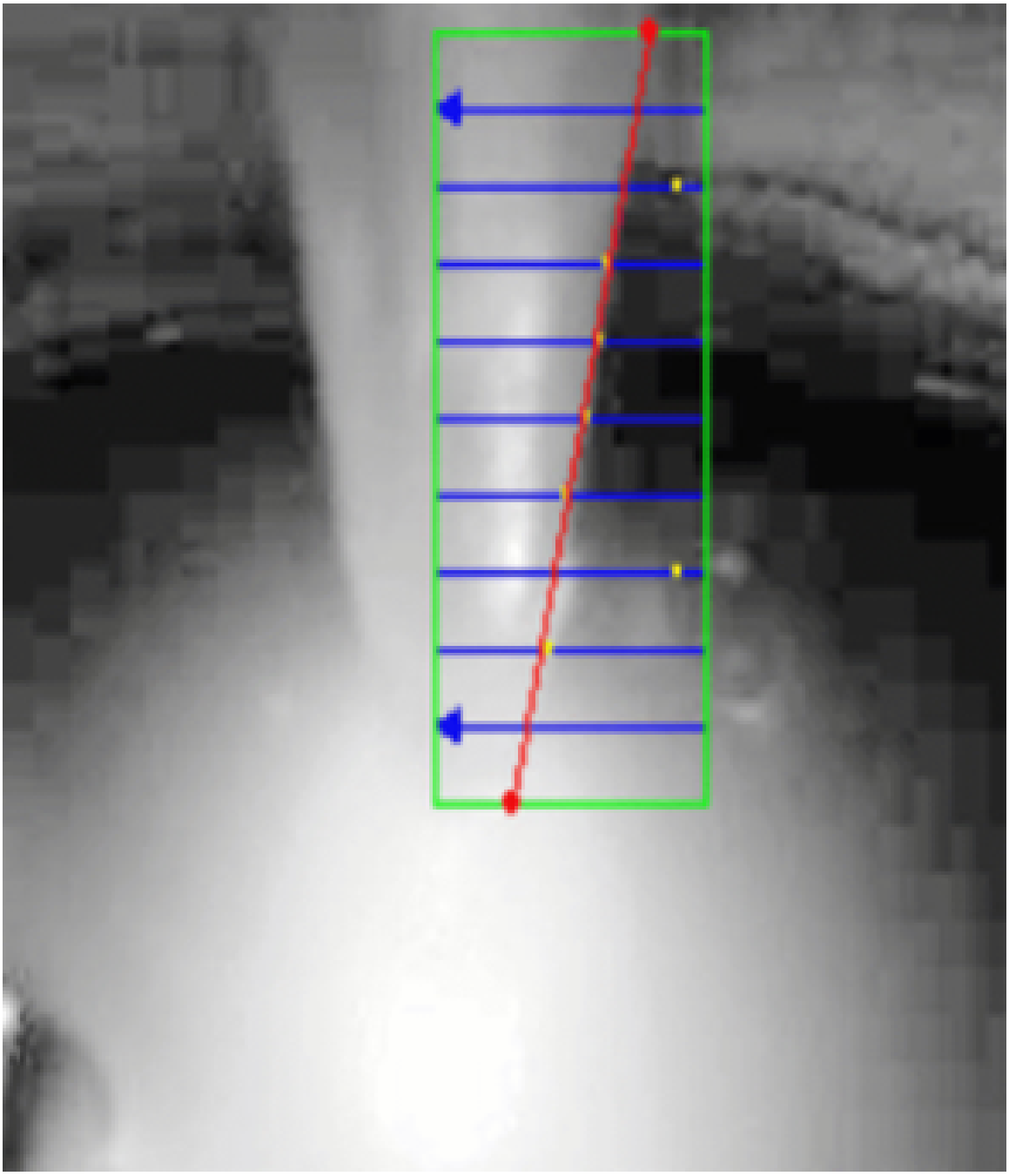


Figure A.10: Tungsten Tip Edge Detection Tracking

A.3 Experimental Method

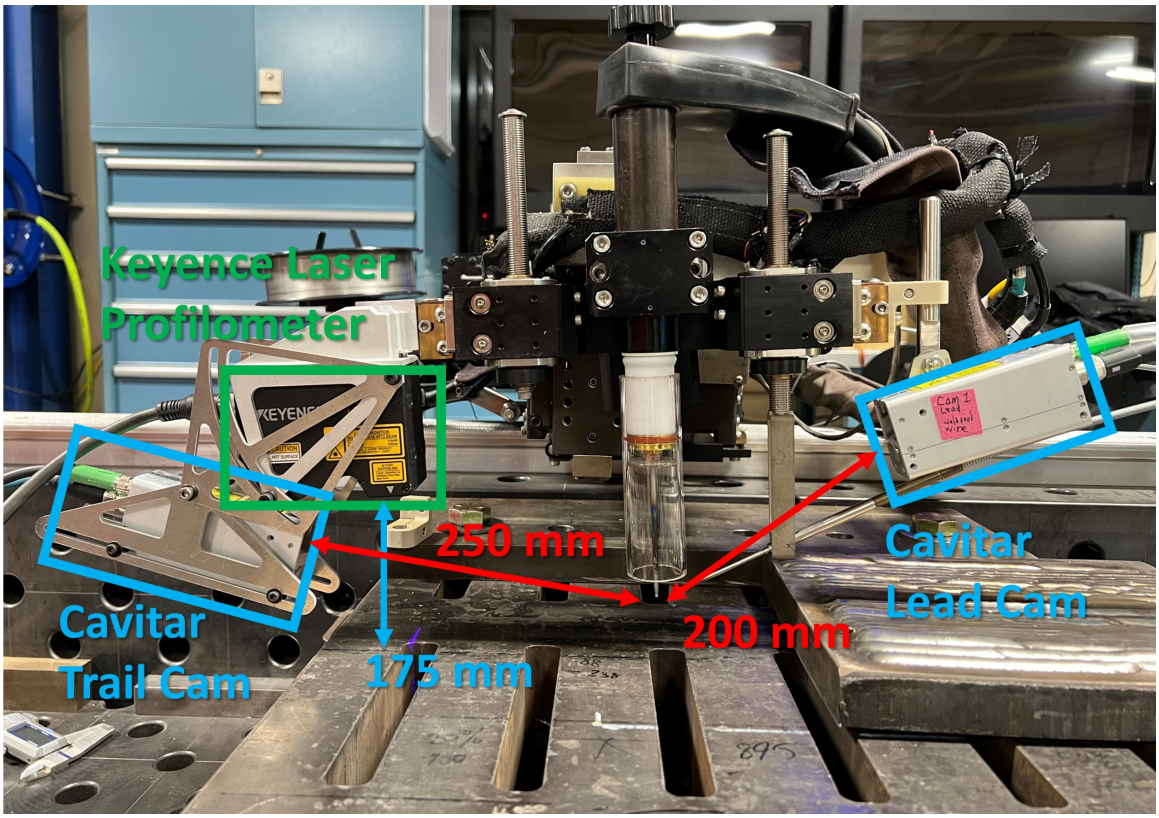


Figure A.11: Liburdi G Head Initial Setup

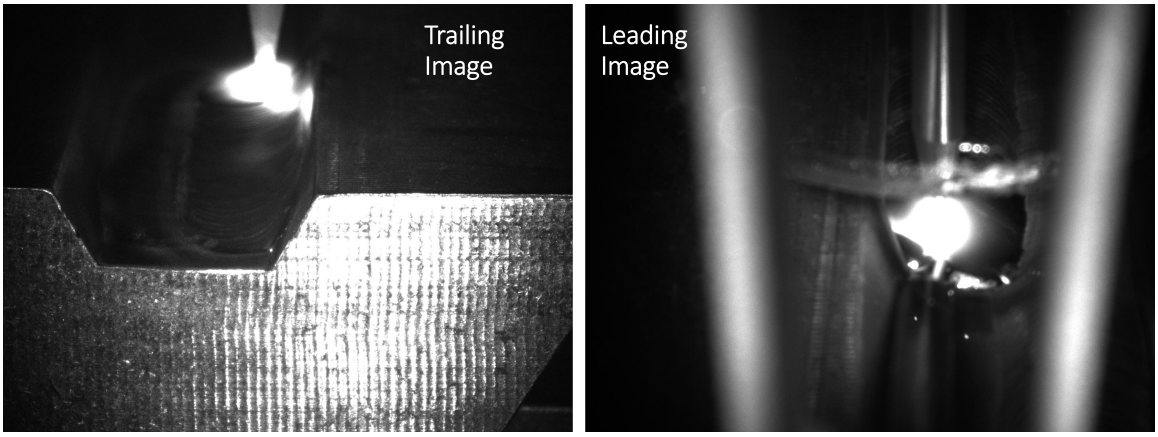


Figure A.12: EPRI Liburdi G Head Mod 1 Cavitar Lead (Left) & Trail (Right) View

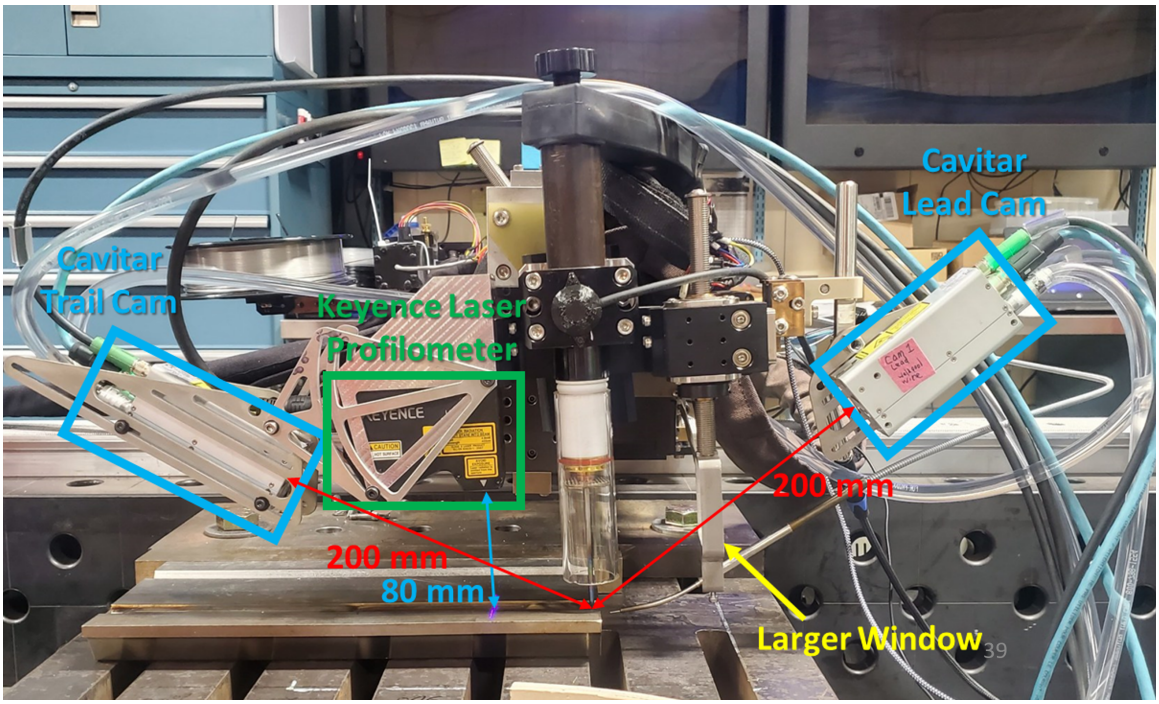


Figure A.13: EPRI Liburdi G Head Final Setup

Table A.1: P300 Power Supply Registers Monitored

Num	Type	Register #	Register Name	Units
1	Output	260	Primary Current	Amps
2	Output	261	Background Current	Amps
3	Output	305	Primary Volts	Volts
4	Output	306	Background Volts	Volts
5	Output	311	In Dwell	seconds
6	Output	312	Out Dwell	seconds
7	Output	310	Excursion	inches
8	Output	262	Pulse Frequency	Hertz
9	Output	263	Pulse Width	%
10	Input	268	Wire Position	_
11	Input	3	Wire Feed Telemetry	_
12	Input	294	Raw Wire	_
13	Input	296	Raw Hot Wire	_
14	Input	291	Raw Amps	_
15	Input	293	Raw Volts	_

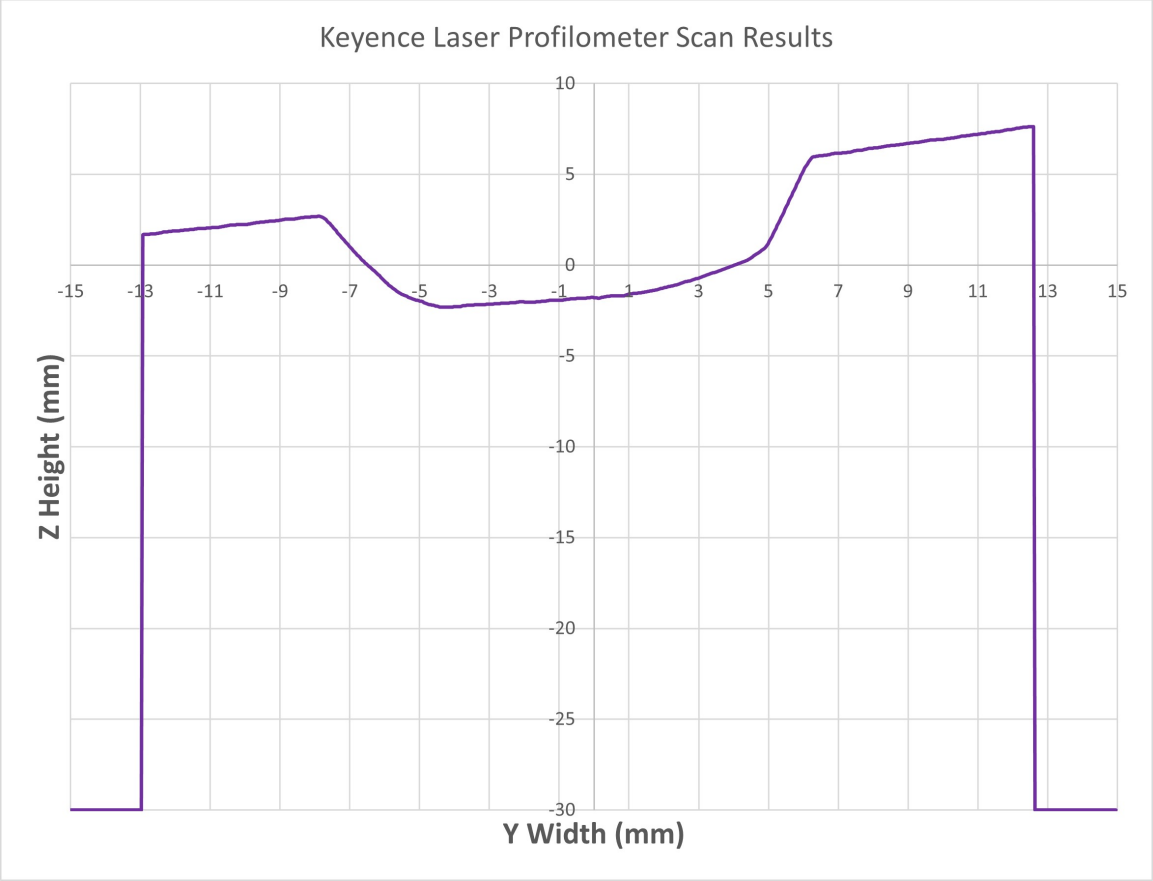


Figure A.14: Keyence Laser Profilometer Scan Plot

Table A.2: Weld States on the Liburdi P300 Registers

Num	State	Record Data?
1	Idle	No
2	Sequence Start	No
3	Position Travel	No
4	Pre Purge	No
5	Electrode Touch	No
6	Electrode Lift	No
7	Arc Start - HF	No
8	Arc Start - Touch	No
9	Arc Start - Scratch	No
10	Arc Start - MIG	No
11	Weld Start	No
12	Segment	Start Yes
13	Downslope	Yes
14	Arc Stop	Stop No
15	Weld Stop	No
16	Post Purge	No
17	Sequence Stop	No
18	Sector	No
19	Crater Fill	No
20	Bum Back	No

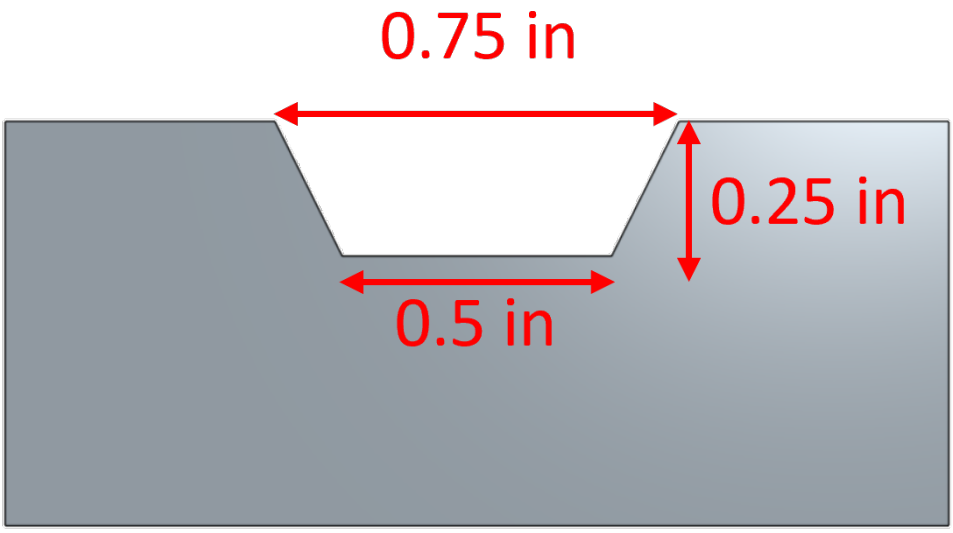


Figure A.15: Groove Geometry

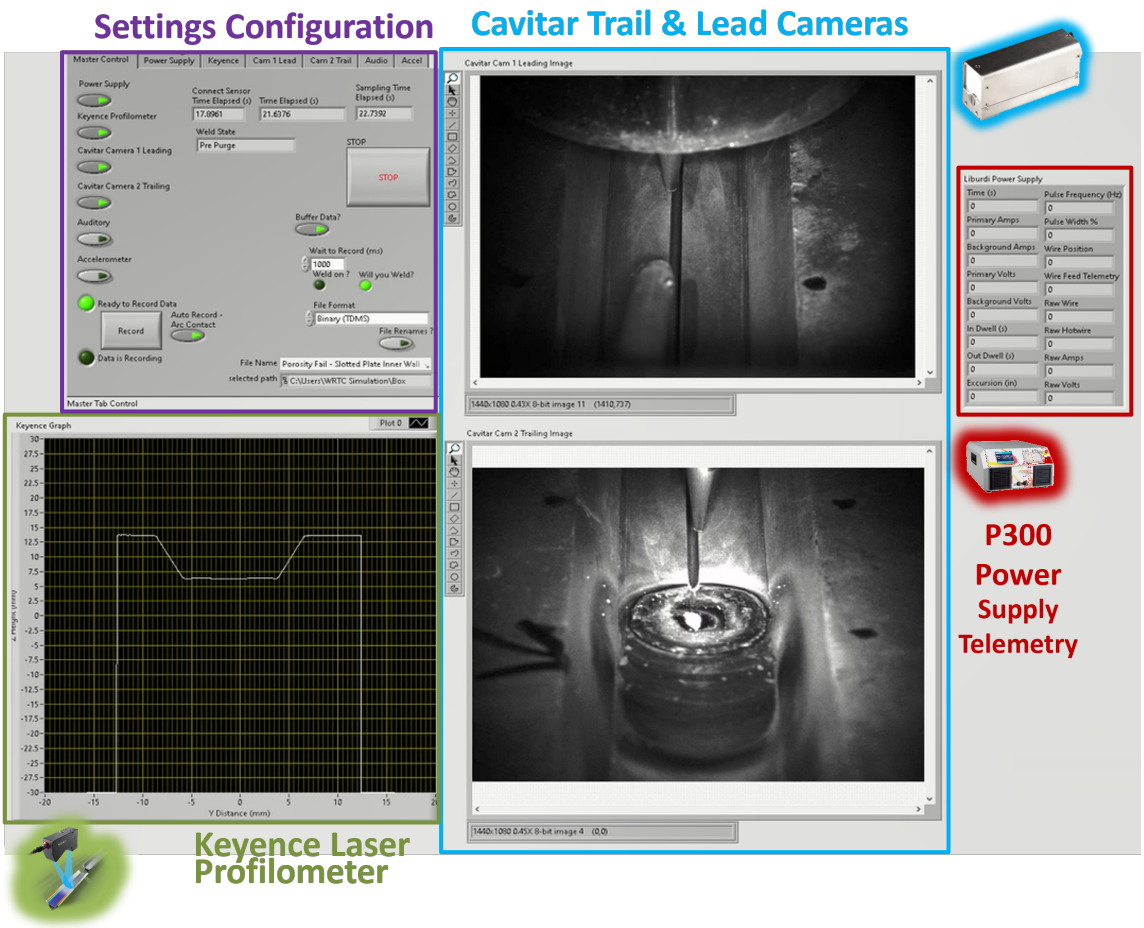


Figure A.16: EPRI G Head Data Collection Interface - LabVIEW Front Panel

Table A.3: Liburdi G Head Power Settings

Setting	Primary	Background	Units
Set	**High**	**Low**	**Units**
Current	270	170	Amps
Volts	10.9	8	Volts
Wire	42	38	IPM
Wire Diameter	316 stainless steel	0.035	inches
Travel		2.4	inch/min
Travel		1	mm/s
Arc Pulse		1.4	Hz
Pulse Width	Equal Split	50	%

Table A.4: Data Collection Settings

Sensor	Series	Side	Sample Rate
Cavitar	C300	Lead	16 Hz
Cavitar	C300	Trail	16 Hz
Keyence	LJ-V7080	Trail	16 Hz
Power Supply	Liburdi P300	N/A	16 Hz

Table A.5: Surface Porosity Test Matrix

	Groove	Hole	Layer	Loc	Case	Weld Condition
1	Flat V	No	Base Plate	Right	Clean	Empty Groove
2	Flat V	No	2nd Layer	Right		Weld on Second Bead
3	Flat V	No	2nd Layer	Middle	Gas	Cut Argon Gas
4	Flat V	No	2nd Layer	Middle		Blew on Weld
5	Flat V	Yes	Base Plate	Right	Oil	Marvel Air Tool Oil
6	Flat V	Yes	Base Plate	Right		Texeco Way Lubricant 68 Oil
7	Flat V	Yes	Base Plate	Right		Mobile Vactra Oil no. 2
8	Flat V	Yes	Base Plate	Right		Hydraulic Mobil Dte 24
9	Flat V	Yes	2nd Layer	Left		Propolyne Glycol - HF
10	Flat V	Yes	2nd Layer	Left		Tapmatic
11	Flat V	Yes	Base Plate	Left	Paint	UNI Oil Based Paint
12	Flat V	Yes	Base Plate	Left		Sharpie Oil Based Paint
13	Flat V	No	Base Plate	Left	Rust	Rust Accelerator on 308 Steel
14	Flat V	No	Base Plate	Right		Oxides
15	Flat V	No	2nd Layer	Right	General	Weld on Prior Defects
16	Flat V	Yes	Base Plate	Left		Drill Holes in Base Plate
17	Flat V	Yes	2nd Layer	Left		Base Holes with Contaminants
18	Flat V	Yes	Base Plate	Right		Shaft inserted into Weld
19	Flat V	Yes	Base Plate	Right	Groove	Good Weld on Various Grooves
20	Flat V	Yes	Base Plate	Right		Compressed Air in Cavity

Table A.6: Tie-In Test Matrix

Order	**Weld Layer**	**Bead Loc**	**Category**	**Cause of Tie-in**
1	Empty Groove	Middle	Good Weld	None
2	Empty Groove	Middle		Oxides
3	2nd	Right		None
4	Empty Groove	Middle	Y Osc Moce	Y Axis Osc Move
5	Empty Groove	Middle		Y Axis Osc Move
6	2nd	Right Wall		Y Axis Osc Move
7	2nd	Middle	Y & Wire	Wire Rot & Y Axis
8	2nd	Left Wall	Wire Manip	Wire In
9	2nd	Left Wall		Wire Out
10	2nd	Middle		Wire Out
11	2nd	Right Wall		Low Wire
12	Top	Right		High Wire
13	Top	Right Wall		Wire In
14	Top	Middle		Wire In
15	Empty Groove	Left Wall	Surface	Wire on Tungsten
16	Empty Groove	Left Wall		Rust
17	Empty Groove	Left Wall		Slotted Geometry
18	Empty Groove	Middle		Slotted Geometry
19	Empty Groove	Middle		Compressed Air
20	Empty Groove	Right Wall		Paint
21	Empty Groove	Right Wall		Holes
22	Top	Left Wall		Oil
23	2nd	Middle		Gas Coverage
24	2nd	Right Wall		Oil

A.4 Experimental Results

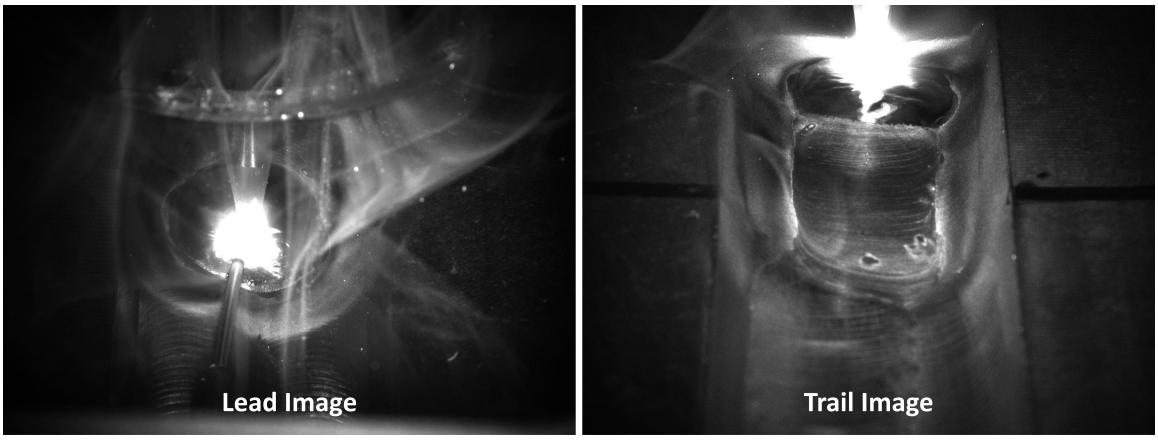


Figure A.17: Cut Gas Coverage Test Case for Surface Porosity

Table A.7: Surface Porosity Results

	Case	**Weld Condition**	**Porosity?**	**Defects?**
1	Clean	Empty Groove	No	Clean Weld
2		Weld on Second Bead	No	Clean Weld
3	Gas	Cut Argon Gas	No	Splatter
4		Blew on Weld	No	Splatter
5	Oil	Marvel Air Tool Oil	No	Clean Weld
6		Texeco Way Lubricant 68 Oil	No	Clean Weld
7		Mobile Vactra Oil no. 2	No	Clean Weld
8		Hydraulic Mobil Dte 24	No	Clean Weld
9		Propolyne Glycol - HF	No	Poor Tie-in
10		Tapmatic	No	Poor Tie-in
11	Paint	UNI Oil Based Paint	No	Tie-in Oxide
12		Sharpie Oil Based Paint	No	Tie-in Oxide
13	Rust	Rust Accelerator on 308 Steel	No	Clean Weld
14		Oxides	No	Oxide
15	General	Weld on Prior Defects	No	Tie-in Voids
16		Drill Holes in Base Plate	No	Clean Weld
17		Base Holes with Contaminants	No	Tie-in
18		Shaft inserted into Weld	No	Clean Weld
19	Groove	Good Weld on Various Grooves	No	Clean Weld
20		Compressed Air in Cavity	No	Splatter



Figure A.18: Cut Gas Coverage Resulting Weld Bead

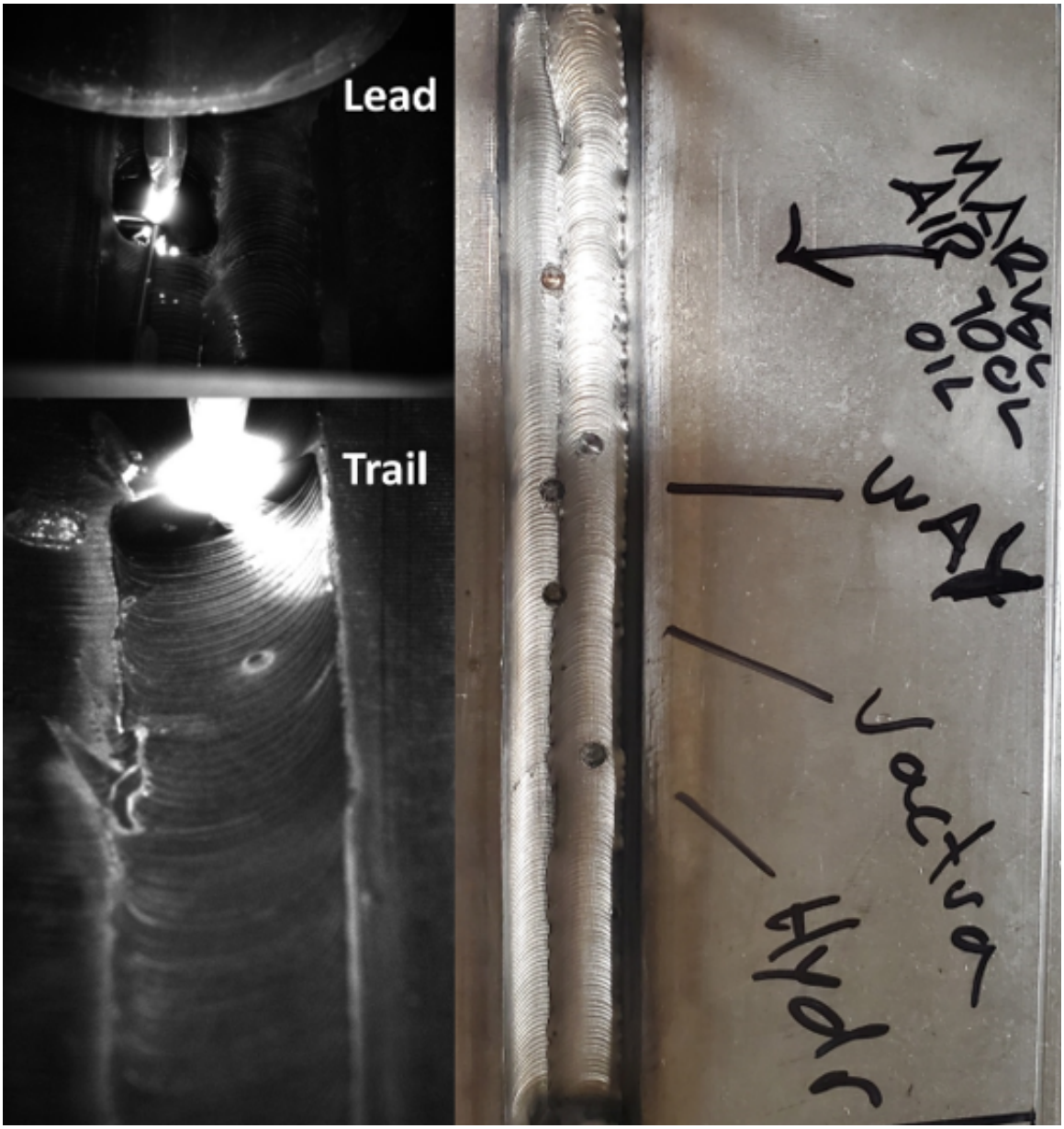


Figure A.19: Oil Contaminants for Surface Porosity

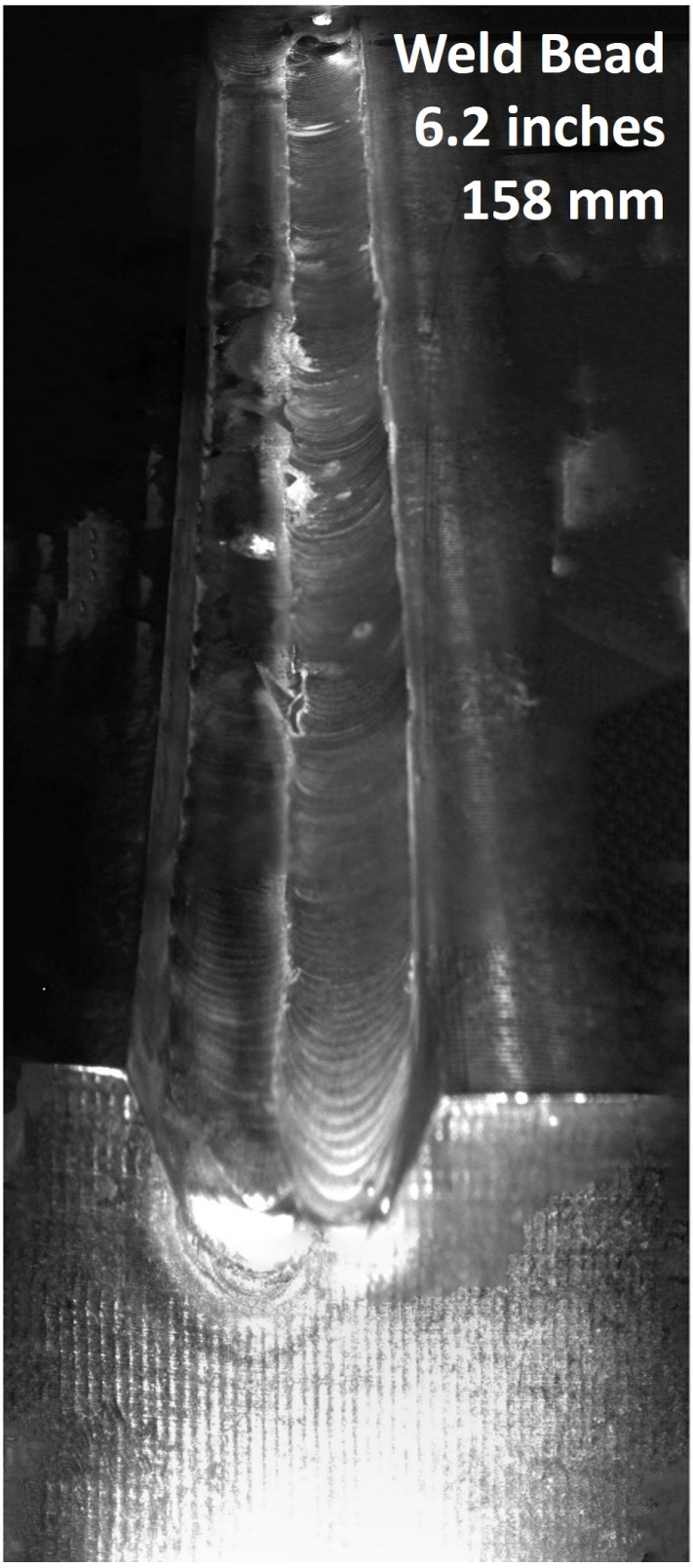


Figure A.20: Oil Contaminants Resulting Weld Bead



Figure A.21: Paint Contaminants for Surface Porosity



Figure A.22: Paint Contaminants Resulting Weld Bead

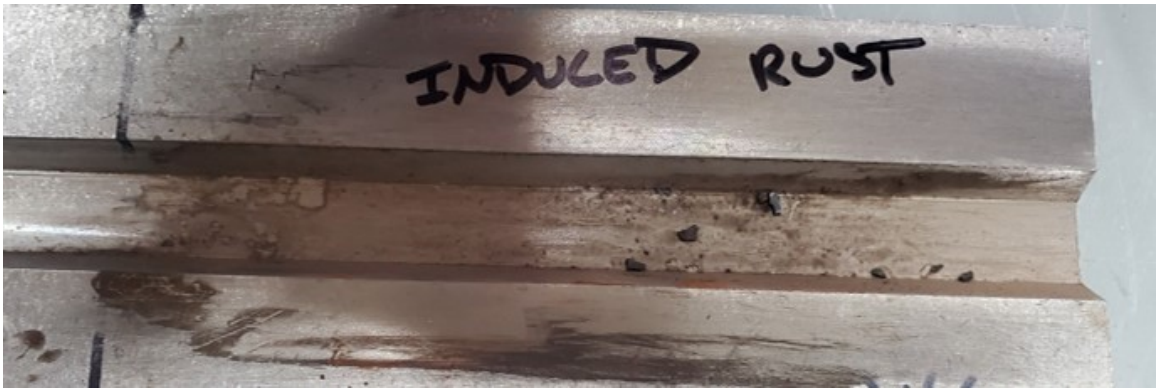


Figure A.23: Induced Rusted Surface Contaminants



Figure A.24: Rusted Surface Contaminants Resulting Weld Bead

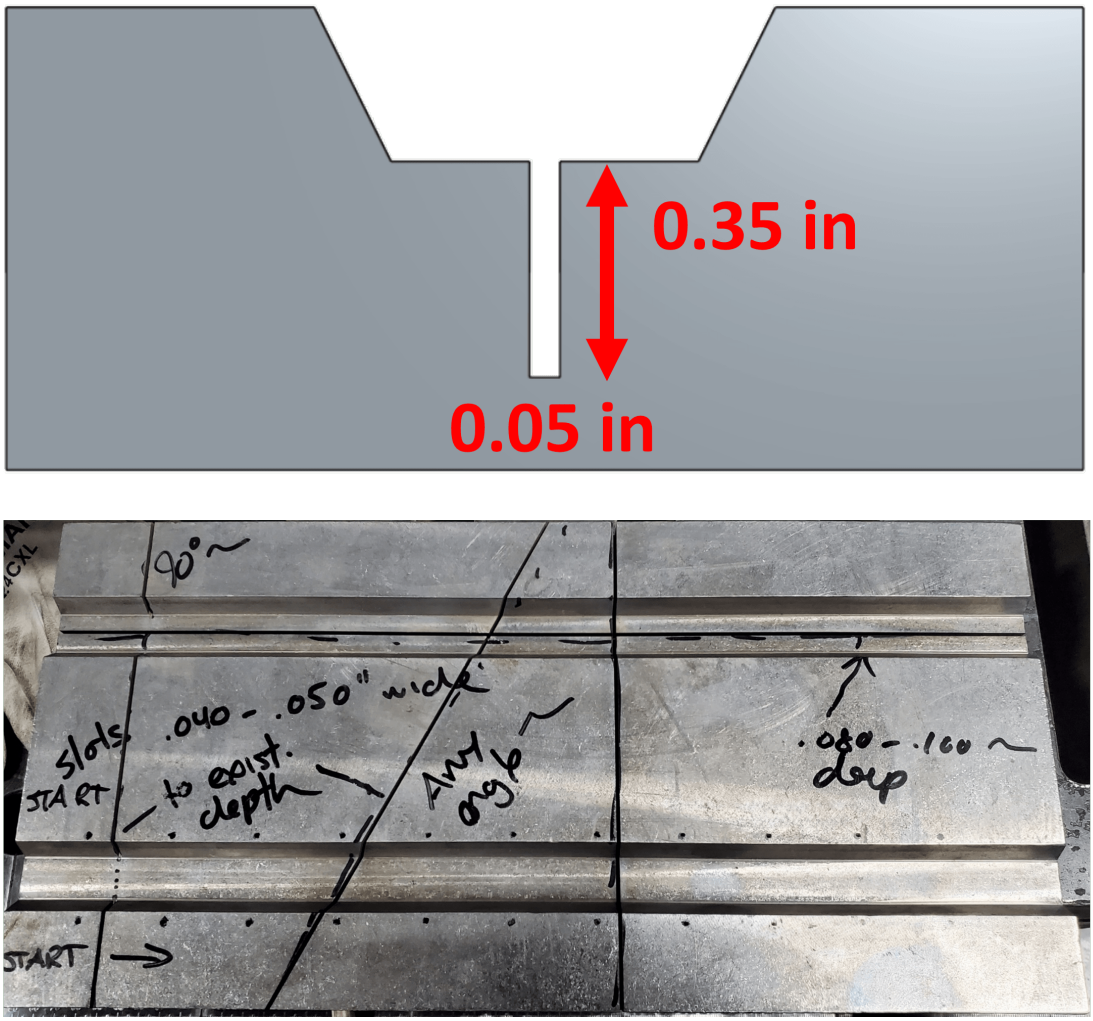


Figure A.25: Different Groove Geometry Test Case

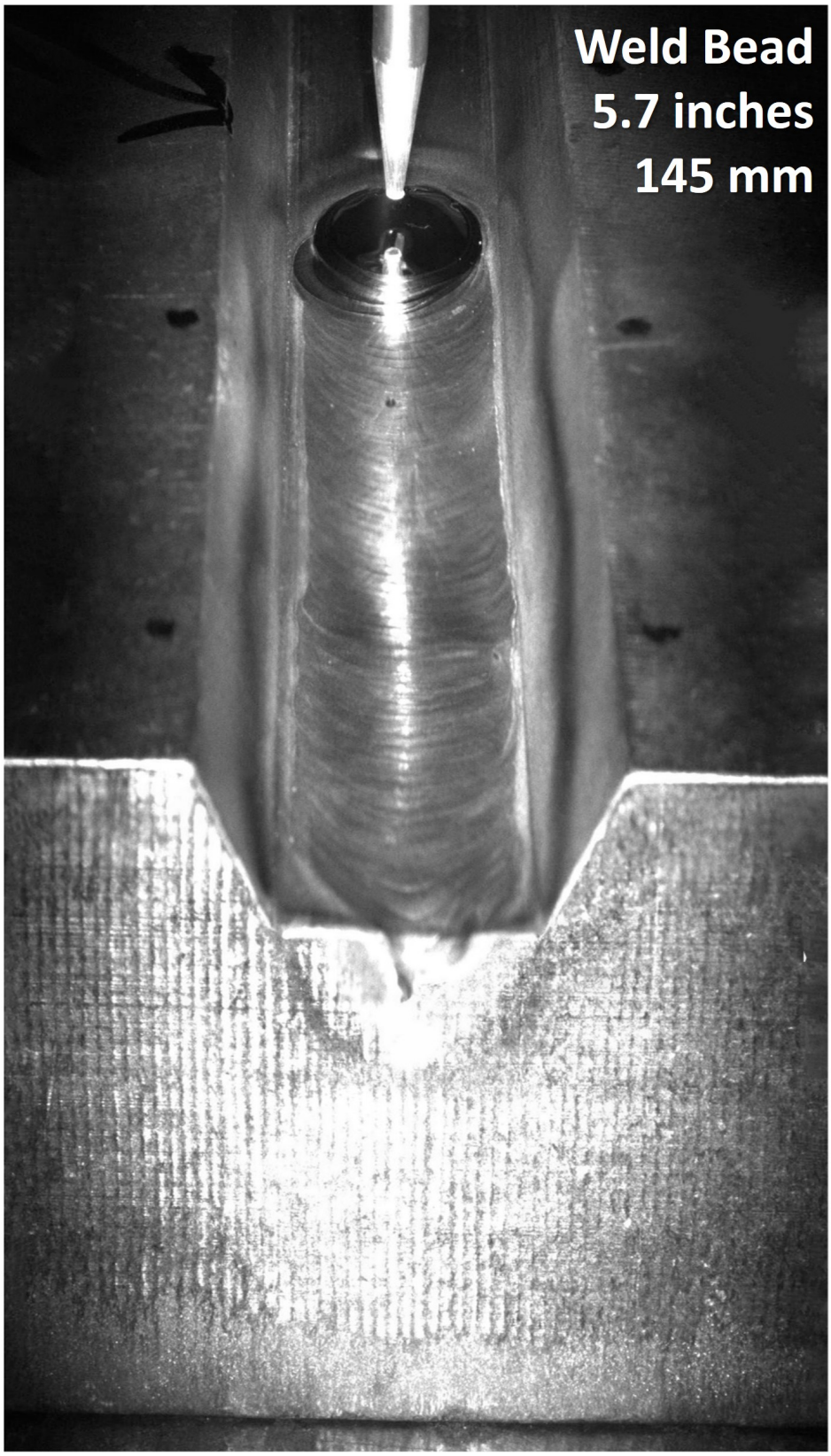


Figure A.26: Slotted Plate Resulting Weld Bead

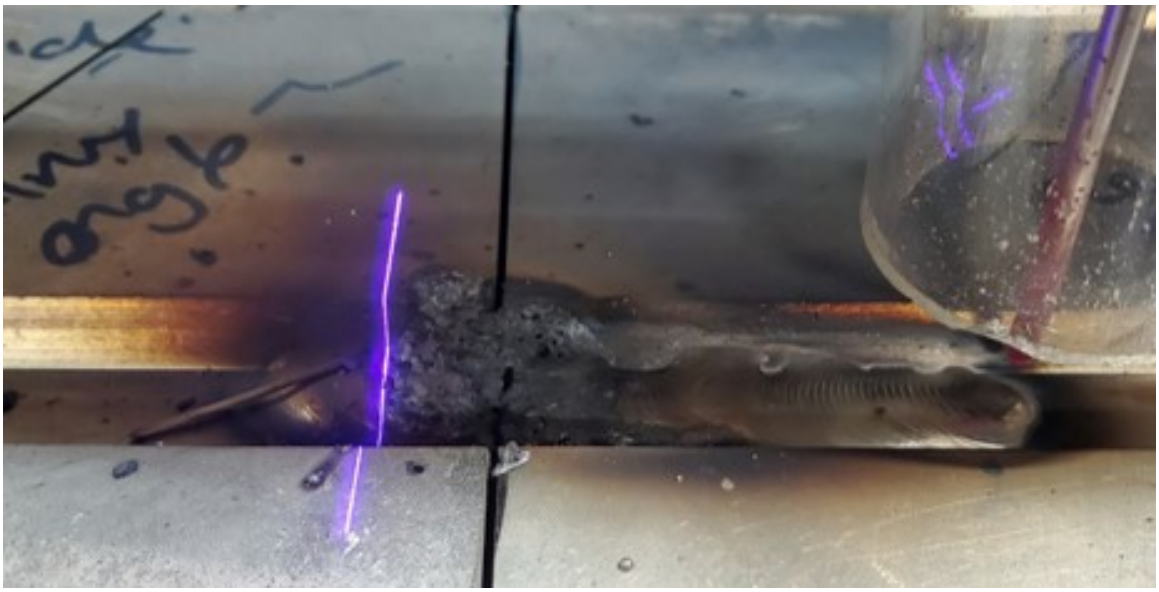


Figure A.27: Slotted Plate Compressed Air Damage

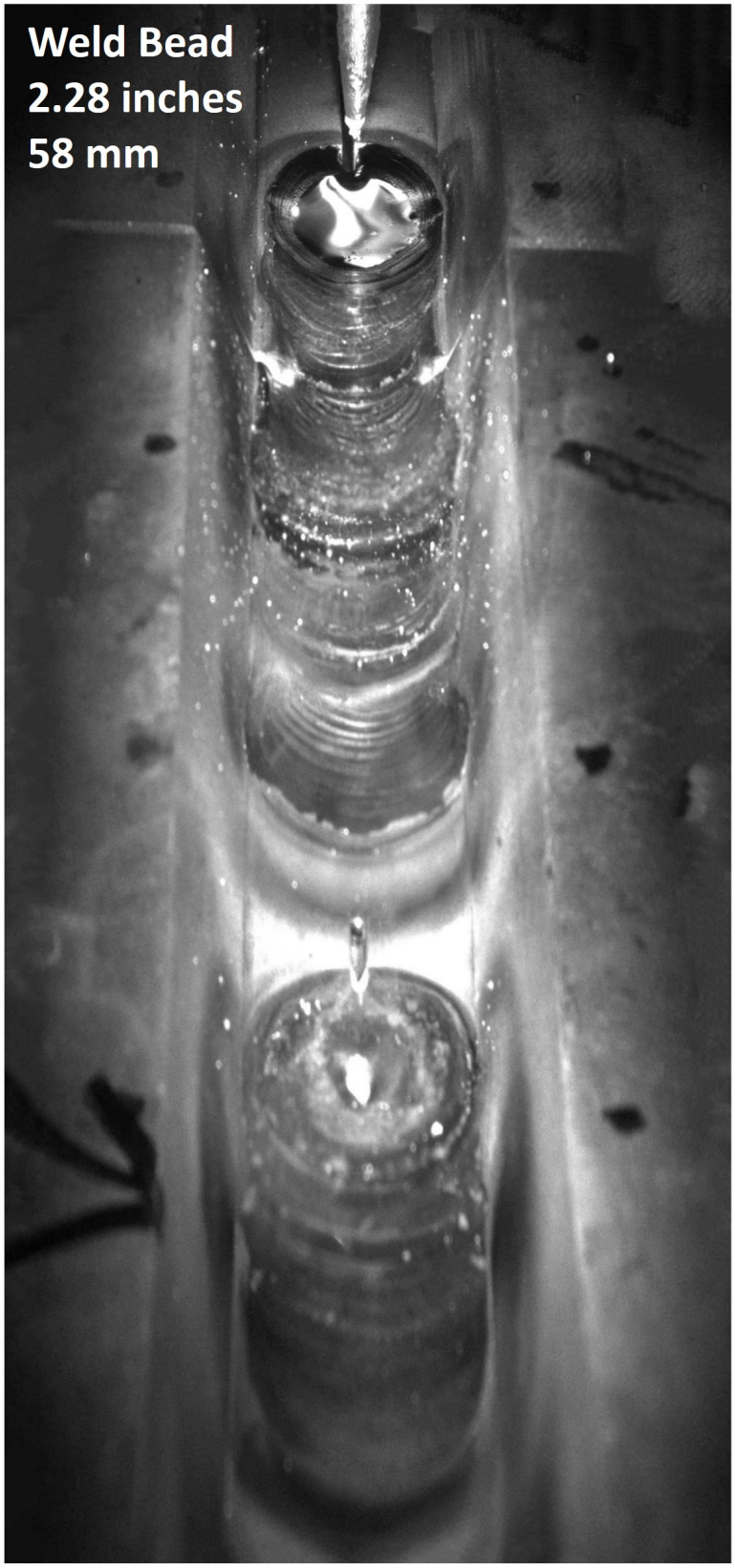


Figure A.28: Slotted Plate Compressed Air Inner Wall Resulting Weld Bead

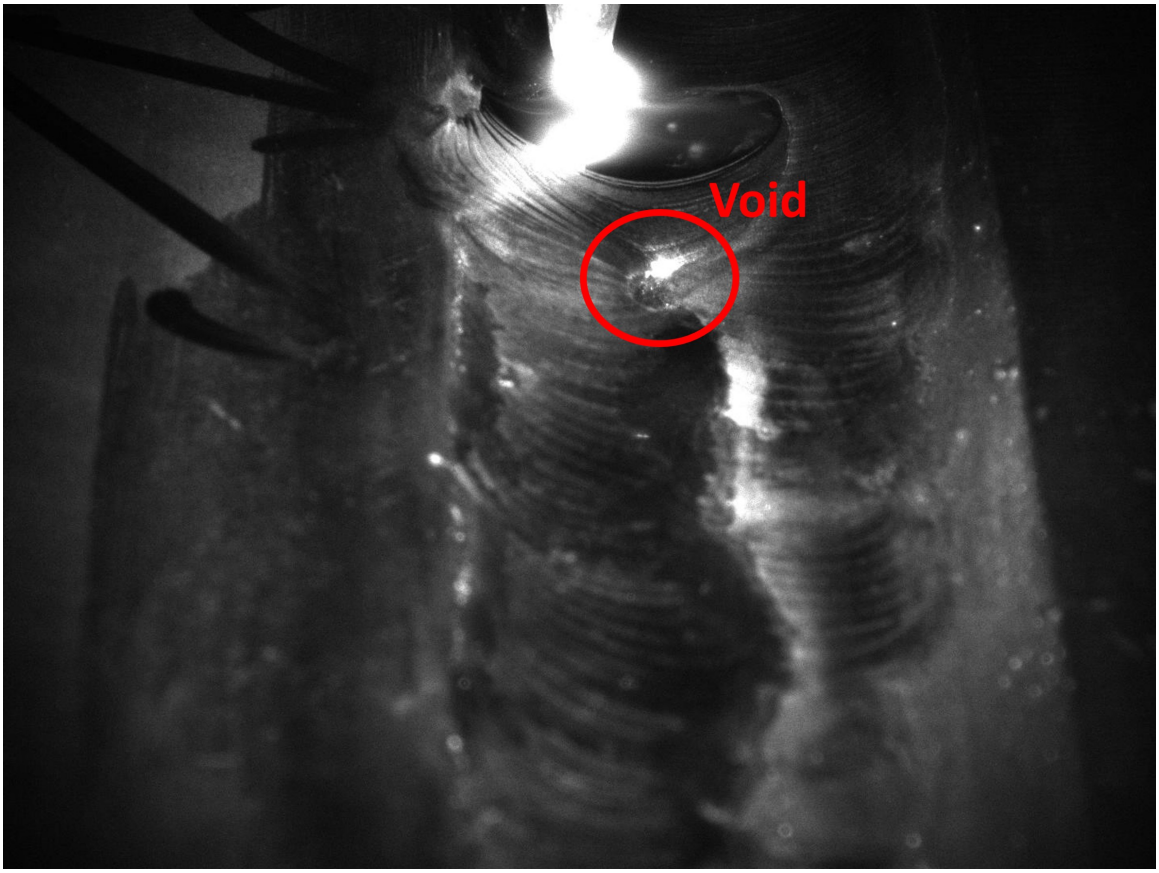


Figure A.29: Void Instance in Surface Porosity Test with Tapmatic

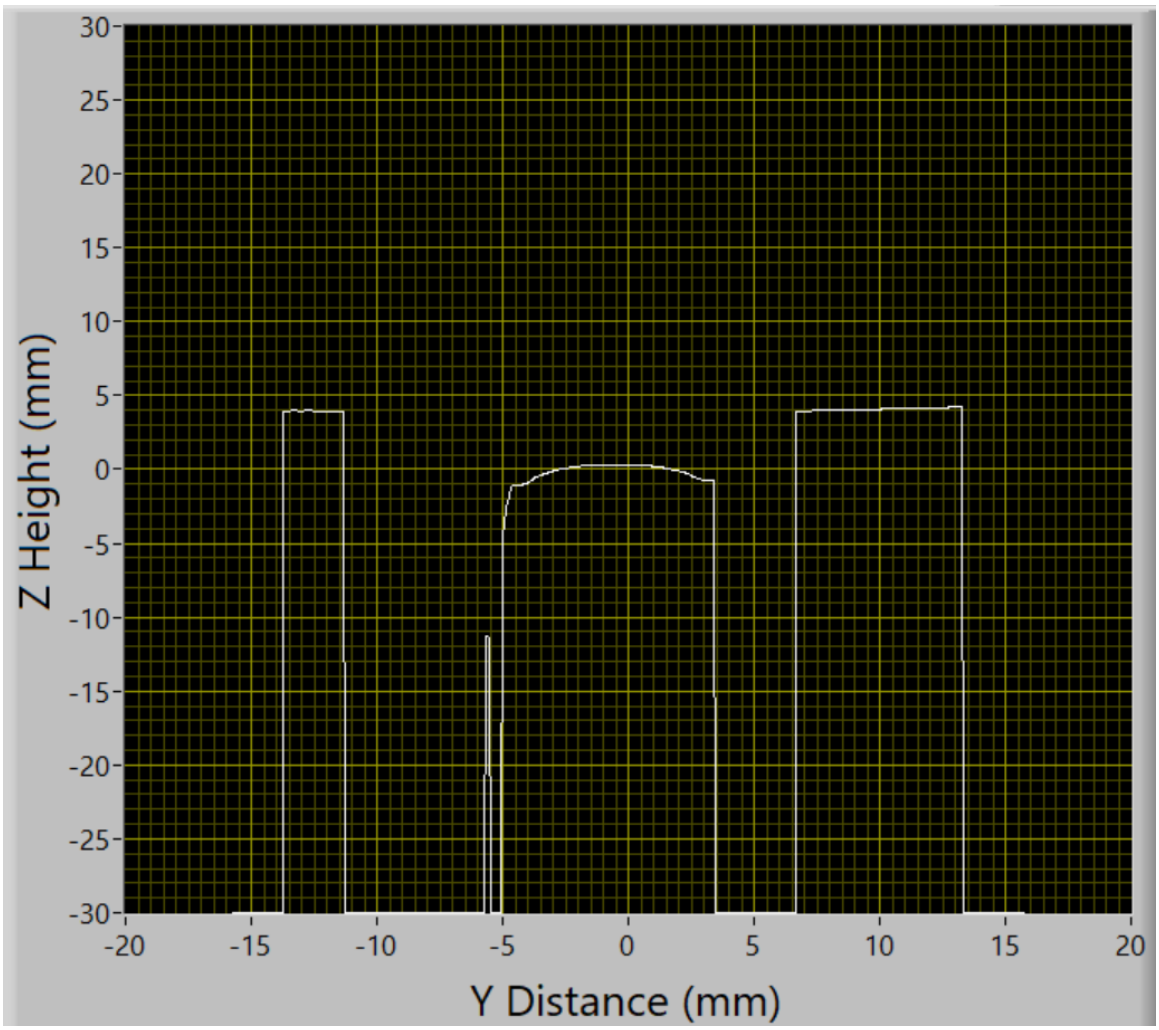


Figure A.30: Keyence Failed Detection

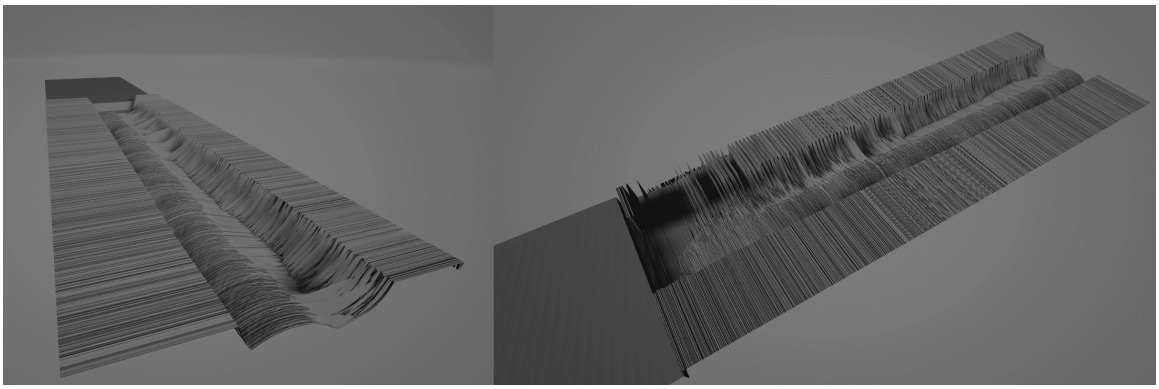


Figure A.31: Heavily Filtered Keyence 3D Weld Groove Scan

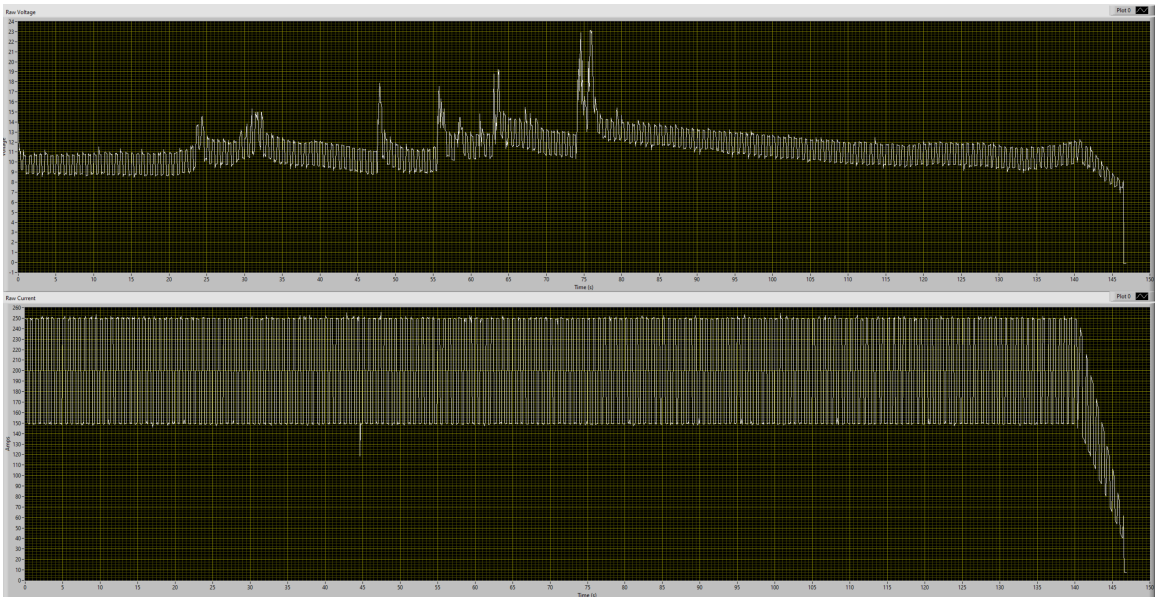


Figure A.32: P300 Power Supply Raw Current & Voltage Telemetry

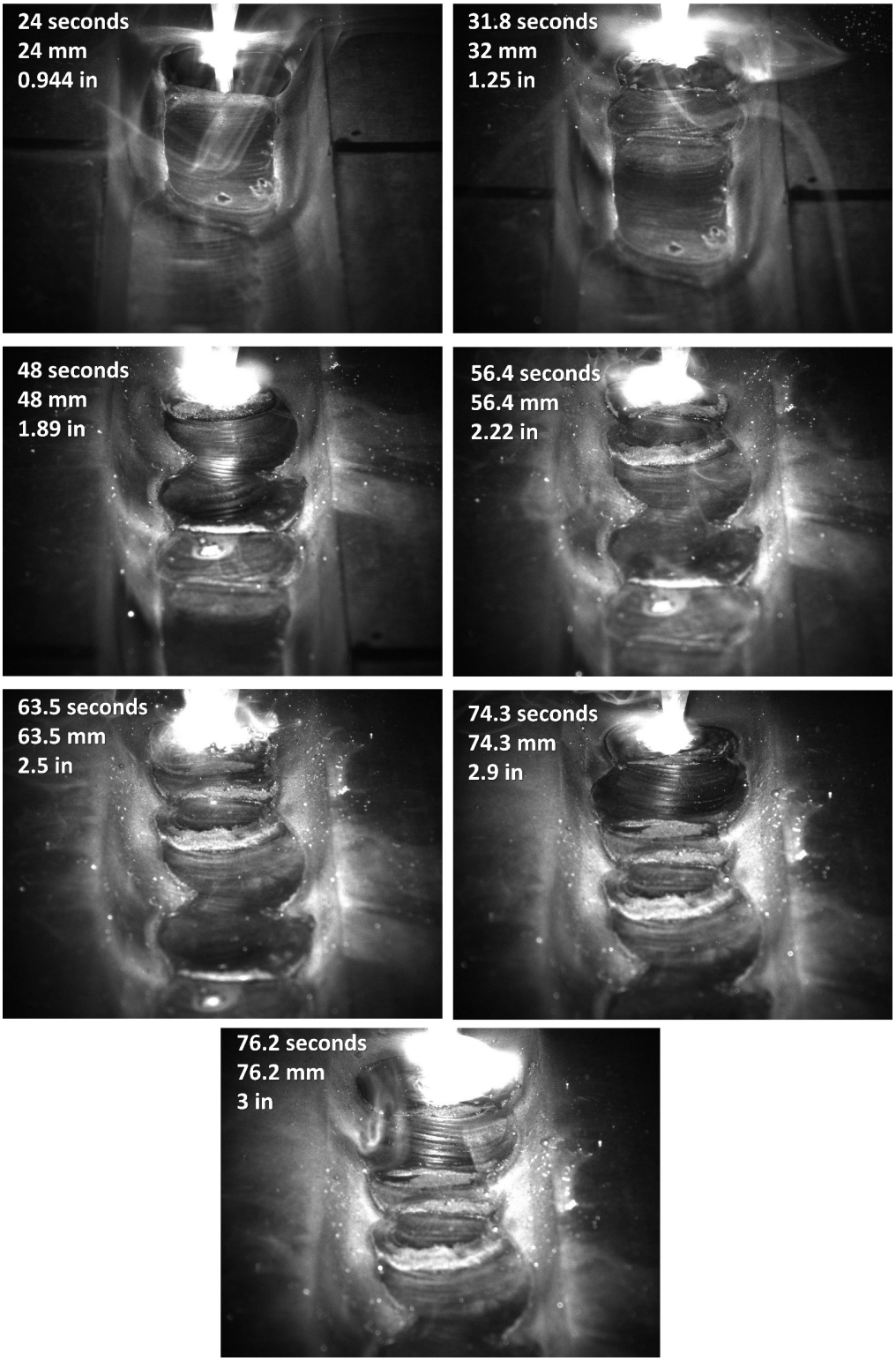


Figure A.33: Cut Gas Coverage Raw Volts Spike Locations

A.5 Tie-In Image Algorithm

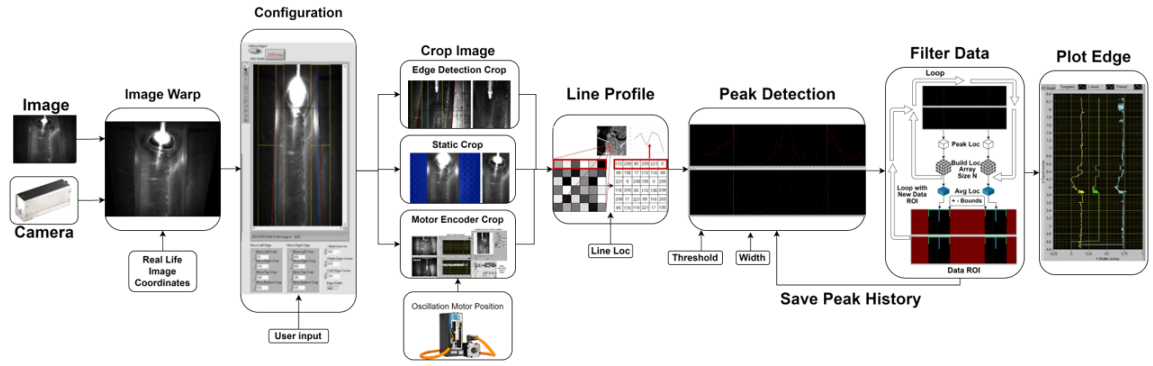


Figure A.34: Tie-In Edge Detection System Diagram

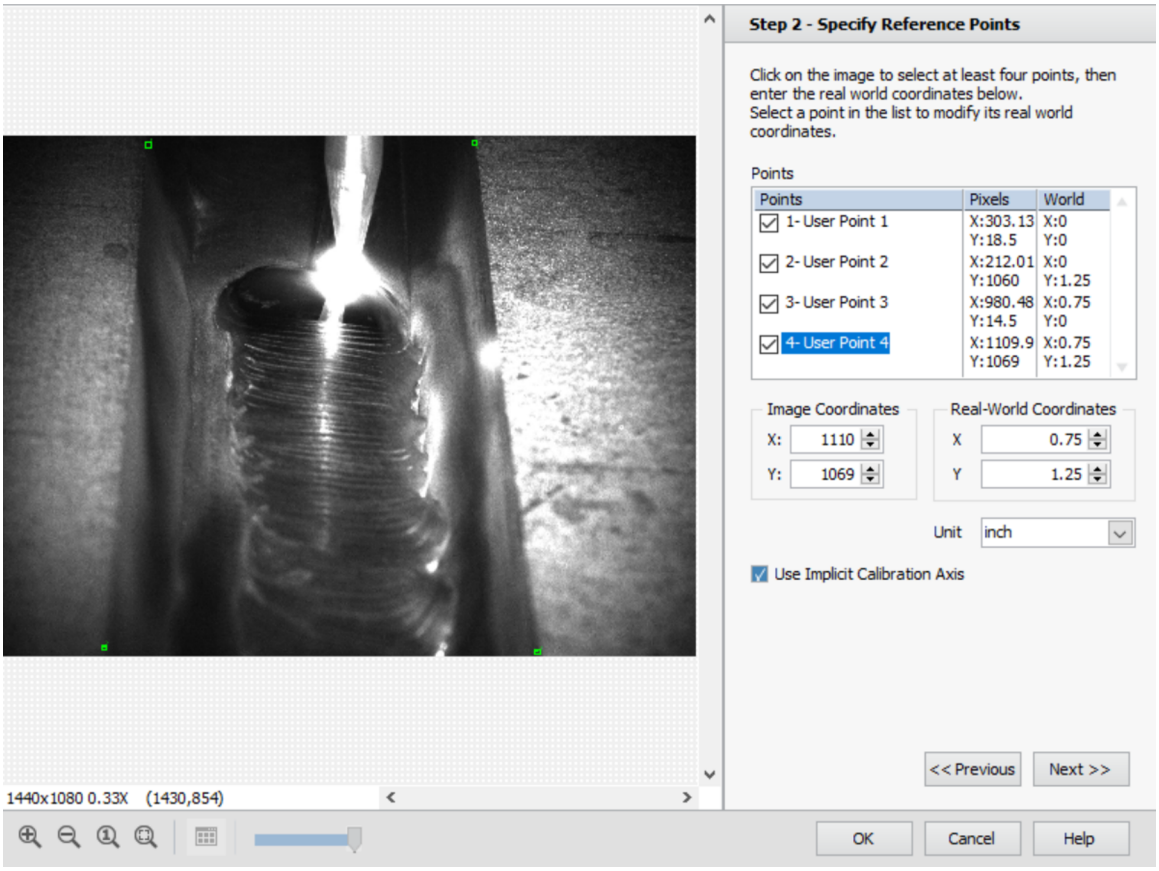


Figure A.35: Image Warping in NI Vision Assistant

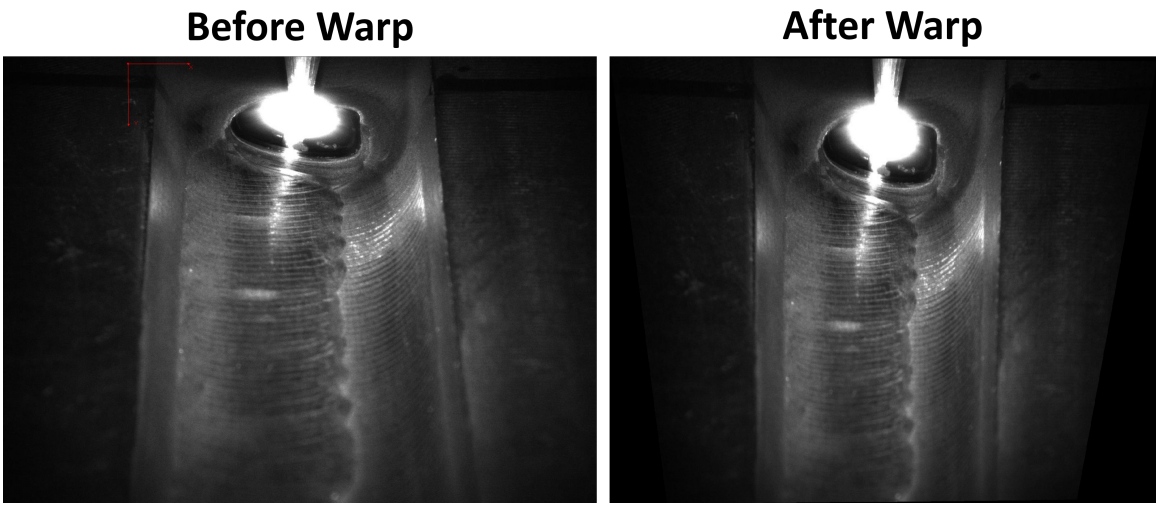


Figure A.36: Image Warping Before & After

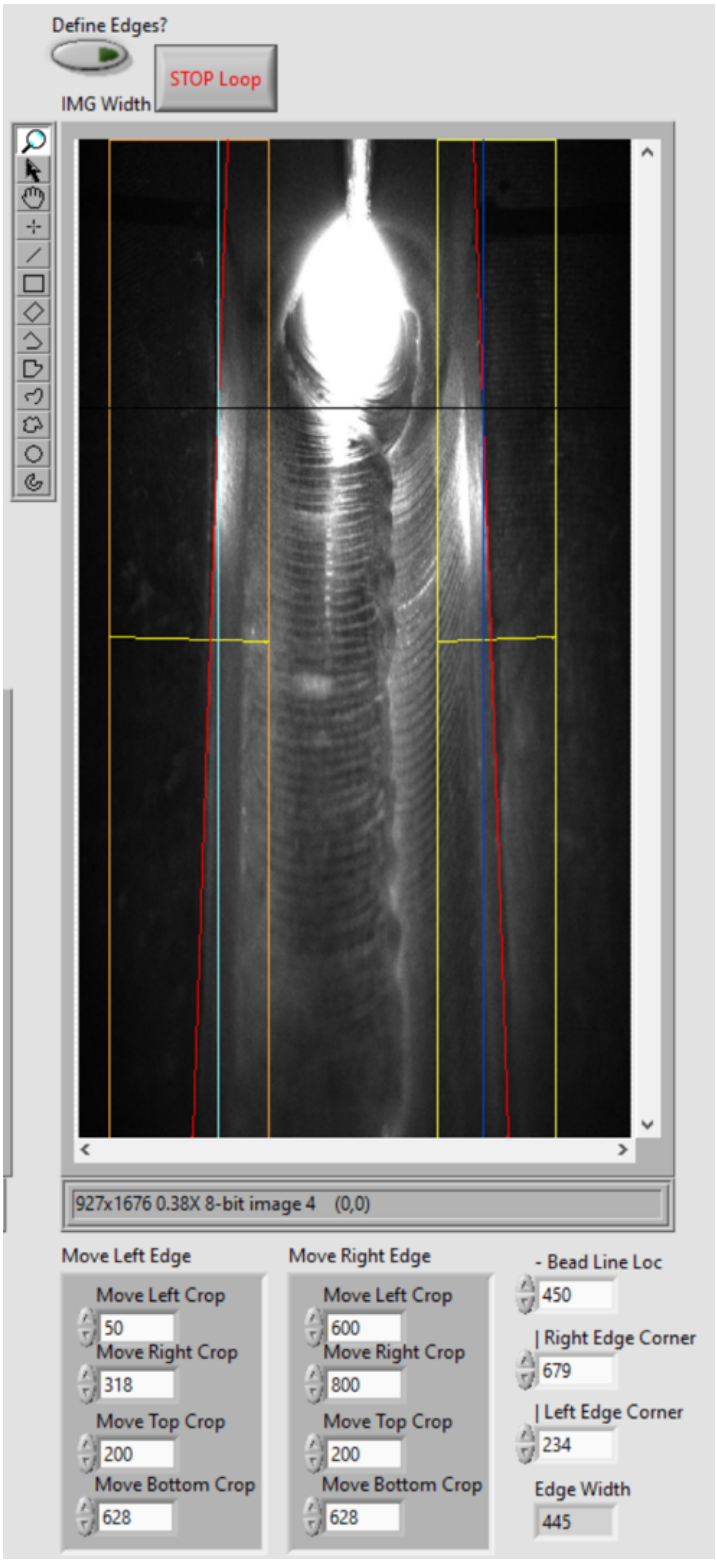


Figure A.37: LabVIEW Tie-In Configuration

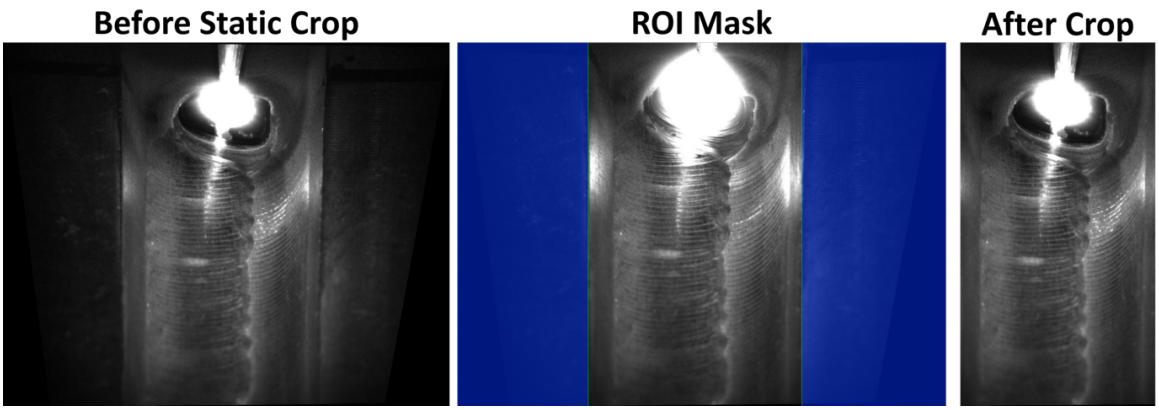


Figure A.38: LabVIEW Static Crop

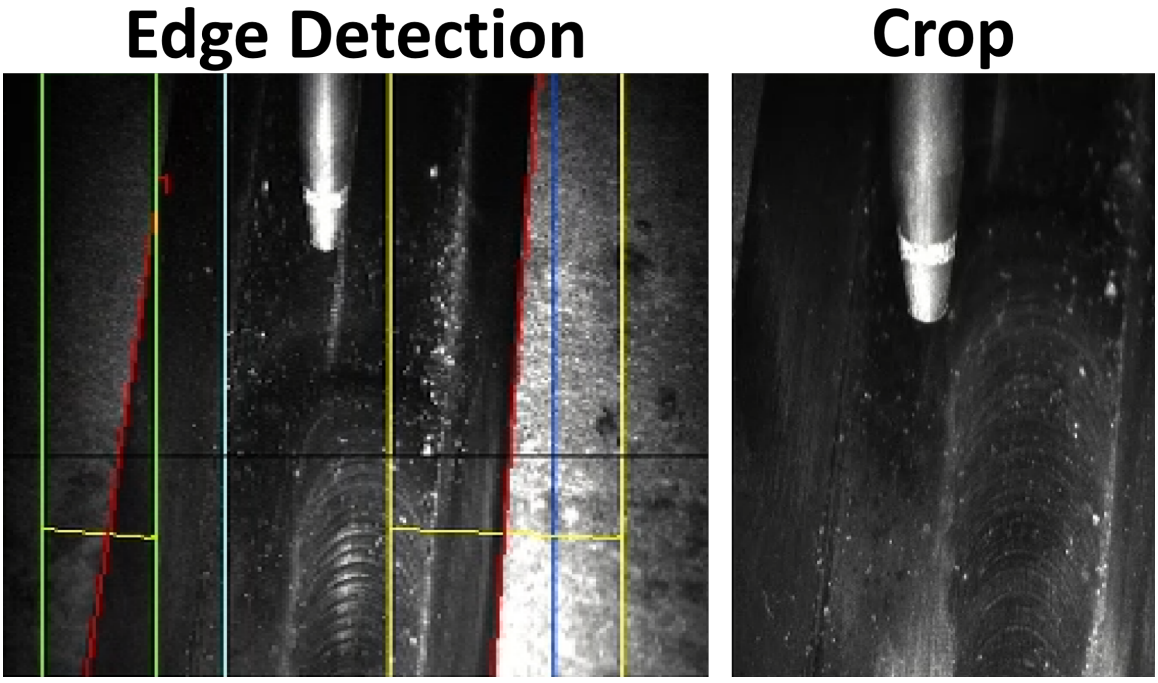


Figure A.39: Edge Detection Cropping

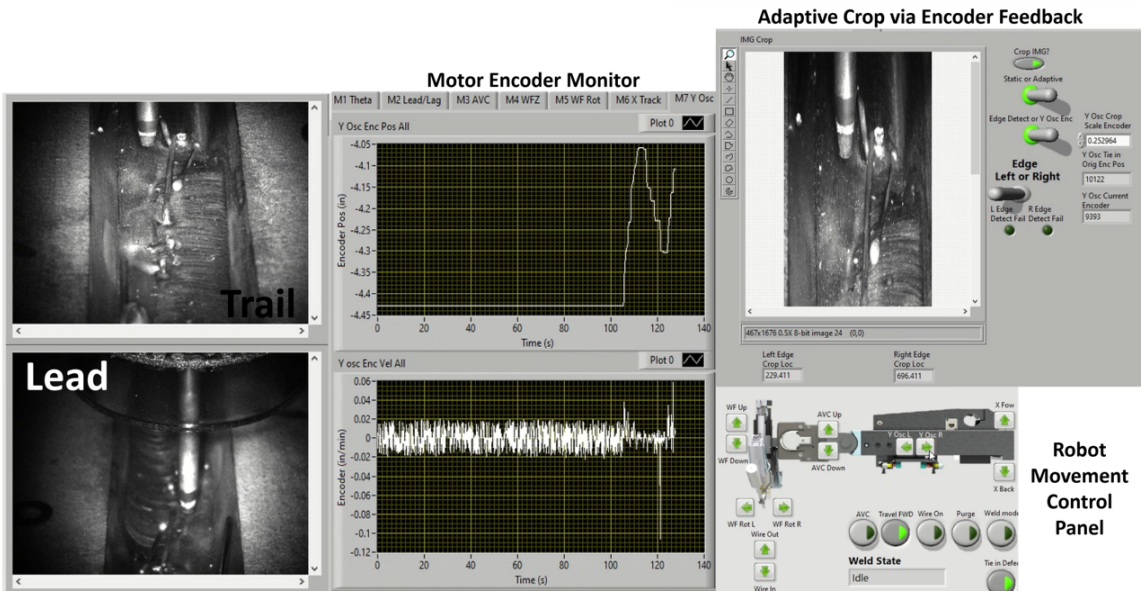


Figure A.40: Y Axis Oscillation Motor Encoder Position Cropping on MK II Head

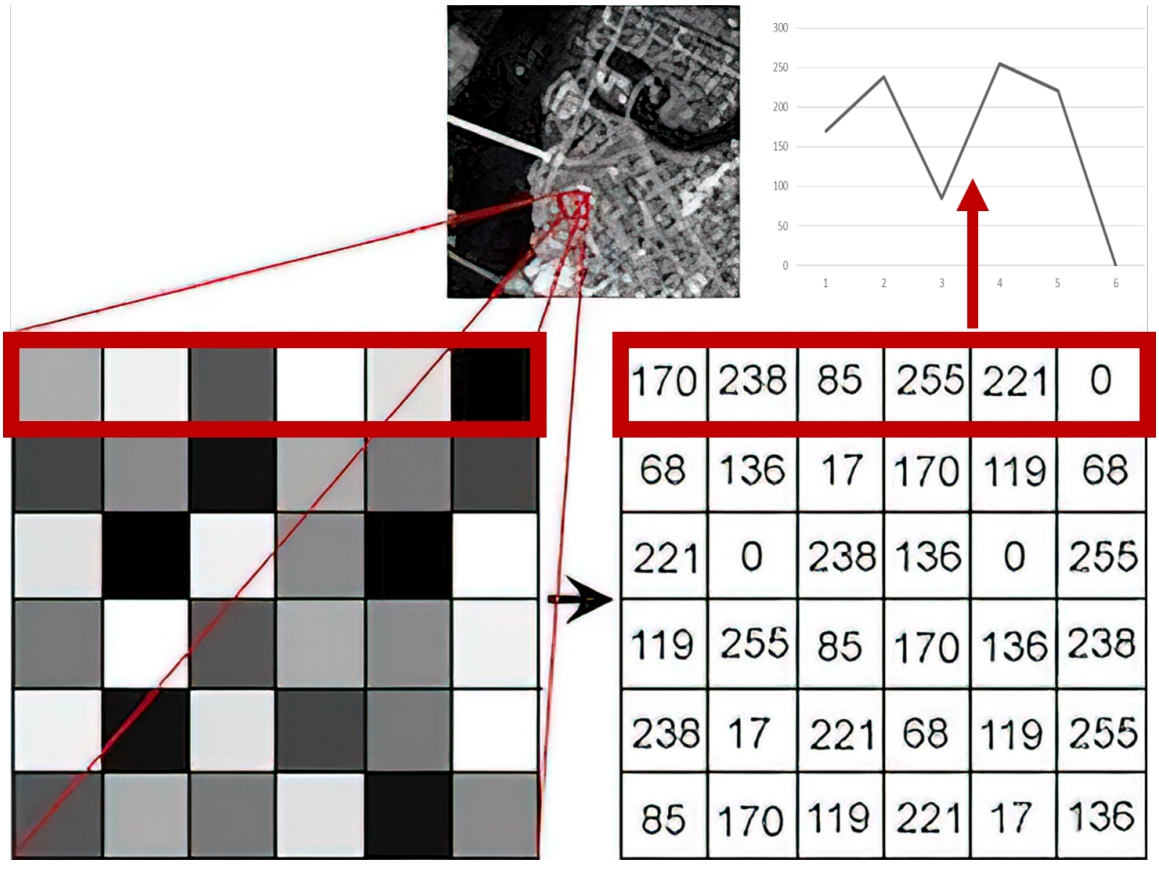


Figure A.41: Image to Matrix to Line Profile Plot

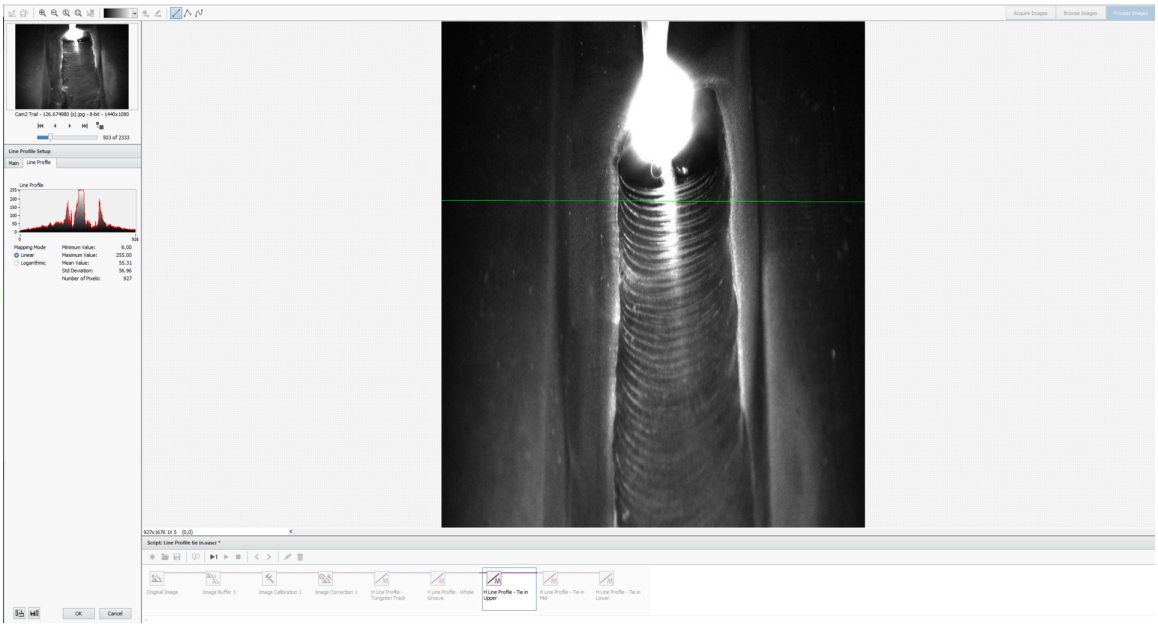


Figure A.42: NI Vision Assistant Line Profile

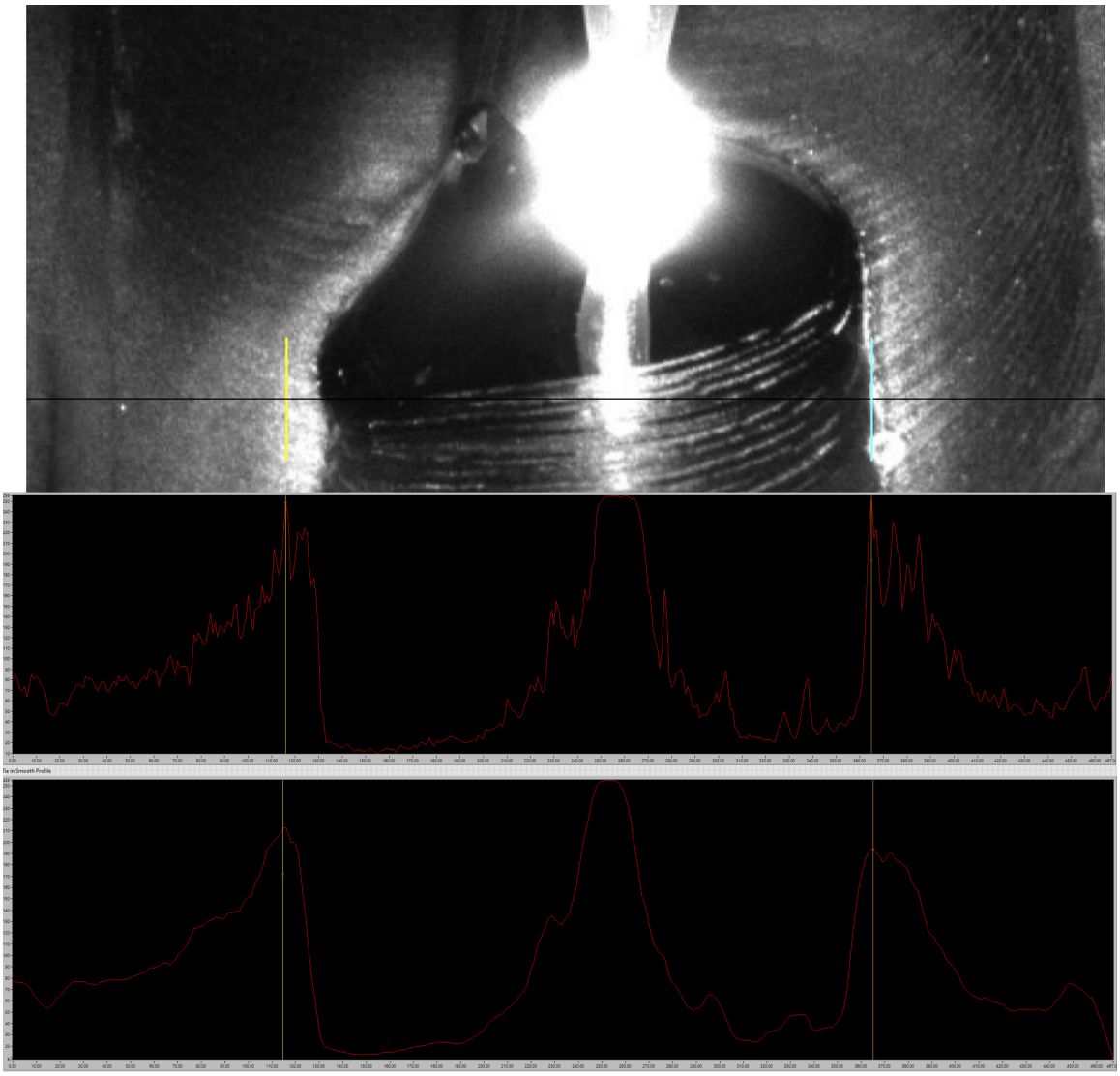


Figure A.43: Average Smoothing Line Profile Peak Detection & Edge Tracking

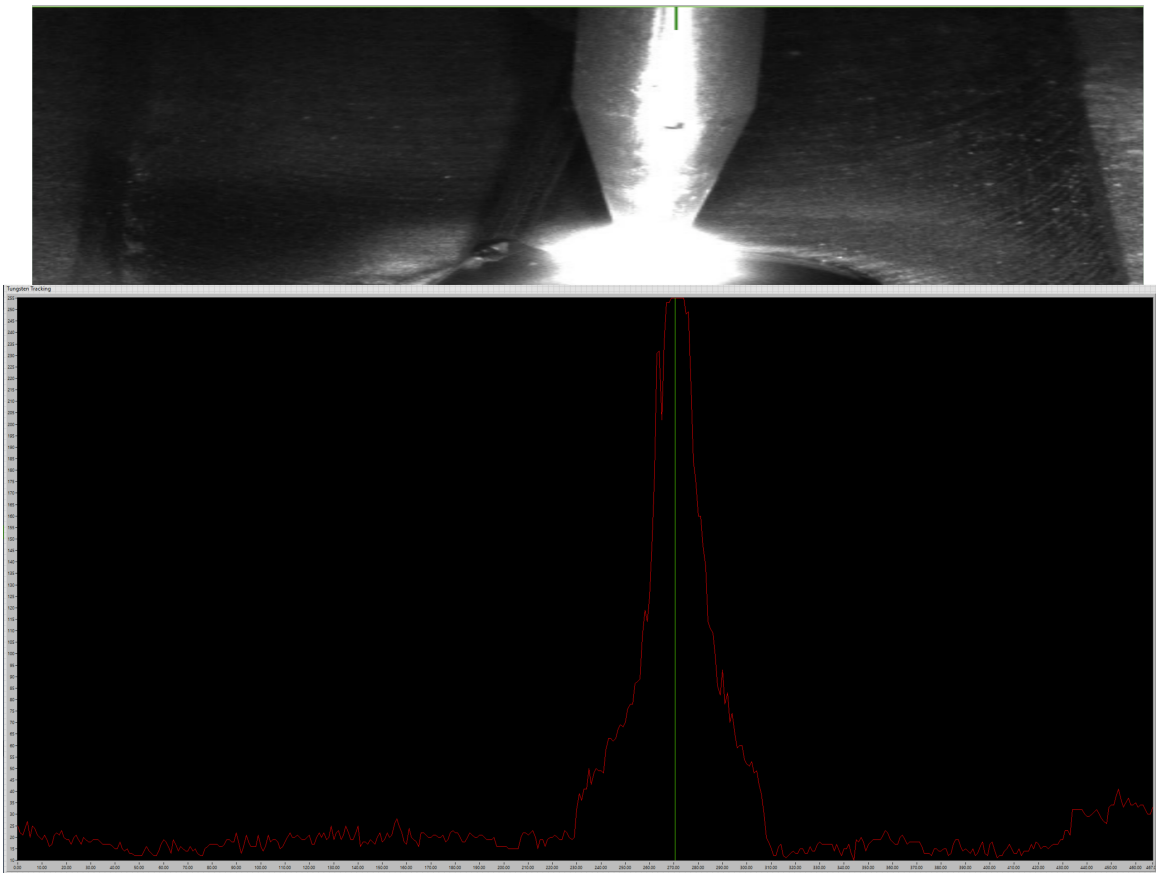


Figure A.44: Tungsten Tracking Line Profile Peak Detection

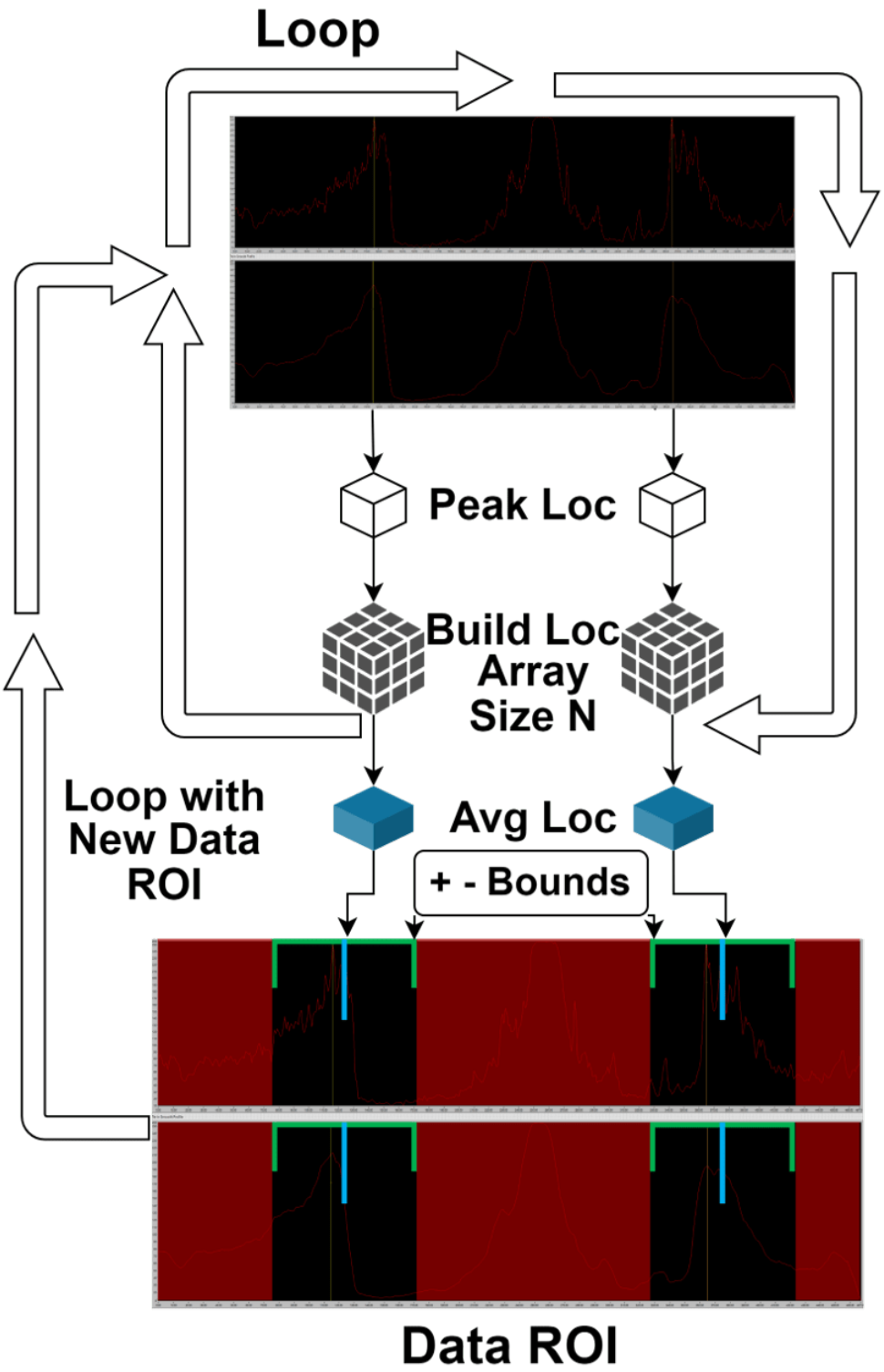


Figure A.45: ROI Data Filter Process Diagram

A.6 Tie-In Algorithm Results

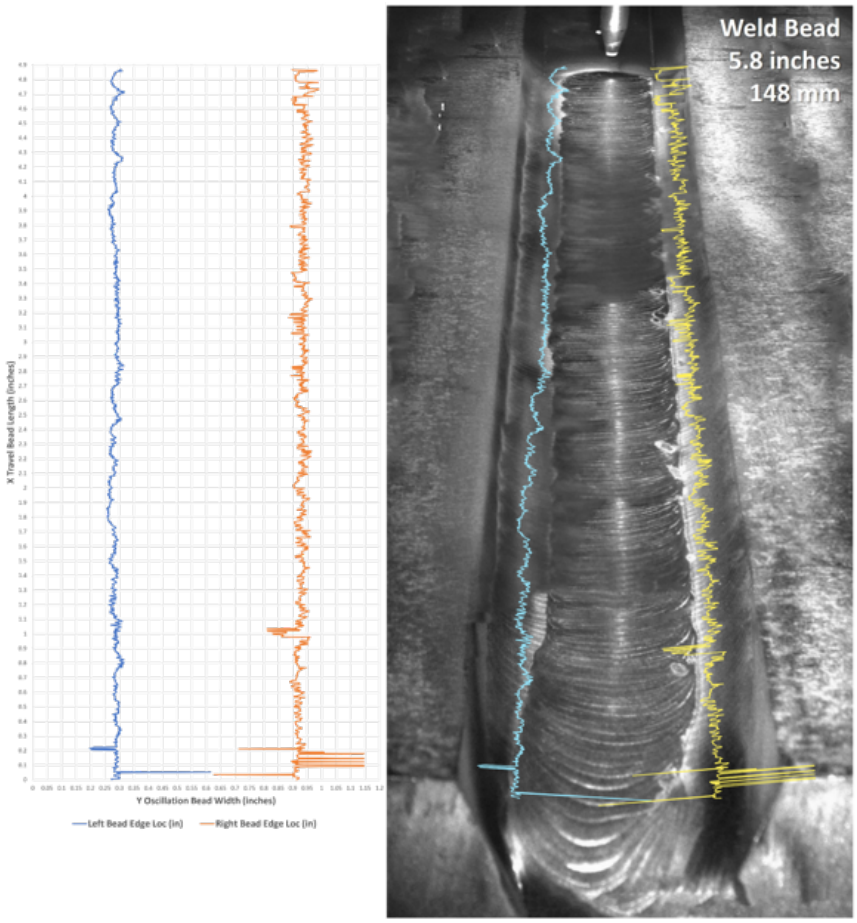


Figure A.46: Clean Weld Center Bead Tie-In Algorithm Test

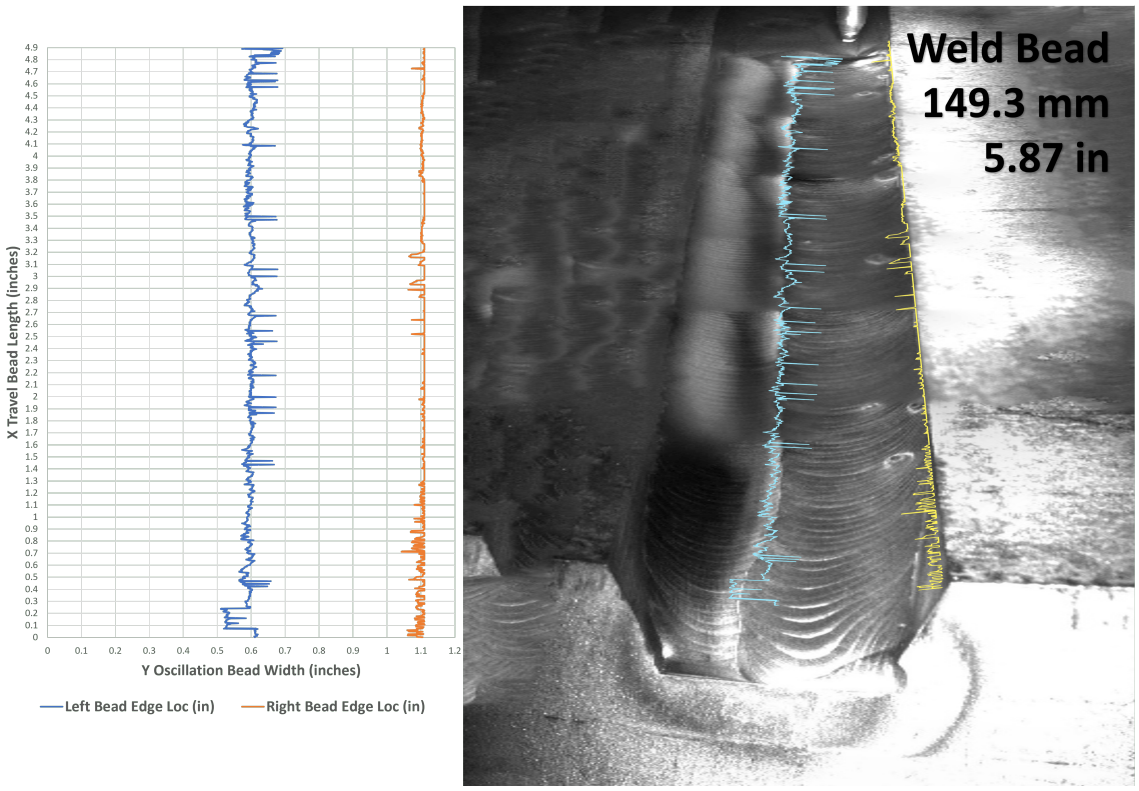


Figure A.47: Clean Weld Outer Wall Tie-In Algorithm Test

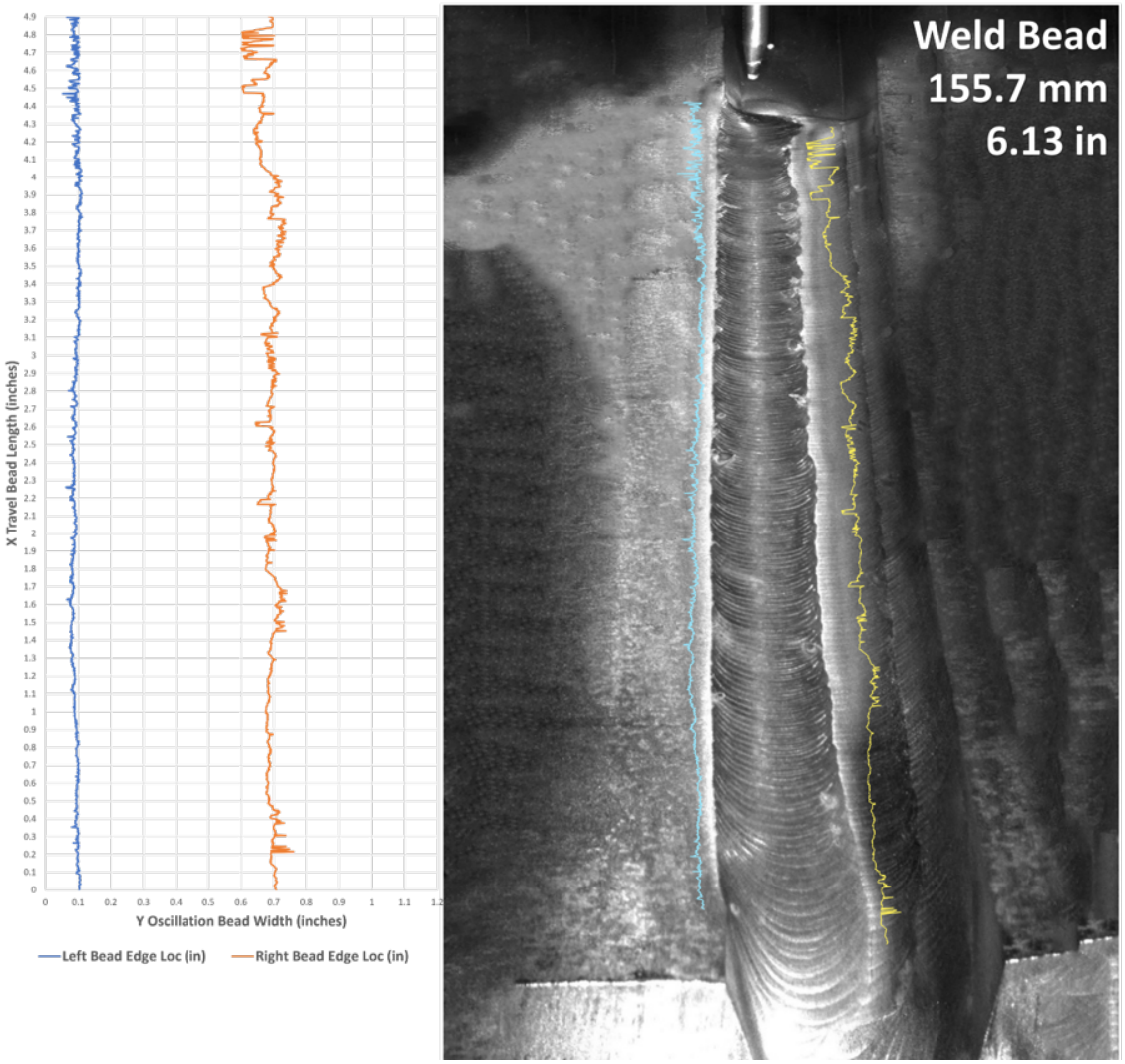


Figure A.48: Clean Weld Inner Wall Tie-In Algorithm Test

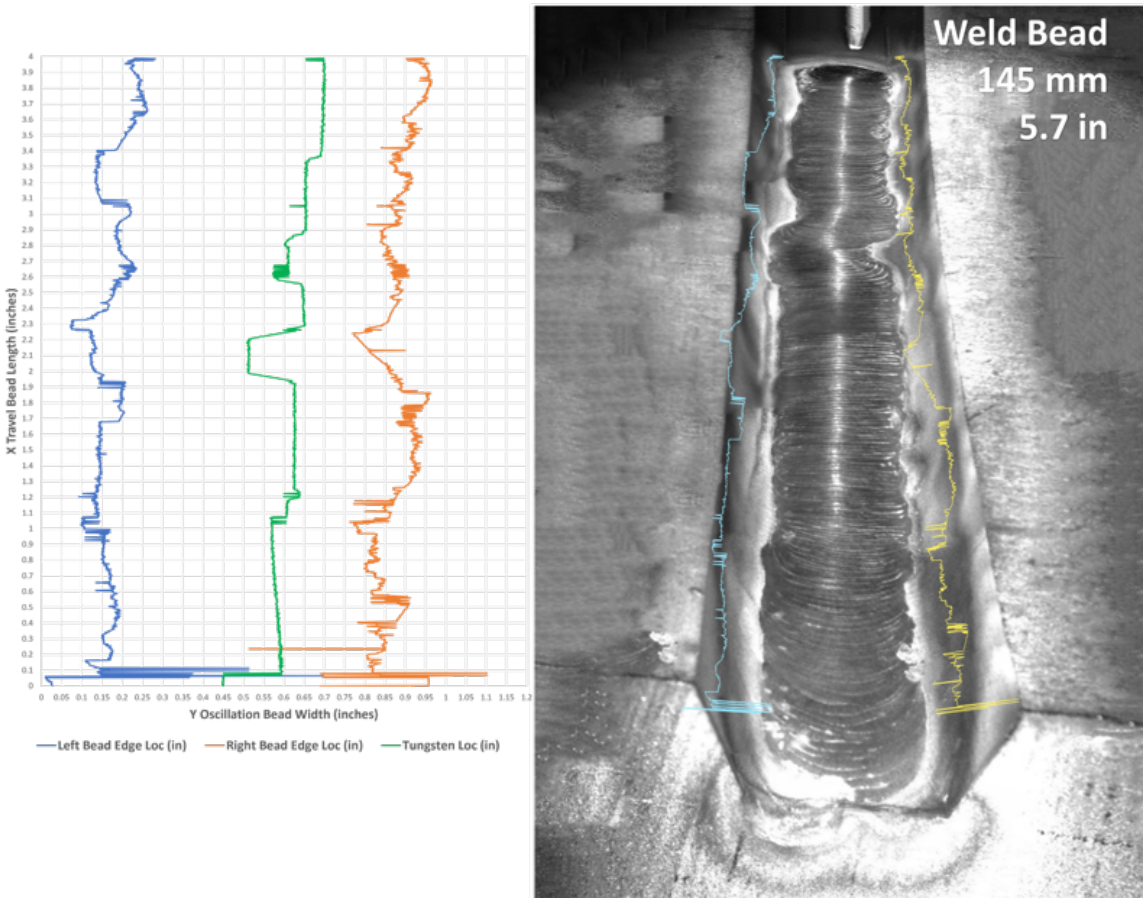


Figure A.49: Adaptive Cropping Moving Y-Axis Oscillation Tie-In Algorithm Test

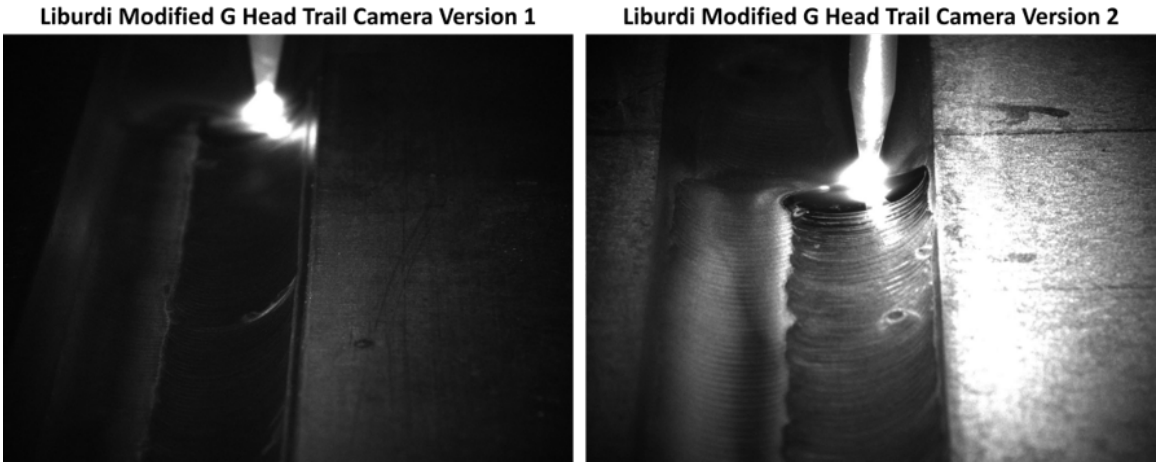


Figure A.50: Poor Camera Angle from First Test Run Comparison

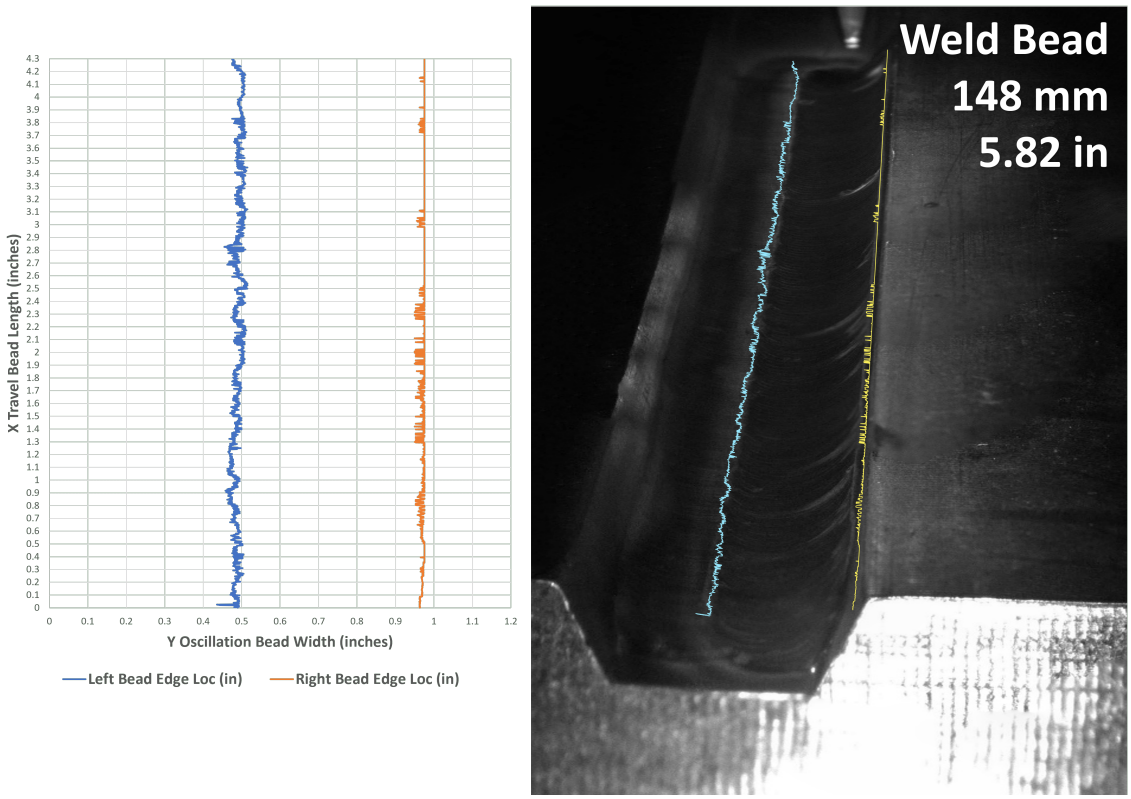


Figure A.51: Poor Camera Angle & Focal Length for Tie-In Algorithm Test

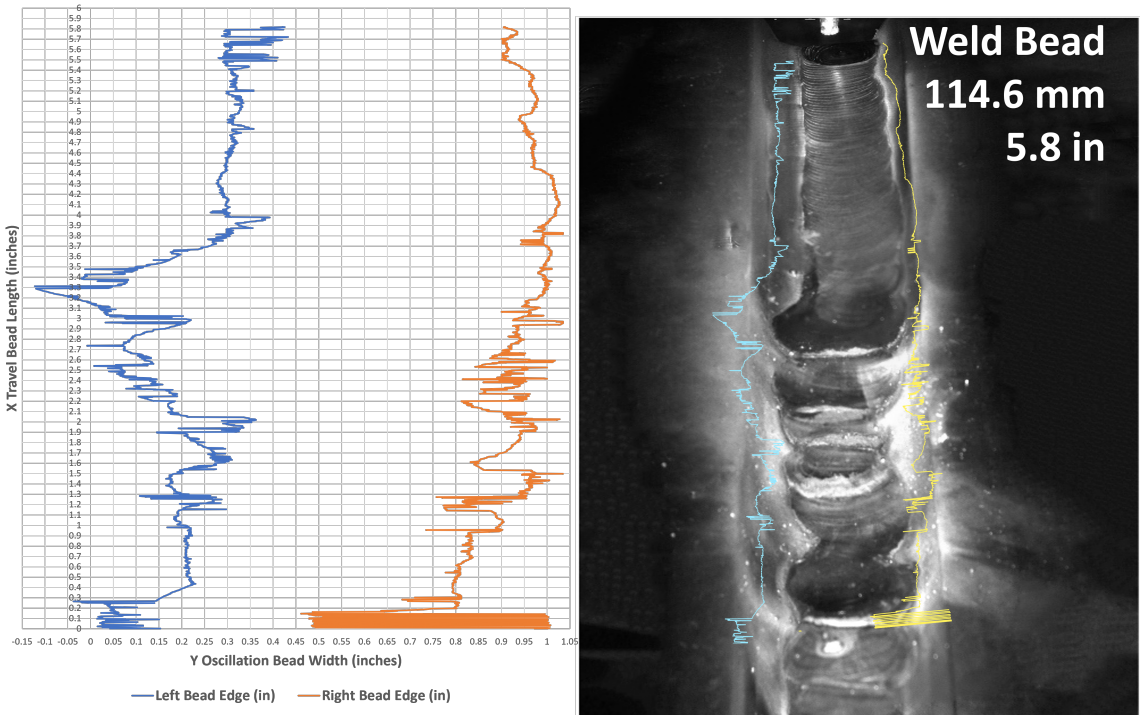


Figure A.52: Tie-In Cut Argon Gas Coverage

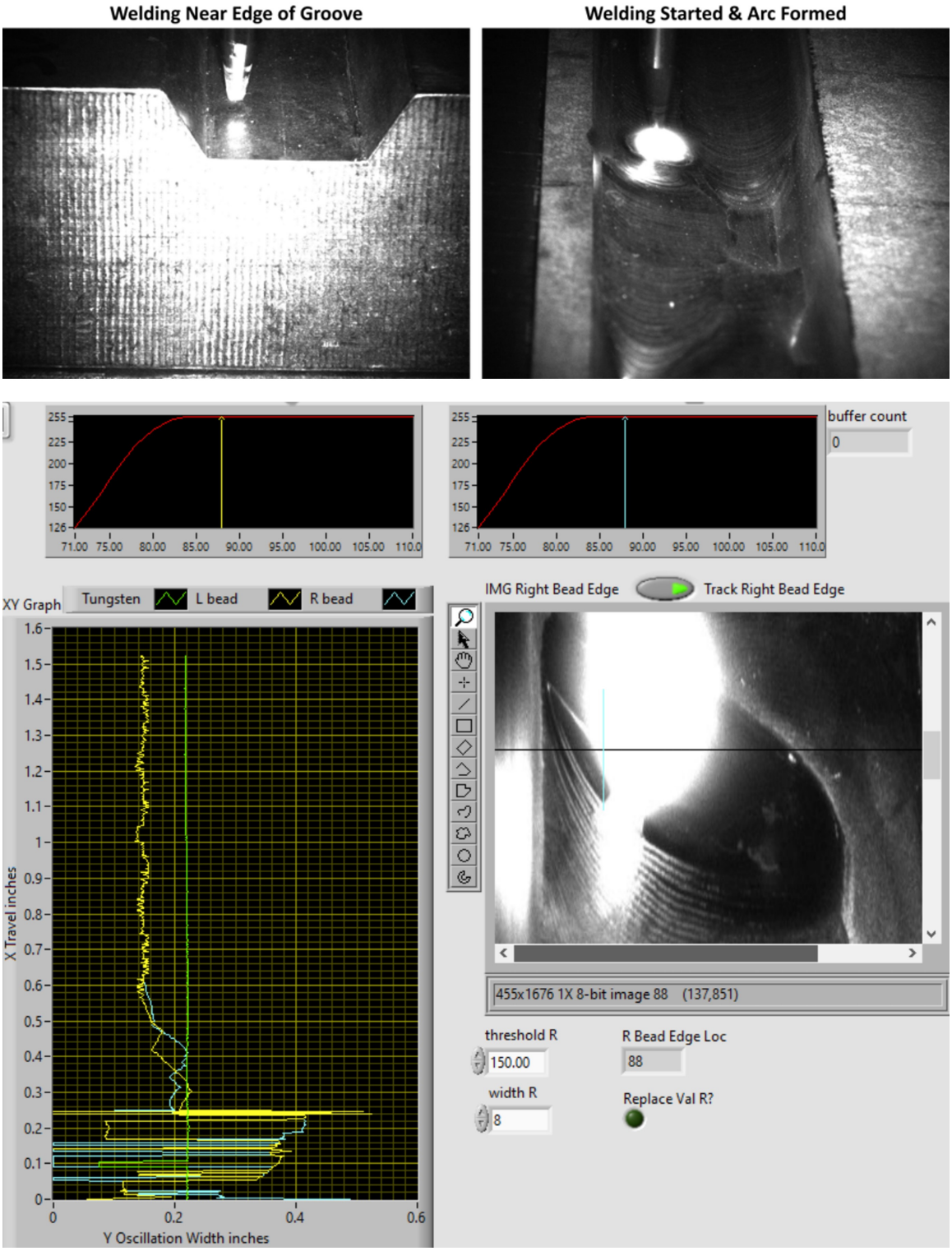


Figure A.53: Result of Bad Algorithm Start Data (Bottom)
Example of Bad Start Data (Top):
Welding Near Edge of Groove (Top Left)
Welding Started with Arc Formation

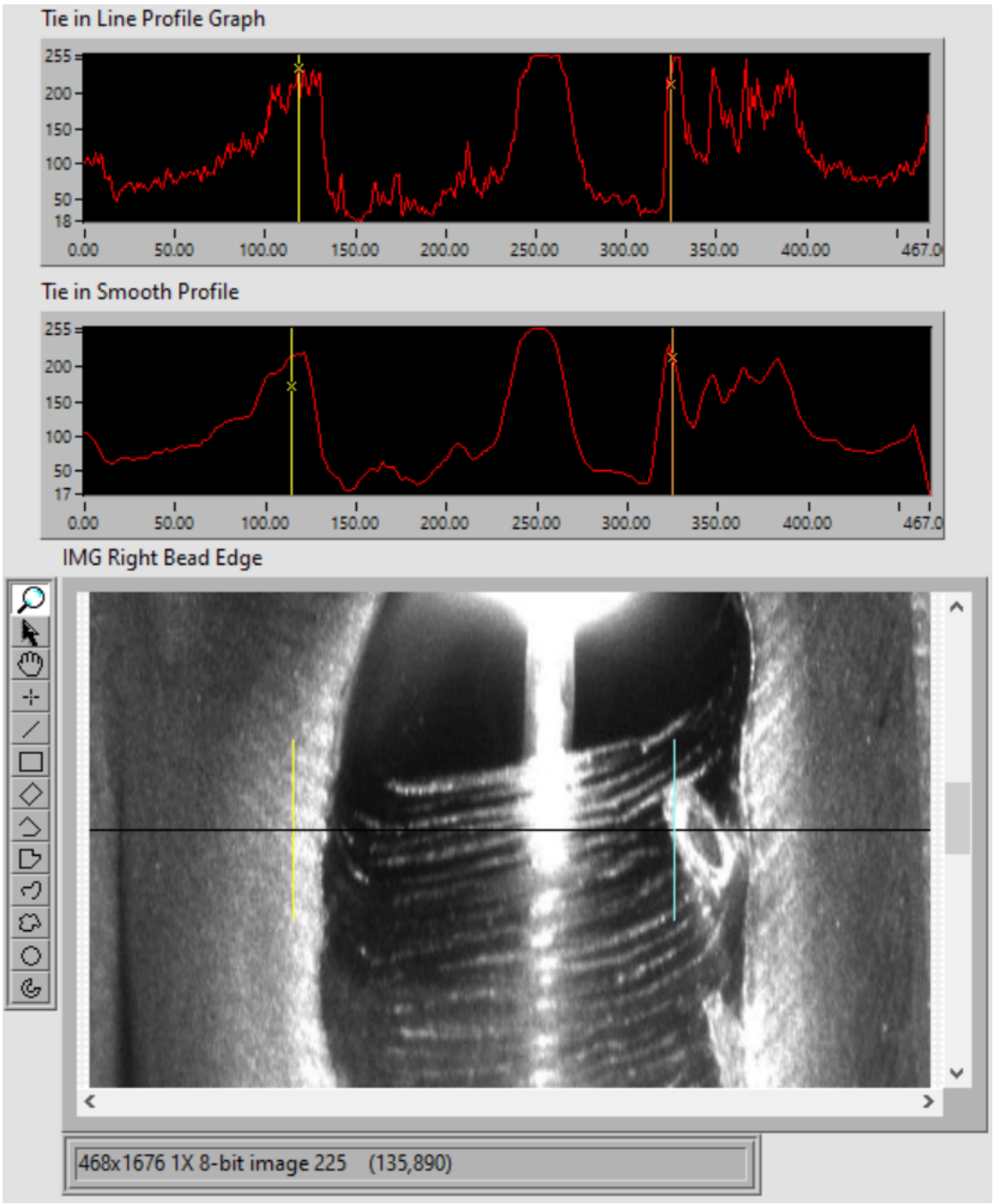


Figure A.54: Algorithm Detects Oxide Close to Right Edge

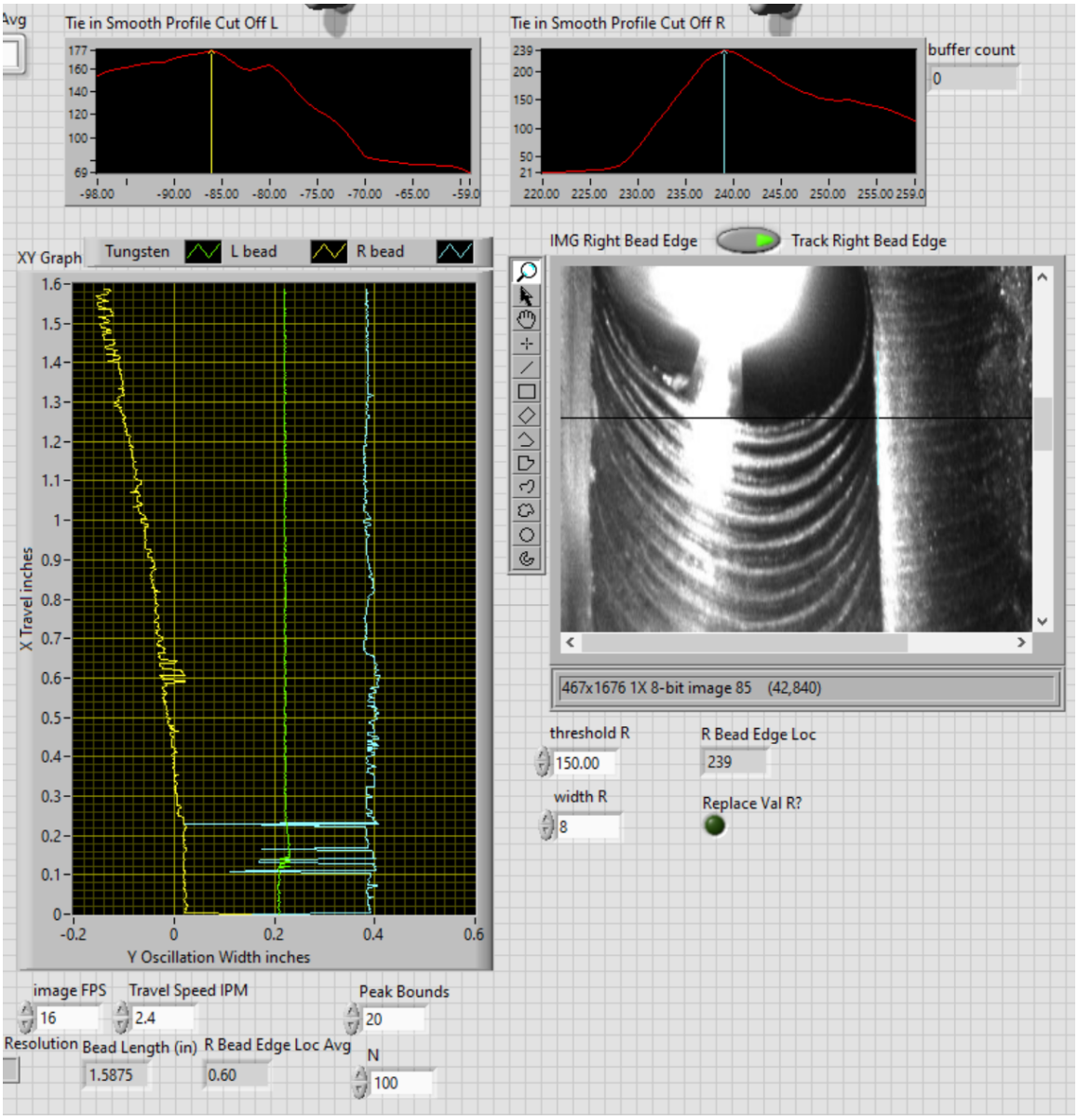


Figure A.55: Instance of Algorithm Diverging from Poor Start Data

A.7 MK II Custom Weld Head

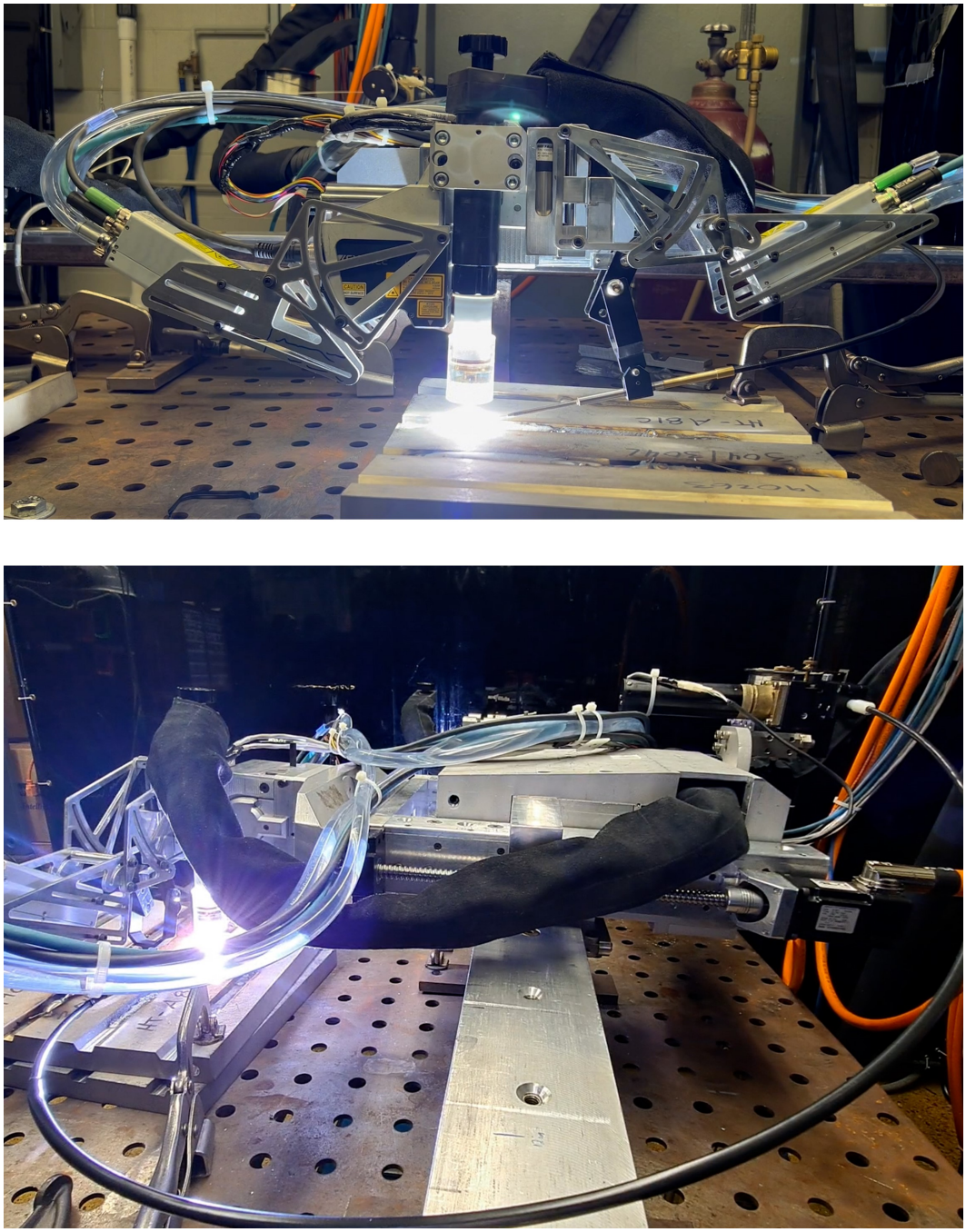


Figure A.56: Current MK II Weld Head Actively Welding: Front View (Top) Side View (Bottom)

			F Head	Mod F Head	G Head	Mod G Head	MK II Head
							
Motors	X - Travel	Manual Move	Yes	Yes	Yes	Yes	Yes
		Motorized	Yes	Yes	Yes	Yes	Yes
		Encoders	No	Yes	No	Yes	Yes
		Control Feedback	No	No	No	No	No
	Y - Oscillation	Manual Move	Yes	Yes	Yes	Yes	Yes
		Motorized	Yes	Yes	Yes	Yes	Yes
		Encoders	Yes	Yes	Yes	Yes	Yes
		Control Feedback	No	No	No	No	No
	Z - AVC	Manual Move	Yes	Yes	Yes	Yes	Yes
		Motorized	Yes	Yes	Yes	Yes	Yes
		Encoders	No	Yes	No	No	Yes
		Control Feedback	No	No	No	No	Yes
	Wire Feed Height	Manual Move	Yes	Yes	Yes	Yes	Yes
		Motorized	No	Yes	No	Yes	Yes
		Encoders	No	Yes	No	Yes	Yes
		Control Feedback	No	No	No	No	Yes
	Wire Feed Rotation	Manual Move	Yes	Yes	Yes	Yes	Yes
		Motorized	No	Yes	No	Yes	Yes
		Encoders	No	Yes	No	Yes	Yes
		Control Feedback	No	No	No	No	Yes
	Theta Pitch	Manual Move	Yes	Yes	Yes	Yes	Yes
		Motorized	No	No	No	No	No
		Encoders	No	No	No	No	No
		Control Feedback	No	No	No	No	No
	Lead/Lag Roll	Manual Move	No	No	No	No	No
		Motorized	No	No	No	No	No
		Encoders	No	No	No	No	No
		Control Feedback	No	No	No	No	No
			F Head	**Mod F Head**	**G Head**	**Mod G Head**	**MK II Head**
Sensors	Cavitar Cameras	Lead	No	No	No	Yes	Yes
		Trail	No	No	No	Yes	Yes
	Keyence	Laser Profilometer	No	Yes	No	Yes	Yes
	Power Supply	P300	No	Yes	No	Yes	Yes
	Motor	Encoders	No	Yes	No	No	Yes
			F Head	**Mod F Head**	**G Head**	**Mod G Head**	**MK II Head**
Data Collection	Cavitar Cameras	Lead	No	No	No	Yes	Yes
		Trail	No	No	No	Yes	Yes
	Keyence	Laser Profilometer	No	No	No	Yes	Yes
	Power Supply	P300	No	No	No	Yes	Yes
	Motor	Encoders	No	No	No	No	Yes

Figure A.57: Evolution of Robot & Comparison

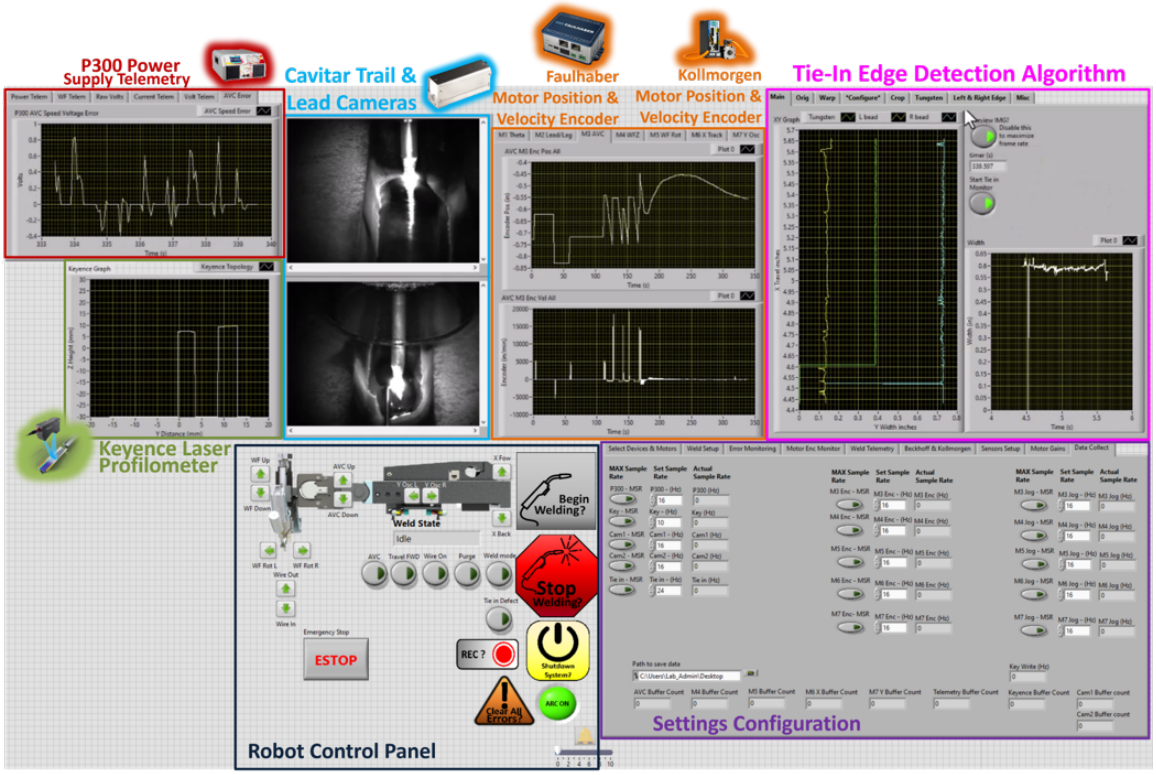


Figure A.58: Current State of MK II Weld Head LabVIEW Interface

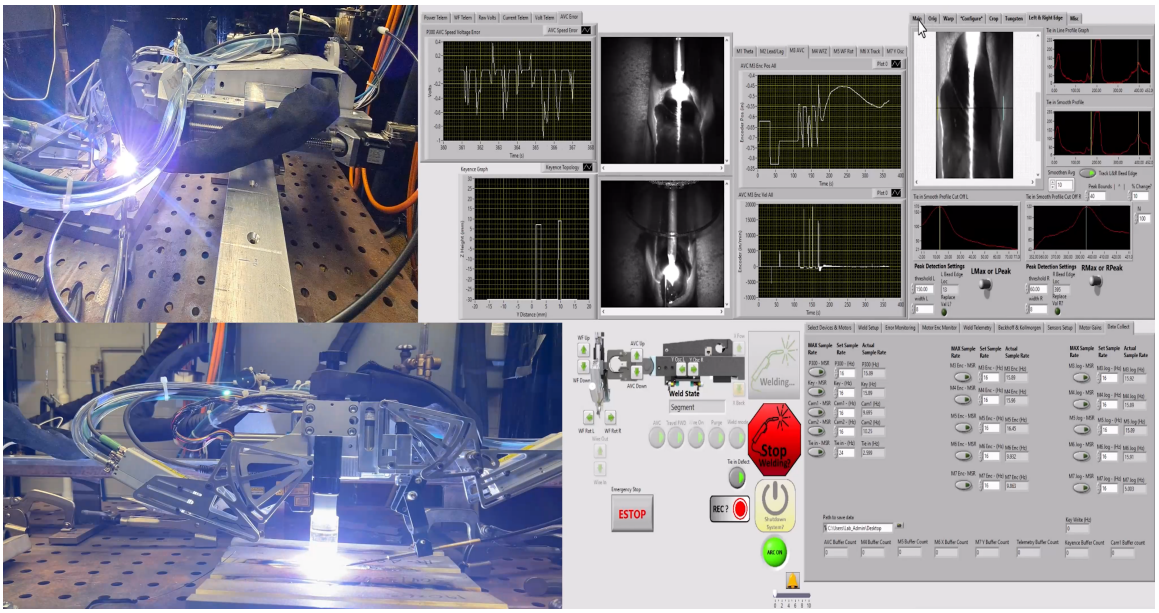


Figure A.59: Live Tie-in Robot Control

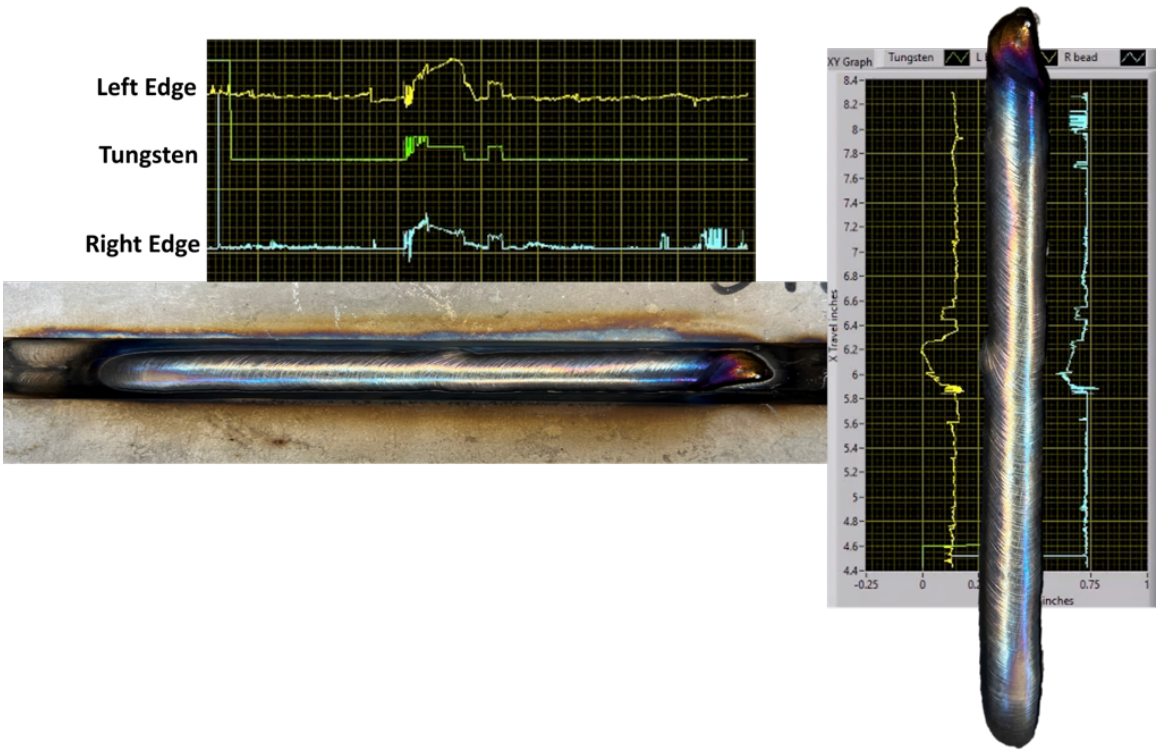


Figure A.60: Results of the Live Tie-In Algorithm on the MK II System

A.8 LabVIEW Code

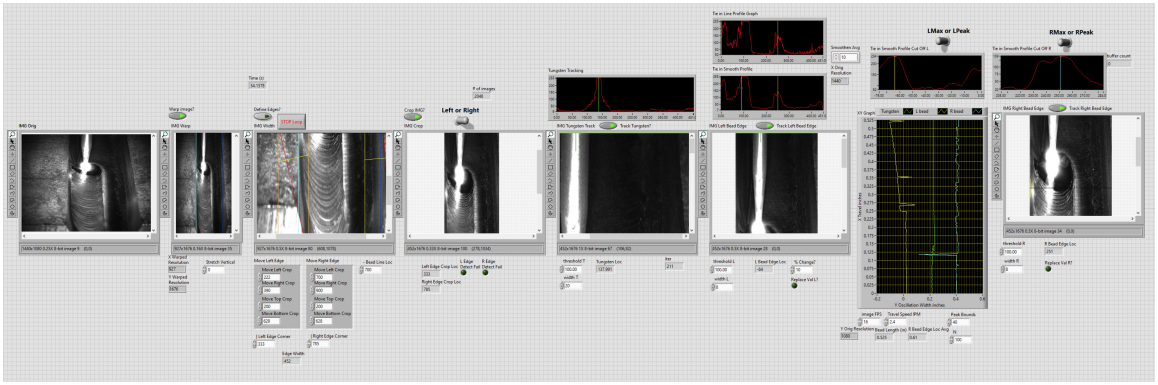


Figure A.61: LabVIEW Front Panel - Standalone Tie-in Algorithm



Figure A.62: LabVIEW Back Panel - Standalone Tie-in Algorithm

Vita

Shems-Eddine Belhout first began pursuing engineering after discovering his love for film making. In high school, he would create videos for classes. He would even start creating his own indie film. Building props for this films and bringing his ideas from fantasy into reality was what inspired him to pursue engineering. He began engineering school at the University of Tennessee and quickly settled on pursuing mechanical engineering. Right before the start of the Covid Pandemic, Shems began working for the Neutron Physics Group where he designed CAD supports for their Beamline experiments. After meeting Ethan Vals during a Study Abroad trip, Engineering in London, Ethan recomended Shems to join a welding research lab for graduate school. Shems began working as an undergraduate research assistant at the University of Tennessee under Dr. Bradley Jared, with his research focused on the Adaptive TIG Welding for Nuclear Pipe Applications. After graduating with his Bachelors in mechanical engineering, Shems began his Masters in mechanical engineering with a focus on hardware and software integration in mechatronics. Shems work experience includes multiple design projects, LabVIEW programming of a custom built TIG welding robot, hardware integration over software, designing systems for data collection. In his free time, Shems enjoys producing indie films with his friends, and spending time with family.